HB

EX 1000 + C1

K^0 Production in μ–tagged jets at the CERN $p\bar{p}$ Collider

I. E. Zacharov

K^0 production in μ–tagged jets at the CERN $p\bar{p}$ Collider

Academisch Proefschrift

ter verkrijging van de graad
van doctor aan de Universiteit van Amsterdam,
op gezag van de Rector Magnificus prof. dr. S. K. Thoden van Velzen
in het openbaar te verdedigen in de Aula der Universiteit
(Oude Lutherse Kerk, ingang Singel 411, hoek Spui),
op woensdag 18 januari 1989 te 15 uur

door

Igor Evgenievitch Zacharov

geboren te Odessa

Promotor: Prof. Dr. A.N. Diddens
Co-promotor: Dr. D. J. Holthuizen
Dr. A. Norton

Het in dit proefschrift beschreven onderzoek werd uitgevoerd als onderdeel van het onderzoeksprogramma van de Stichting voor Fundamenteel Onderzoek der Materie (FOM) welke financiëel gesteund wordt door de Nederlandse Organisatie voor Wetenschappelijk Onderzoek (NWO).

Chapter 1

Introduction.

This thesis is based on the work within the UA1 Collaboration[1] in the 'heavy flavour group' carried out at the European Laboratory for Particle Physics (CERN) in Geneva and at the National Institute for Nuclear and High Energy Physics (NIKHEF) in Amsterdam.

A Collider experiment at CERN was originally proposed by Rubbia, McIntyre and Cline [1] to establish experimentally the mediators of the weak force — the W and Z vector bosons. These bosons with masses around $90\,GeV/c^2$ were predicted by the theory which gives a unified description of the electromagnetic and weak interactions between elementary particles [2]. For the development of this theory Glashow, Weinberg and Salam were awarded the Nobel prize in physics in 1979.

To produce the W and Z particles the proton Synchrotron at CERN (SPS) had to be converted into a Collider of counter-rotating beams of protons and antiprotons. The antiproton beam had to be prepared with the technique of stochastic cooling developed by van der Meer [3]. The collisions would have $540\,GeV$ of center of mass energy; since each quark in a proton or an antiproton carries about 1/6 of the proton momentum (gluons carry 1/2 of the proton momentum), the vector bosons could be created in these collisions. The largest of the Collider experiments — the UA1 experiment, headed by Rubbia, proposed a detector with almost 4π solid angle coverage in 1978 [4]. The first W particles were captured in 1982, the Z boson was captured in 1983 [5]. For this pioneering work Rubbia and van der Meer were awarded the Nobel prize in physics in 1984.

The success of the unified electroweak interaction inspired the development of Quantum Chromodynamics, a theory describing strong interactions between elementary particles [6]. According to this theory elementary interactions between the quarks in the proton–antiproton collisions should among other produce heavy quarks — the charm, bottom and top quarks. Since the top quark is supposed to be quite heavy it has not been directly produced yet [7]. On the other hand the bottom and the charm quarks are abundantly produced in the proton–antiproton collisions at the CERN Collider. The measurement of the properties of the heavy quarks leads to a better understanding of the strong interactions and supports the unified description of the electroweak and the strong interactions in the 'Standard Model'.

Heavy quarks are produced in jets. Jets appear to the observer as a collimated stream of particles. It is extremely difficult to distinguish the type of quark or gluon, which has produced the jet. In the UA1 experiment the jets produced by heavy quarks (bottom and charm quarks)

[1] The UA1 Collaboration consists (in 1987) of institutes in Aachen, Amsterdam (NIKHEF), Annecy (LAPP), Birmingham, CERN, Harvard, Helsinki, Kiel, London (Imperial College and Queen Mary College), Madrid (CIEMAT), MIT, Padua, Paris (College de France), Riverside, Rome, Rutherford (Appleton Laboratory), Saclay (CEN), Victoria, Vienna, Wisconsin.

were selected by the measurement of a high energetic muon in that jet; this muon is assumed to come from a weak decay of heavy quarks in the jet [8].

The method of the heavy quark investigation is qualitatively different from the method used for the measurement of the W and Z bosons. For the W and the Z discovery the invariant mass of the decay products from the $W^{\pm} \rightarrow e^{\pm}\nu$ or $Z \rightarrow e^{+}e^{-}$ decays were measured and it provides a direct evidence for the production of these particles. The same method can be applied for a subsample of events containing bound states of charm and bottom quarks in the J/ψ and Υ particles, which can decay into opposite charged lepton pair (hidden flavour) [8]. On the other hand in a large majority of the events the heavy quarks (open flavour) are established by comparing quantities as muon isolation, relative transverse momentum of the muon in the jet, etc. to the corresponding values calculated by a Monte Carlo program assuming a heavy quark production. In the latter case we may speak of circumstantial evidence for heavy quark production. This is also true for the measurement of the bottom quark production in the so called J/ψ events (via the process $B \rightarrow J/\psi + X$) [9]. The investigation of the heavy quark production is possible by carefully tuning the Monte Carlo program to model the 'Standard Model' and the detector response to the muon coming from the interaction region [10].

The muon is selected in the jet study, because it can be easily identified in the UA1 detector. Electrons can not be identified in jets with the present UA1 detector and therefore can not be used to tag a bottom or charm decay. Other particles, that can be identified in the UA1 detector are the neutral kaons and lambdas. These particles are recognized by the observer from their typical V^0 decay pattern that they can leave in the detector. The algorithm for V^0 reconstruction in the UA1 detector has been initially formulated by Karimäki [11]. Although lambdas can also be identified in the UA1 detector the same way kaons are identified, lambdas are produced less abundantly than kaons. Therefore we focused our research on kaons in the first place.

There are several points of interest. Heavy quarks can produce neutral kaons in their decay, because the favored decay mode of, for instance, a bottom quark is $b \rightarrow c \rightarrow s$ and the s quark can form a K^0 meson. The kinematical properties of these kaons can be studied with the aim to use them as a tag of heavy quark production. The selection of events with a neutral kaon in the J/ψ data sample might allow a direct measurement of the bottom quark production from the $B \rightarrow J/\psi + K^0$ decay. Another possible investigation consists of the reconstruction of a $K^{*\pm}$ from its decay into $K^0\pi^{\pm}$; even more particles could be taken together, up to the B meson.

The latter possibility proved to be very difficult. The first results of the reconstruction of the $B \rightarrow J/\psi + K^0$ decay were very promising, but more J/ψ events are needed for a conclusive measurement [12]. More events are expected when the upgrade program of the CERN Collider (ACOL) is carried out (1988).

In this thesis we investigate the possibility of using the K^0 particles for jet identification, like it is done presently with muons. For this work we used a data sample with one reconstructed muon (called single muon data), because it has been shown to contain a substantial amount of heavy quark jets [10] and because of the high number of events in this sample ($\approx$ 20000 events). Since neutral kaons can be identified in jets, they could possibly be used to study the properties of heavy quarks without relying on the muon information.

This thesis is organized as follows. We review briefly the 'Standard Model' in chapter 2. A brief discussion of the UA1 detector is the subject of chapter 3. The K^0 reconstruction in jets and the reconstruction efficiency are considered in chapters 4, 5. The efficiency determination is used to calculate the cross section of K^0_S production in the single muon data sample, see chapter 6. Chapter 7 is devoted to the discussion of the use of the neutral kaon for heavy quark tagging. Finally, chapter 8 contains the summary and conclusions.

Chapter 2

Theory of the $p\bar{p}$ collisions.

2.1 Introduction.

The Standard Model has been extremely successful in its description of interactions between elementary particles at least at energies below the masses of the W and Z bosons. The Standard Model is the theory of the strong, the electromagnetic and the weak interactions. The electromagnetic and weak interactions have been unified and the resultant electroweak interaction is described by the Weinberg-Salam-Glashow model [2]. The theory of strong interactions is described by Quantum Chromodynamics (QCD) [6]. Both, the electroweak and the QCD are combined in the Standard Model.

2.2 Theory of Quantum Chromodynamics.

2.2.1 Introduction.

QCD is a renormalizable langrangian quantum field theory of the strong interactions. Its fundamental constituents are spin 1/2 fermions called quarks which carry color charge and fractional electric charge and non–abelian spin 1 gauge fields called gluons which interact with the quarks as well as among themselves [6].

There are 6 quark flavours (n_f) in QCD arranged in 3 families, as shown in table 2.1. Technically, a family is a doublet of the weak isospin eigenstates. All quarks, except the top quark have been established experimentally. Since the top quark is supposed to be quite heavy ($m > 44\,GeV/c^2$ [7]) only a lower limit on top production has been measured so far. There is an indirect evidence for its existence, however, based on the success of other predictions of the Standard model [13] [14].

Table 2.1: Some quark properties.

charge/family	I	II	III
$+\frac{2}{3}$	up (u)	charm (c)	top (t)
$-\frac{1}{3}$	down (d)	strange (s)	bottom (b)

The division of leptons and quarks in families is important, since due to lepton number conservation lepton families do not mix among themselves. Family mixing occurs in the weak decays of quarks; the relative strengths are given by the Kobayashi-Maskawa matrix (U_{KM}) [15].

2.2.2 The Quark-Parton Model.

All hadrons consist of quarks and gluons (jointly called partons) in the Parton Model based on QCD. In the Parton Model the charged partons are the quarks and the neutral ones are the gluons [16]. Quarks are called valence quarks, if they build up the quantum numbers of a hadron. Mesons contain a quark–antiquark pair as valence quarks and baryons contain three valence quarks, held together by the strong force mediated by the gluons. For the description of the strong interaction between the quarks and the gluons in the parton model, it is important to include the contribution from the virtual quarks and gluons excited from the vacuum. The quarks excited from the vacuum are called sea quarks. The momentum of a hadron is a sum of momenta of its constituents (valence and sea quarks and gluons). The parton momentum is described in the framework of the Parton Model by the parton distribution functions $f_i(x_i)$, where parton (i) carries fraction (x_i) of the hadron momentum. In first approximation in QCD the parton distribution function depends only on a dimensionless variable x, which is the fraction of total hadron momentum carried by the parton (scaling). The parton distribution functions have been measured in ep and νp collision experiments.

Qualitatively, the valence quark distributions (in the proton) peak at $x \approx 0.2$ and fall to zero for $x \to 0$; the gluon distribution functions peak at $x \to 0$, because of a high probability of soft gluon emission from quarks and gluons predicted by QCD. The distributions of the sea quarks also peaks at $x \to 0$. In summary, about half of the hadron momentum is carried by the quarks and another half by the gluons.

The analysis of deep inelastic ep scattering has shown, that the parton distribution functions in the proton depend logarithmically on the momentum transfer $Q^2 = -(p^e_{in} - p^e_{out})^2$ (scaling violation) [17]. The quantitative dependence of the parton distribution functions on Q^2 has been calculated by Altarelli and Parisi [18]. Qualitatively, the contribution from the virtual quark or gluon splitting to the parton distribution function increases with growing Q^2. The main effect of these virtual corrections is the softening of the valence and the sea distribution functions (they peak at smaller x) with growing Q^2.

We point out, that the parton distribution functions also contain a contribution from heavy quarks. This is especially important for higher Q^2, since due to the scaling violation the interaction with the virtual heavy quark pair increases. Several parametrizations of the structure functions exist, we have used Solution 1 of Eichten et al. [19] in the ISAJET Monte Carlo program (see section 2.3.1).

2.2.3 Parton confinement.

As measured in deep inelastic scattering experiments, the QCD coupling constant (α_s) varies as function of the momentum transfer squared Q^2 of the scattered particle. This dependence is calculated in QCD [17]:

$$\alpha_s = \frac{12\pi}{(33 - 2n_f)\ln(\frac{Q^2}{\Lambda^2})} \tag{2.1}$$

Equation 2.1 shows the basic property of QCD ($n_f = 6$): at high Q^2 (i.e. small interaction distances) the coupling strength of QCD becomes weak.

Therefore at large Q^2/Λ^2, when α_s becomes small a hadron can be treated as if it was kinematically composed of free partons with a specified momentum distribution. On the other hand at small momentum transfer of the scattered particle and consequently at large α_s, the quarks appear to be strongly bound inside the hadrons. A large value of the strong coupling constant for undisturbed partons in a hadron is believed to cause the so called confinement of quarks and gluons. In equation 2.1 Λ is the confinement scale. It gives a measure of the deviation from free-field behavior. Currently, $\Lambda \approx 0.2\,GeV$ (a range of 0.2 to $0.4\,GeV$ is used in the calculations), therefore the QCD perturbation theory is said to be applicable above $Q^2 > 10\,GeV^2$ ($\alpha_s < 0.3$ with $n_f = 6$) [20]. However, there is some uncertainty in the choice of the Q^2 calculation when used for the treatment of $p\bar{p}$ collisions. Several Q^2 definitions are in use. For instance the ISAJET Monte Carlo program uses $Q^2 = 2stu/(s^2 + t^2 + u^2)$, where s,t,u are the Mandelstam variables of the parton-parton scattering process [21] (see also [23]), whereas the Eurojet Monte Carlo program uses $Q^2 = p_t^2 + m_Q^2$, referring to the outgoing quark Q [22].

Coming back to the confinement we remark, that free quarks are not observable for the following reason. Quarks in a hadron can be considered to scatter among themselves; the momentum transfer Q^2 is inversely proportional to the distance between the quarks. Thus, when two quarks are separated the coupling constant grows with the distance between the quarks as given by equation 2.1. Therefore when two quarks are separated their interaction potential grows, until the corresponding energy is sufficient to create a quark-antiquark pair and we have a system of two mesons. This process is known as the process of quark hadronization.

2.2.4 Fragmentation of quarks and gluons in jets.

The main property of the high energy inelastic $p\bar{p}$ scattering is the creation of jets. Jets are highly collimated streams of particles with small transverse momentum relative to the jet axis ($p_t \ll p_{||}$). According to the Parton Model jets are created in the process of fragmentation of a quark or a gluon after their interaction. Fragmentation is a process of repeated hadronization. Energy is transferred during the interaction to partons in the hadron. An outgoing quark takes an antiquark from the sea of the $q\bar{q}$–pairs and becomes a hadron; the remaining quark repeats this process until all energy, that has been transferred during the interaction is dissipated. At the end a jet of particles is created close to the initial quark direction.

In the fragmentation model of Field and Feynman [23] it is assumed, that each quark fragments independent of the others and the fragmentation process is independent of the production process. However, there is a problem with the last quark, which has not enough energy to excite a new $q\bar{q}$–pair from the sea. In the ISAJET Monte Carlo program this quark is discarded [21] and the conservation of color quantum number is violated. In the Eurojet Monte Carlo the last quark is coupled to the remaining quarks from other fragmentations to achieve the conservation of color quantum number [22]. If the last, low momentum quark is discarded like in ISAJET program, the color compensation has to be assumed.

According to the so called 'soft color-screening' hypothesis mutual color compensation for partons produced in a hard process is not associated with significant redistribution of energy and momentum among the jets [16]. On the contrary, fast particles in a jet 'remember' the quantum numbers of the parton that has created the particles [23]. At the Collider energies however, large particle multiplicities make it very difficult to disentangle the original flavour. A very important tool of jet identification used in the present experiment is the semileptonic decay of the jet particles, see section 2.2.5. Jets from heavy quarks for instance, can be statistically identified if they contain a lepton from the heavy quark decay, by selecting events with certain kinematical parameters of the leptons.

The main characteristic of the fragmentation process is the ratio (z), defined as $z = (E + p_l)_h/(E + p_l)_q$, where p_l is the longitudinal momentum of the created hadron (h) or the longitudinal momentum of the quark (q) (with respect to the quark direction). The transverse momentum of the hadron with respect to the quark direction is connected to the brownian motion of the partons in the hadron and has a distribution with a width of typically $p_t < 0.3\,GeV$. The probability to create a hadron (h) with a given z from quark (i) is described by the fragmentation function $D_i^h(z)$. For the light quarks (q) u,d,s or a gluon the fragmentation function can be written as

$$D_q^h(z) = 1 - a + a(b+1)(1-z)^b \tag{2.2}$$

with adjustable parameters a,b. Peterson et al. proposed the following form of the fragmentation function for the heavy quarks c,b,t (Q) [24]:

$$D_Q^h(z) = \frac{N}{z[1 - \frac{1}{z} - \epsilon_Q \frac{1}{1-z}]^2} \tag{2.3}$$

with $\epsilon_Q \approx (m_q/m_Q)^2$, where m_q is the mass of the light quark (q) taken by the heavy quark (Q). N follows from the requirement $\sum_h \int dz D_Q^h(z) = 1$ for all hadrons (h) created in the fragmentation of the heavy quark Q. The dependence of the parameter ϵ_Q on the heavy quark mass m_Q has an important consequence: the fragmentation function of heavy quark will produce harder mesons, compared to the momentum of mesons created in a light quark fragmentation process at the same energy. For instance the B–meson will get on average as much as 80% of the initial b–quark momentum. Another consequence is the shorter fragmentation chain of the heavy quarks, compared to the light quarks, since the hadrons from the heavy quarks obtain more energy.

2.2.5 Weak decays of the heavy quarks.

As a quark fragments into hadrons large number of resonances are created which decay into stable (quasistable) particles with π and γ emission (strong and electromagnetic interactions). These decays occur between the members of the same family. When strong or electromagnetic decays are not possible, the decay proceeds via the weak interaction and quark families are mixed.

Special interest of the present study is devoted to the fragmentation products of the b and c quarks. A b-quark can take a light quark from the sea to become a B meson, which decays weakly via a semileptonic or a hadronic channel (the $B^\pm$ life time is about $10^{-12}\,sec$ [25]). The relative probabilities of the flavour changing transitions in weak decays are given by the Kobayashi-Maskawa matrix U_{KM} [15]. Experimental evidence for U_{KM} is such, that the mixing between quark families becomes weaker with growing family number and in addition with the distance between the families. Therefore cascade decays (like $b \to c \to s$) are more probable than direct transitions (i.e. $b \to s$).

Of special importance for the present experiment are the semileptonic heavy quark decays into a muon and a muon neutrino (branching ratio is about 12% for the $B^\pm$ meson and 18% for the $D^\pm$ meson [25]). Muons in jets can be identified with the UA1 detector (see chapter 3) and used as a signature for a heavy quark production.

Note the appearance of the s-quark at the end of the decay chain ($b \to c \to s$ or $c \to s$). This s-quark can create a K_S^0 in some fraction of the events, which can be reconstructed in the UA1 detector (see chapter 3). In the present study we investigate the possibility to obtain additional evidence for the heavy flavour production at the CERN Collider by an appropriate K_S^0 selection (see chapter 5).

2.3 Summary of hadron production.

To calculate the hadron scattering cross section we assume the validity of the factorization scheme, in which the scattering cross section is described by the convolution of the elementary scattering of the constituents with their structure functions. Then, for the description of the production processes of hadrons we have to know four quantities, which are functions of several variables.

- First, the differential cross section of the elementary subprocess ($d\hat{\sigma}$) must be calculated. These are the processes of quark-quark, quark-gluon, etc. collisions. Since the colliding objects have no structure (they are pointlike) and occur at large Q^2 (at the $Sp\bar{p}S$), the cross sections can be calculated in the QCD perturbation theory. The largest contribution to the invariant matrix element (A) in a first order QCD calculation is given by the scattering process $gg \to gg$ ($|A(\theta_{CM})|^2 = 30.4$ in relative units for massless partons and polar angle $\theta_{CM} = \frac{\pi}{2}$ [20]), followed by the process $qg \to qg$ ($|A(\frac{\pi}{2})|^2 = 6.11$) and $qq \to qq$ ($|A(\frac{\pi}{2})|^2 = 3.26$).
- Second, the parton structure functions $f_i(x, Q^2)$ must be known. The structure functions are assumed to depend mainly on the fraction (x) of the parton momentum, the dependence on the momentum transfer Q^2 being due to the QCD corrections to the first order (Born) approximation for the elementary subprocess (Altarelli-Parisi equations, see section 2.2.2).

The combination of these two points gives the inclusive cross section for the scattering of proton (a) and (anti)proton (b) to hadron (c) and anything (X) [20]:

$$d\sigma(a+b\to c+X) = \sum_{ij}\frac{1}{1+\delta_{ij}}\int dx_a dx_b\ [\ f_i^{(a)}(x_a,Q^2)f_j^{(b)}(x_b,Q^2) + f_j^{(a)}(x_a,Q^2)f_i^{(b)}(x_b,Q^2)\ ]\ d\hat{\sigma}(i+j\to c+X)$$

where $f_i^{(a)}(x_a, Q^2)$ is the probability that proton (a) contains parton (i) which carries a fraction x_a of the proton's momentum; $d\hat{\sigma}$ is the cross section of the subprocess as before.

- Third, a fragmentation model has to be applied. Each quark coming from the interaction region has to be converted to one or more colorless objects, according to the confinement hypothesis. We use the Field and Feynman fragmentation model, where each quark fragments independently from all other quarks (see section 2.2.4).
- Fourth, unstable particles have to decay into stable ones to be analyzed at the detector level. The decay can proceed also via the electroweak interaction.

For the explicit calculation of the cross sections and the spectra of the outgoing particles we used the ISAJET Monte Carlo program [21] (version 5.23) and (to a lesser extend) the Eurojet Monte Carlo program [22]. The Monte Carlo program calculates the matrix elements for the subprocesses, integrates over the fragmentation functions and includes branching ratios and the decay kinematics.

2.3.1 ISAJET Monte Carlo program.

Heavy quarks (Q) are produced in the QCD processes of flavour creation (1), flavour excitation (2) and final state gluon splitting (3), each accounting for about 1/3 of the calculated cross section of the heavy quark production:

$$\begin{array}{lll} (1) & gg \to Q\bar{Q} & q\bar{q} \to Q\bar{Q} \\ (2) & qQ \to qQ & gQ \to gQ \\ (3) & g \to Q\bar{Q} & \end{array}$$

Hard scattering cross sections for these subprocesses are calculated using QCD matrix elements of lowest order in α_s (eq. 2.1). In the heavy flavour excitation mechanism a heavy quark from the sea undergoes a hard scattering with a light quark or a gluon from the other incident hadron. As mentioned in section 2.2.2 the Eichten et al. structure functions (solution 1) have been used. Higher order matrix elements are not included directly in ISAJET, but they are approximated by the basic QCD branching processes $q \rightarrow qg$, $g \rightarrow gg$ and $g \rightarrow q\bar{q}$ applied to the partons of the hard scattering (shower approximation). The collinear singularities of the radiation processes are absorbed by the structure functions. They are handled by introducing a cut off in the momentum transfer at 6 GeV/c [21]. Thus, heavy quark production in gluon splitting occurs for gluon momenta above 6 GeV/c; below that energy the gluon is hadronized.

The independent fragmentation model of Field and Feynman has been used (see section 2.2.4) with a cut off at 6 GeV on the parton shower evolution. In ISAJET a gluon is fragmented as if it were a light quark or an antiquark, except that gluons radiate more in the evolution process. Heavy quarks are fragmented with the Peterson et al. function (see section 2.2.4) into a leading heavy flavour hadron in the proportions $Q\bar{u} : Q\bar{d} : Q\bar{s} : Qqq = 38.7\% : 38.7\% : 12.6\% : 10\%$. The ratio of spin 1 to spin 0 (spin 3/2 to spin 1/2 for baryons) is assumed to be ≈ 3 [10].

The remaining spectator quarks from the proton and the antiproton are fragmented to reproduce the observable particle distributions. The global multiplicity distribution was adjusted so that it reproduces the height of the rapidity plateau in high E_t jet events far away from the jet axes [10]. The average transverse momentum of primary mesons is adjusted using the same jet data and fixed at $< p_t >= 0.45\,GeV/c$.

Relative contributions of the three processes to the $b\bar{b}$ cross section at the CERN Collider are shown in fig. 2.1 taken from ref. [26]. Although the three processes contribute about equally to the total cross section, they result in topologically distinct jet configurations. In the process of flavour creation the two heavy quarks are produced back to back in their CM system. In the laboratory system they might be boosted in the direction of the beam, but retain maximal separation in the azimuthal angle. The flavour excitation mechanism leads to a configuration where one high p_t heavy quark is produced at large angle and is balanced in momentum by a light quark or a gluon. The other heavy quark tends to be produced more in the forward direction (large rapidity). Gluon splitting produces a $Q\bar{Q}$–pair which tends to have a small opening angle. Fig. 2.2 taken from ref [10] shows the difference in the azimuthal angle between the two muons, coming from a semileptonic heavy quark decay for each of the three processes.

The total cross section for $b\bar{b}$ pair production has been calculated using the single muon cross section $\sigma(p\bar{p} \rightarrow \mu + X)$ with a kinematical cut off $10 < p_t(\mu) < 15\,GeV/c$ and $|\eta(\mu)| < 1.5$ [26]. The average semileptonic branching ratio of a B-meson of 12% has been used. The integration of the cross sections to $p_t(b) = 0$ and for all rapidities using QCD calculations of Nason et al. gives $\sigma(p\bar{p} \rightarrow b\bar{b} + X) = 10.2 \pm 3.3\mu b$ [26]. The error is a propagation of the experimental errors, assuming no further error from the uncertainty in the shape of the theoretical distributions used for the extrapolation. The experimental errors include the statistical error on the sample, the errors due to the subtraction of background of muons not coming from the $b\bar{b}$ decays and the errors on integrated luminosity and muon acceptance. The measurement of the muon spectrum is treated in chapter 5.

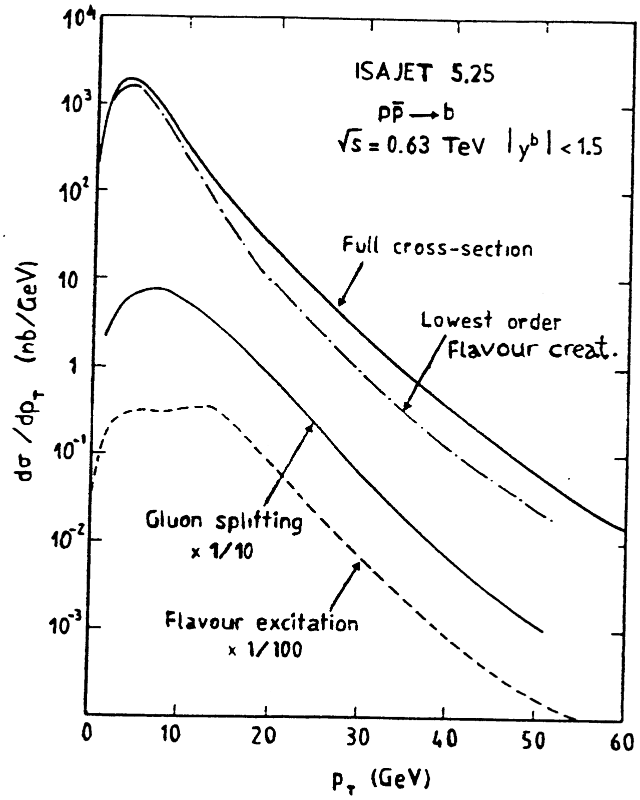

Figure 2.1: *The inclusive differential bottom cross section as estimated by the ISAJET Monte Carlo program (version 5.25) in the central rapidity region $|y| < 1.5$ for $p\bar{p}$ collisions at $\sqrt{s} = 0.63\,TeV$ (full line). Individual processes: flavour creation (dash-dotted line), gluon splitting scaled down by 1/10 (lowest full line), flavour excitation scaled down by 1/100 (dashed line).*

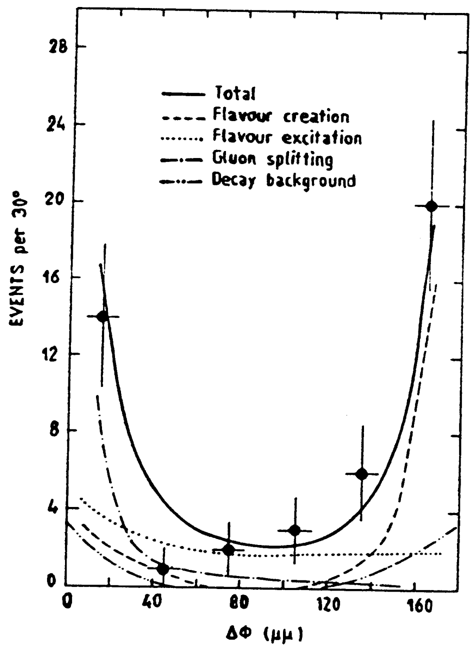

Figure 2.2: *The azimuthal angle difference between two muons in jets coming from the processes of flavour creation (dashed line), flavour excitation (dotted line) and gluon splitting (dash-dotted line). Real data is shown for events with $p_t^{\mu_1} > 7\,GeV/c$, $E_t^{jet1} > 12\,GeV$ and $p_t^{\mu_2} > 3\,GeV/c$ and with $\sum E_t > 6\,GeV$ in a cone of $\Delta R < 0.7$ around the first muon (non-isolated).*

Chapter 3

Description of the UA1 experiment.

3.1 $Sp\bar{p}S$.

Data analyzed in this thesis was taken at the CERN $Sp\bar{p}S$, the proton - antiproton collider at the CM energy of $\sqrt{s} = 630\,GeV$. The performance of the accelerator is described by a machine parameter called luminosity (L) [27]:

$$L = \frac{n \cdot f \cdot N(p) \cdot N(\bar{p})}{A} \qquad (3.1)$$

Here $N(p)$ and $N(\bar{p})$ are the number of protons and the number of antiprotons per bunch respectively; n is the number of bunches; A is the effective area of overlap of the proton/antiproton bunches at the interaction point; f is the revolution frequency. Luminosities in the order of $0.5\,\mu b^{-1}s^{-1}$ have been achieved in the $Sp\bar{p}S$ in the year 1986.

The number of events (N) is calculated from the integrated luminosity and the cross section (σ) for the process which produces the events:

$$N = \sigma \times \int Ldt \qquad (3.2)$$

Single muon data used for the analysis for this thesis were collected during the years 1985, 1986 of the collider run. The total integrated luminosity is $556\,nb^{-1}$. The integrated luminosity has been measured with an accuracy of 15%.

3.2 The Detector.

The detector has been built around a beam intersection point known as the Underground Area 1 (UA1). It has a solid angle coverage of nearly 4π (holes less than $0.2°$ for the beam pipes). It consists of a multiwire drift chamber in a uniform magnetic field (Central Detector, CD), electromagnetic and hadronic calorimeters and drift chambers for muon detection (muon chambers) [4]. The geometrical structure of the detector is shown in figure 3.1. The UA1 detector can measure electrons, muons, hadrons and photons; neutrinos are measured by the energy imbalance transverse to the beam.

At $0.2\mu b^{-1}s^{-1}$ the rate of proton-antiproton collisions is approximately $6.2\,kHz$ Clearly, at this rate most of the initial data stream contains events not interesting for the physics analysis in the UA1 experiment (and also beam gas interactions, etc.). The data rate has to be reduced to $< 5\,Hz$ for the recording on a magnetic tape. Interesting events are selected on line by the trigger electronics. There are two levels of triggering.

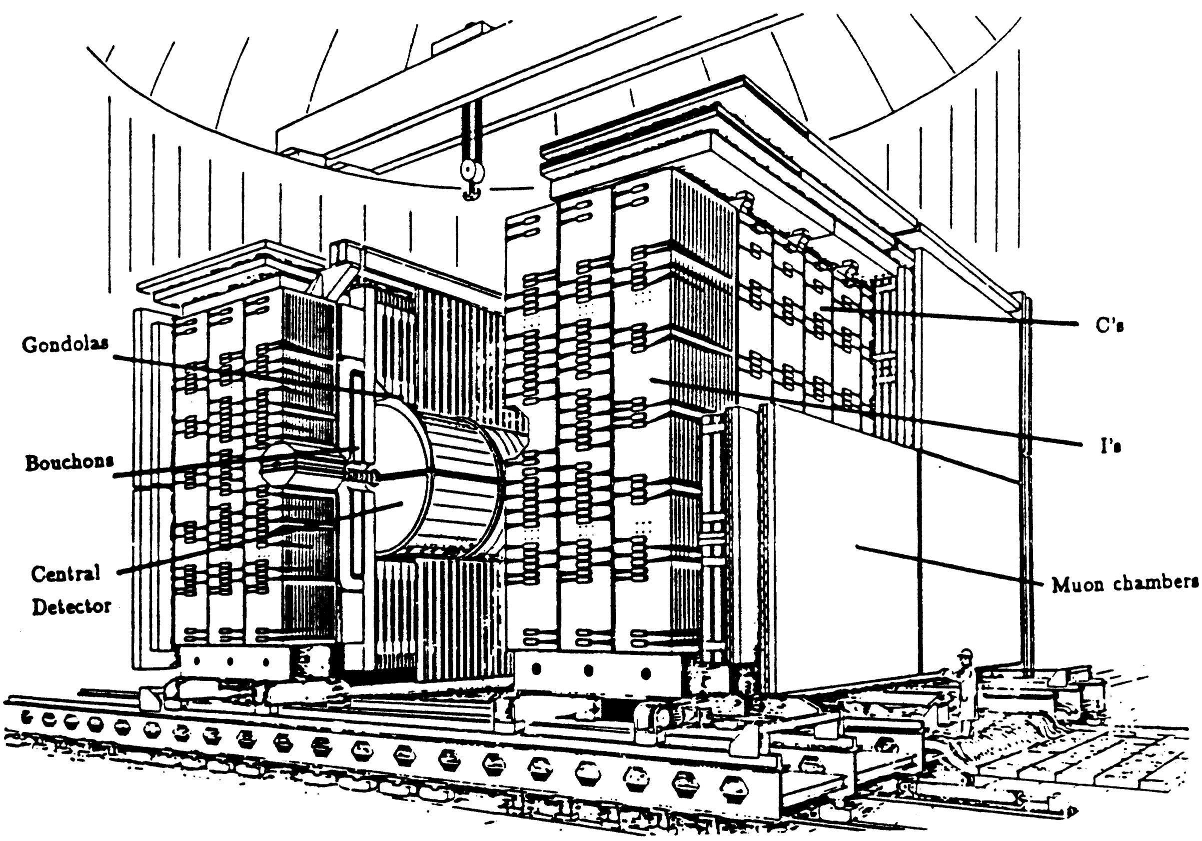

Figure 3.1: *The UA1 detector with the two halves separated, showing the Central Detector, electromagnetic calorimeters (Gondolas and Bouchons), hadron calorimeters (C's and I's) and the muon chambers.*

The first level trigger consists of a pre–trigger, separate triggers for the muon chambers and the calorimeter, and the final decision system, which combines this information [28]. The data rate is reduced to about $10\,Hz$ (at $0.2\,\mu b^{-1}s^{-1}$) after the application of the first level trigger. The second level trigger does a partial event reconstruction, combining the information given by different detector parts. About 60% of the events are rejected at this level, so that the data rate is reduced to $< 5\,Hz$ for the recording to the magnetic tape [29].

We want to describe the function of the pre–trigger. It is based on four planes of scintillator hodoscopes symmetrically placed on the two ends of the UA1 detector, covering the angular range around the beam pipe from 0.6° to 25°. The pre–trigger condition is satisfied when at least two pairs of hodoscopes have fired at both ends of the detector in a tight coincidence with a bunch crossing. On special occasions, data taking is initiated with at least the pre–trigger condition satisfied (other trigger signals are ignored). These data mainly contain events of the non-single diffractive $p\bar{p}$ interactions, called minimum bias events. The efficiency of the pre–trigger for the non-single diffractive events is $96 \pm 2\%$ [30].

About 40% of the events written to tape passed the muon trigger. For the events with the muon chamber hits, the first level trigger takes the hit-pattern and rejects the event if the pattern does not match a pre–calculated pattern stored in a lookup table. In the second level trigger, employed for the events with a single muon, the timing information from the muon chambers is also used (MUTIME algorithm [29]). The second level trigger is about 90% efficient for the events with $p_t(\mu) > 6\,GeV/c$ and nearly 100% efficient for events with a muon $p_t(\mu) > 8\,GeV/c$.

3.3 Event reconstruction in the Central Detector.

The Central Detector (CD) is a cylindrical multiwire drift chamber of 5.8 m in length and 2.3 m in diameter, made of eight independent chambers. The CD covers the polar angles from 5° to 175° with respect to the beam direction. It is located in a dipole magnet generating a uniform field of 0.7 T. The direction of this field is horizontal and perpendicular to the beams. All wires in the chambers are strung along the magnetic field direction, as indicated in fig. 3.2. The distance between the sense wires is 1 cm.

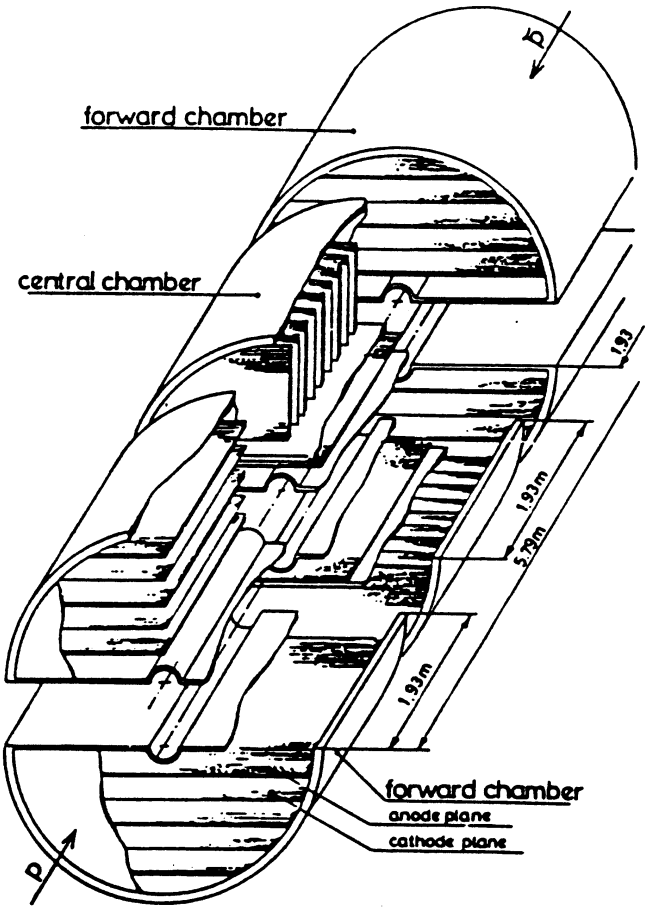

Figure 3.2: *The UA1 Central Detector, showing the geometrical structures of six chambers and the wires. Two small chambers between the central chamber and the beam pipe are not shown.*

The passage of a charged particle ionizes the chamber gas, creating free electrons which drift in a uniform electric field toward the sense wires. In the proximity of the sense wires the field is not uniform any more and the drift time of the electrons depends on the angle of sense wire approach. Corrections are applied for the track reconstruction to compensate for this effect. The charge collected on a sense wire produces a pulse which is measured and read out on both ends of the wire [4]. The measured drift time appears to be also a function of the pulse size, because smaller pulses rise more slowly than large pulses in the read out electronics. The so called time-slewing corrections of the form $\delta t = -const/E$, where E is the pulse size (ionization) of the hits are applied to compensate for this effect.

The recorded information consists of

- the drift time measurement combined with the known wire position. The precision of this measurement is about 0.25 mm.

- the position along the wire, calculated from the difference in the pulse height on both ends of the wire. This so called charge division measurement is accurate to about $4\,cm$ ($\approx 1.7\%$ of the wire length).
- the energy loss dE/dx of the particle is measured by the sum of the pulse heights on both ends of the wire. This information is not used for the analysis described in this thesis, because the energy loss is not sensitive to particles with high momentum, as required in the present work.

For each event, the recorded digitizings have to be reduced to particle trajectories. The parameters of these trajectories should be obtained at the interaction point. The interaction point is the position of the $p\bar{p}$ interaction at the beam crossing. Since the beam bunch has extended dimensions, this position is not known beforehand. Only the transverse beam position is well determined at fixed beam momenta (within $100\,\mu m$, the beam dimensions in the y and the z-directions), while the interaction region is several centimeter long.

The particle trajectory in the CD is parametrized by a helix curve. In the drift plane (the xy-plane perpendicular to the magnetic field direction) the projection of this helix is a circle with a radius of curvature R_{xy} (in meters) given by

$$R_{xy} = \frac{p \cdot cos\lambda}{0.2998 \cdot B} \tag{3.3}$$

where p is the momentum of the particle in GeV/c, λ is the angle of particle trajectory with respect to the xy-plane, B is the magnetic field strength in Tesla. Under the normal operating conditions B=0.7 T. The helix coordinate along the field is represented by a straight line in the coordinates (s,z):

$$z = c_1 s + c_2 \tag{3.4}$$

where s is the track length in the xy-projection and z is the coordinate along the field; c_1 and c_2 are constants.

Event reconstruction in the CD proceeds in two stages, the so called 'track finding' and 'track fitting' [31]. Track finding is done by identifying track segments (three to eight unused points lying on a line) and by combining the track segments to a single track of constant curvature. This global track construction gives first two groups of track candidates corresponding to the bottom and top chambers of the CD. The track candidates from these two groups are combined to a single track, when possible. Track fitting is done by a least squares fit in projections, a circle in the xy-plane and a line in the sz-plane, as described above [32].

The position of the interaction vertex is determined from the extrapolations of the tracks to the beam line in the xy-plane [33]. The crossing or nearest point to the beam is entered into a histogram. The biggest cluster is selected as the position of the primary interaction point (primary vertex). The accuracy of the vertex position depends on the number of tracks in an event, it is typically in the order of $2\,mm$ in the x-direction. Figure 3.3 shows the error distribution of the vertex position in the x-direction for the minimum bias events and the single muon events. The track density in single muon events is typically a factor 2 to 3 higher than the track density in minimum bias events. Therefore the position of the primary interaction point can be estimated with a higher precision. Vertices other than beam-beam interactions are found with the same method, if they are near to the beam line.

A special search is done for vertices caused by a decay of a neutral particle, resulting into two charged particles leaving a typical V^0 - track pattern. The reconstruction of the decays of neutral kaons and lambdas, leaving a V^0 - track pattern is the main subject of this thesis. The method used for the V^0 search will be discussed in detail in chapter 4.

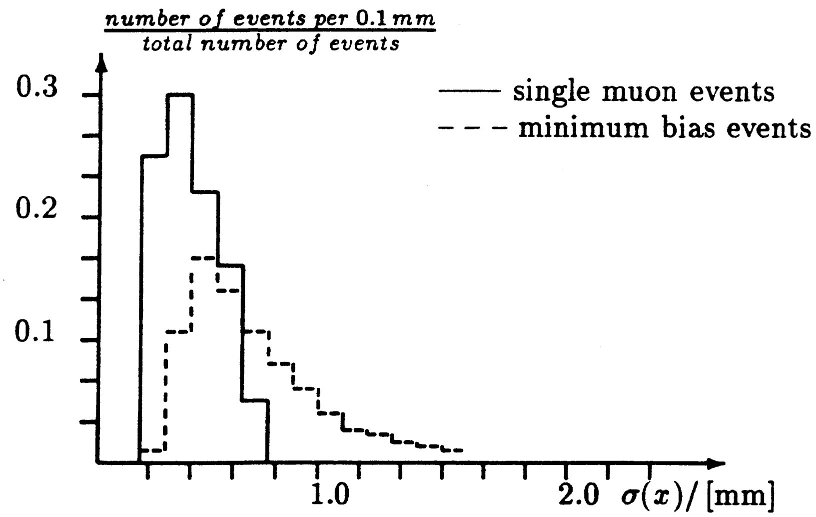

Figure 3.3: *Distribution of the estimated error in the vertex position in x-coordinate for the minimum bias and single muon events.*

The track association to the vertices takes into account the nearest distance of the track to the vertex point in the statistical sense. So, tracks which extrapolate to within ± 3 standard deviations of the fitted vertex position are defined to be 'associated to the vertex'. The trajectories of these tracks are then refit, using the vertex as an additional point in the fit.

3.4 Jet reconstruction.

The physics of jet phenomena has been described in chapter 2 of this thesis. In general, a jet consist of a group of high energy particles which are spatially near to one another. Jets can be readily recognized in a reconstruction of charged particle trajectories and energy depositions in the detector.

In the CD the jet reconstruction is based on the spatial distance (ΔR) between the neighboring tracks:

$$\Delta R = \sqrt{\Delta\phi^2 + \Delta\eta^2} \tag{3.5}$$

where $\Delta\phi$ is the difference in the azimuthal angle between two tracks and $\Delta\eta$ is the difference in their pseudorapidity. The pseudorapidity is calculated from

$$\eta = -\ln(\tan\frac{\theta}{2}) \tag{3.6}$$

where θ is the polar angle around the beam direction. The pseudorapidity is close to rapidity for small particle mass or at high particle energy.

The jet reconstruction proceeds as follows. First, all tracks in the CD with the transverse momentum larger than the threshold of $1\,GeV/c$ are marked. These tracks are called the initiators and they are marked in an order that decreases with p_t. All initiators within a certain ΔR cone (typically $\Delta R < 1$) are added up vectorially to obtain a jet axis, initiators outside this cone are used to define another jet. Then, all other tracks within the same ΔR cone around the jet axis and with p_t above $0.1\,GeV/c$ are added scalarly to obtain the total jet transverse momentum.

This algorithm has been modified slightly for the present analysis by including the reconstructed neutral kaons. This, and some other modifications will be discussed in chapter 5.

Apart from the reconstructed V^0's, neutral particles cannot be measured in the CD and therefore the jet definition with CD-tracks only will in general be distorted. A very important exception are jets with a high momentum muon, where the muon defines primarily the jet axis and transverse momentum left over to escape with neutral particles is low. For the analysis of jets without a muon we used the measurement of the energy deposition in the calorimeters, instead of the tracks in the CD.

An energy deposition in a calorimeter cell is assigned a vector, called a pseudotrack, that points from the interaction vertex to the cell. This vector has a magnitude of the energy deposition. Jet finding with pseudotracks proceeds the same way as for the tracks in the CD, described above. We have used the threshold of $2.5\,GeV$ for the initiators and the threshold of $1\,GeV$ for the other pseudotracks. The jet cone size is $\Delta R = 1$.

The choice of $\Delta R = 1$ for the calorimeter jets is apparent from the calorimeter granularity, see table 3.1. The cell size of the hadronic calorimeter (the so called C's and I's) is about $\Delta R \approx 0.5$. Therefore the requirement of the cone size of $\Delta R < 1$ demands a separation of at least one calorimeter cell between the jets.

Table 3.1: *Main parameters of the calorimeters. For the definition of the calorimeter elements see fig. 3.1. Here X_0 is the radiation length ($\approx 180\,A/Z^2\,gcm^{-2}$) and λ is the nuclear interaction length (see e.g. [34]). The energy (E) is expressed in GeV.*

	Gondolas	Bouchons	C's	I's
Plate thickness	$1.2\,mm$ lead	$4\,mm$ lead	$5\,cm$ iron	$5\,cm$ iron
Scintillator thickness	$1.5\,mm$	$6\,mm$	$1\,cm$	$1\,cm$
Cell size ($\Delta\eta \times \Delta\phi$)	$0.1 \times 180°$	$1.5 \times 11°$	$0.3 \times 15°$	$0.4 \times 15°$
Number of cells	48	64	232	128
Thickness at normal incidence	$26.4\,X_0$ $1.1\,\lambda$	$26.7\,X_0$ $1.2\,\lambda$	$5.0\,\lambda$	$7.1\,\lambda$
Number of depths samplings	4	4	2	2
Energy resolution $\sigma(E)/E$ %	$0.25/\sqrt{E}$	$0.20/\sqrt{E}$	$0.80/\sqrt{E}$	$0.80/\sqrt{E}$

All calorimeter jets have been validated with a CD track or a kaon, both with $p_t > 0.5\,GeV/c$ and within a cone around the calorimeter jet of $\Delta R < 0.4$. This choice of ΔR is also related to the cell size; detector simulation studies have shown that for a jet energy above $10\,GeV$ about 85% of the validated calorimeter jets correspond to one quark fragmentation.

In real events, the CD or the calorimeter jets obtained with the algorithm described above will contain in general a contribution from other jets or from the underlying event. Some of the calorimeter jet energy is lost outside the $\Delta R = 1$ cone. Monte Carlo studies have shown [37], that for jets with transverse energies below $10\,GeV$ the energy dependence on the underlying event is very large and depends on the center of mass energy. For higher jet E_t the energy uncertainty is dominated by energy escaping the $\Delta R = 1$ cone of the jet finding algorithm. The transverse energy resolution ($\sigma(E_t)/E_t$) for jets above $10\,GeV$ is about 25%, approximately independent of jet energy. We have not attempted to correct the jets for the energy escaping the $\Delta R = 1$ cone, or for the underlying event subtraction. Jet energy quoted in this thesis is the uncorrected value from the jet algorithm.

3.5 Muon identification and reconstruction.

The main signature of a muon production is a track in the muon chambers. The muon chambers are the outermost part of the detector. To reach them, a particle has to penetrate the calorimeters and extra iron shielding, adding up to a total of at least 9 interaction lengths. Muons loose only about $2.5\,GeV$ in passing through this material, but non-interacting hadrons are suppressed by $e^{-9} \approx 10^{-4}$.

The muon chambers are covering the range of $10°$ to $170°$ around the beam pipe. For the single muon data some of the muon chamber regions were vetoed for the first level trigger operation. This was done to avoid overflow of the system at high particle luminosities. The muon trigger has good efficiency up to the pseudo rapidity of $|\eta| < 1.5$.

There are two rows of muon chambers, except for the bottom region where, because of lack of space, there is only one row of muon detectors. Otherwise, the distance between the two rows is $60\,cm$. This arrangement of the muon chambers allows to obtain positional and directional information of the particle passage, see fig 3.4.

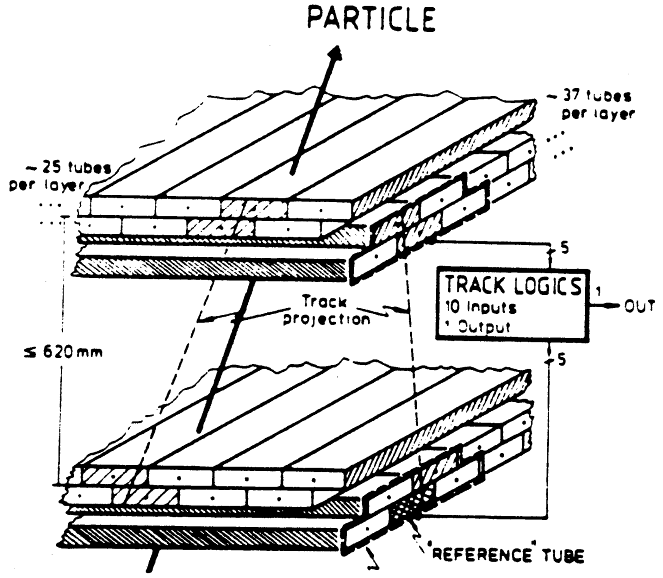

Figure 3.4: *Muon detector arrangement, showing the configuration at the passage of a particle.*

The muon is identified by linking the information recorded from the muon chambers to the rest of the event reconstructed in the CD. All Central Detector tracks are extrapolated through the calorimeters, taking into account the bending in the magnetic field, the energy loss and multiple scattering of a muon candidate. If the track has enough momentum it will traverse the calorimeter and the absorber and will reach the muon chambers, where it is tried to find a matching muon chamber track.

A matching is described by a χ^2 variable, calculated from the differences between the position and the angle of the muon chamber track and the extrapolated CD track. It has four degrees of freedom (NDF) (two positions for the two chambers, angle in the xy-plane and angle out of this plane). A match is accepted, if $\chi^2 < 15$. In this way the background from misassociation is small, compared to the direct decay background.

It should be mentioned, that the matching-χ^2 described above does not correspond to a statistical χ^2 distribution, because there are number of systematical errors entering the calculation. Therefore the cuts like $\chi^2 < 15$ have to be determined experimentally, without any relation to the statistical probability distribution.

The dominant background contribution comes from the $K/\pi^{\pm}$ decays in flight. In the CDvolume pions decay with a probability $0.023/p_t$ and kaons with a probability $0.11/p_t$. These rates of hadron decays are calculated by using a Monte Carlo program and convoluted with the measured inclusive hadron spectrum to obtain the decay muon spectrum.

3.6 Single muon events selection.

The single muon event sample used in the present analysis has been obtained by inclusive selection of events with a muon of $p_t(\mu) > 6\,GeV/c$. Several technical cuts have been applied to ensure a high quality muon sample. In detail, these quality cuts are:

- CD track fit in bending plane, χ^2 should be < 3 per degree of freedom.
- CD track fit out of bending plane, χ^2 should be < 9 per degree of freedom.
- Number of points on CD track should be > 20.
- Length of CD track in bending plane should be $> 40\,cm$.
- Averaged position and angle matching of the CD to muon, χ^2 should be < 15 (NDF=4).
- Kaon decays in the CD were rejected by testing for changing curvature in the tracks ('Kink algorithm') [35].
- Cosmic rays were rejected by testing for interaction point association ('Tkdloo algorithm') [36].
- Fiducial leakage cuts were enforced by testing for cracks in the detector ('Clique algorithm').

After this tight muon selection about 20000 single muon events remain with a muon $p_t(\mu) > 6\,GeV/c$ [10] [38]. The muon rapidity range extends up to $|\eta|$ of 1.5, where the trigger has quite good efficiency. The inclusive total cross section for single muon production can be calculated from

$$\sigma_{tot}(p\bar{p} \rightarrow \mu + X) = \frac{N}{\varepsilon \cdot L} \tag{3.7}$$

where N is the number of events, ε is the muon acceptance and L is the integrated luminosity. Without the acceptance correction the total cross section is $\sigma_{tot} = 36.0 \pm 0.3\,nb$. The acceptance of the muon reconstruction procedure outlined above is estimated to be 0.33 ± 0.02 (statistical error only) [39]. For the low momentum muons the inefficiency of the second level trigger (MUTIME, see section 3.2) is $(90 \pm 5)\%$, therefore the total efficiency for muons with $p_t(\mu) > 6\,GeV/c$ is 0.29 ± 0.03. After acceptance correction the total cross section for single muon production in $p\bar{p}$ collisions is $\sigma_{tot}(p\bar{p} \rightarrow \mu(p_t > 6\,GeV/c) + X) = 124 \pm 13\,nb$. The uncertainty of the given cross section is statistical with the uncertainty in the muon acceptance added up quadratically. The systematic error due to the uncertainty in the luminosity measurement is 15% (see chapter 3.1). It should be emphasized, that the given cross section contains also the large contribution from the muon background sources, mainly the $K/\pi^{\pm}$ decays in flight, that have slipped through the cuts. We have not performed the background subtraction in this work, because the inclusive muon cross section is needed here only for the normalization of the K^0 spectrum (see chapter 6). However, the transverse momentum spectrum of the muons (taken from reference [10]) is shown in fig. 3.5, together with the decay background. The background fraction is up to 70% for the lowest muon momenta, but goes down to 20% for muons above $20\,GeV/c$. The muon spectrum falls steeply for low transverse momenta of the muon and flattens out for transverse momenta above $15\,GeV/c$. The flattening of the momentum spectrum is compatible with muon production in W and Z decays, smeared by the detector resolution. The muons at lower momenta, after background subtraction, are expected to come from heavy flavour decays.

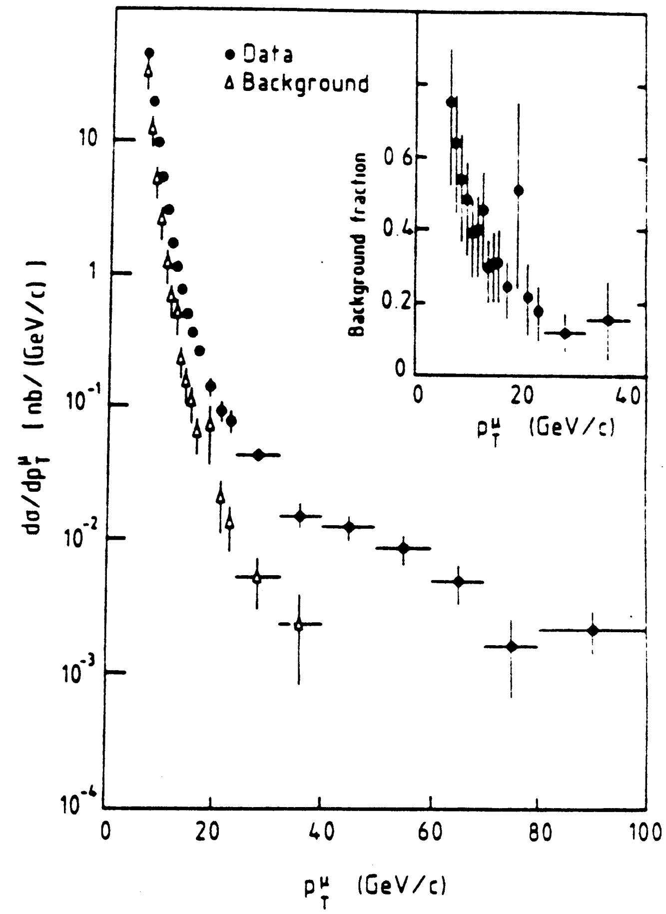

Figure 3.5: *The inclusive muon spectrum and the result of the muon background calculation.*

Chapter 4

V^0 reconstruction in the CD.

4.1 Introduction

We have discussed in chapter 2 that the cascade decays of heavy quarks can lead to neutral kaons in the final state. Charged kaons can be produced as well, but they cannot be distinguished from pions in the UA1 detector. Only charged particles can be directly detected in the UA1 Central Detector (see chapter 3), because only charged particles leave ionization tracks in the gas filling of the multiwire drift chamber. However, neutral kaons and lambdas can be reconstructed in the CD by searching for a typical V^0 pattern of their decay into charged particles which can be subsequently recorded.

As to the K^0, only K^0_S decays into $\pi^+\pi^-$ (branching ratio 68.6% [25]) can be detected. The long living entity K^0_L has a mean flight path of $\gamma \cdot 15\,m$ and therefore will in general decay outside the Central Detector.

The search for a K^0_S in the CD is based on a geometrical property of a V^0 decay: a kaon decaying into a $\pi^+\pi^-$ pair at some distance from the production vertex creates two tracks in the CD, which cross at the decay point and which are not associated to the primary production vertex. In the V^0 search we invert the problem of the decay geometry by looking for crossing tracks of opposite charge, that are required not to originate from the primary vertex. The sum of their momenta must point at the production vertex. The main criterion for a V^0 decay is the invariant mass of the V^0 particle, which should be close to the K^0_S or a $\Lambda/\bar{\Lambda}$ mass.

In the next section we will consider cuts used in the V^0 reconstruction and selection. These cuts have been obtained in the study of the signal to background ratio for a K^0_S mass spectrum. This study is presented in section 4.3. The efficiency of the K^0_S reconstruction for the selected set of cuts will be considered in the next chapter.

4.2 The V^0 finding cuts.

The standard algorithm for the search for V^0 decays in the UA1 CD is described in ref. [11]. The tracks fitted in the CD are input to the 'V0FI processor', which tests all pairs of positive and negative tracks against the V^0 decay kinematics. This is a general algorithm for the V^0 pattern recognition and it is capable of searching for the $K^0_S \rightarrow \pi^+\pi^-$, $\Lambda/\bar{\Lambda} \rightarrow p\pi$ decays and $\gamma \rightarrow e^+e^-$ conversions.

The tracks selected for processing must have more than 20 points in the CD with $\chi_{fit} < 6$ and the accuracy of momentum measurement $\Delta p/p < 0.2$; the individual track momenta are bound to $p > 0.1\,GeV/c$. The logical steps in the V^0 selection algorithm are the following:

- the circles in the xy–plane (perpendicular to the magnetic field) defined by the track segments from the V^0 decay should cross within 3 mm. If successful, this test determines the decay point (in the xy–plane) of the V^0–candidate. One track can cross with more than one other track (ambiguity or track sharing). Many of these additional crossings are rejected by the subsequent cuts. If the ambiguity remains, the best track combination is selected at the end of the V^0 search procedure as the one with the best impact parameter of the resulting V^0, see section 4.3.

- The χ_i^2 parameter of an individual track is defined by its deviation from the primary vertex:

$$\chi_i^2 = \left(\frac{b_i}{\Delta b_i}\right)^2 \tag{4.1}$$

  where b_i is an impact parameter of track i in the xy–plane and Δb_i is its uncertainty at the primary vertex position. The χ_i^2 is required to satisfy $\chi_i^2 > 4$ for both tracks. This cut reduces a large number of tracks coming from the primary interaction point. Since a V^0 decay is expected to occur at some distance from the primary vertex, its decay products should not cross at the primary vertex.

- The impact parameter of the V^0 candidate in the xy–plane satisfies $b(V^0) < 3\,mm$. The V^0 is assumed to come from the primary interaction point with the specified accuracy.

- The decay distance satisfies $d > 0$, so that the two tracks do not cross logically behind the main vertex.

- The track digitizings should start after a track circle intersection in the xy–plane (Causality Condition). The Causality Condition ensures, that the pion tracks from a $K^0 \rightarrow \pi^+\pi^-$ decay start after the K^0 decay point defined by a track circle crossing. We have put a tolerance on this condition of $1\,cm$, which is the distance between two adjacent sense wires in the Central Detector (see chapter 3).

- The tracks are required to cross also in the z–coordinate within 30 cm. This cut is not really restrictive, since the accuracy of the z-coordinate measurement is 4 cm (see chapter 3.3). After this test the sz–fit (described in chapter 3) constrained with the V^0 decay vertex (crossings of the track circles) is repeated for the two tracks. If the track circles cross at two points and no one of the crossings can be rejected by the Causality Condition or positive decay distance requirement, both points are tried in the sz–fit. The crossing ambiguities are resolved by choosing the crossing with the best χ_z^2 of the sz–fit. The sz–fit in V^0 finding is in fact a coplanarity constraint on the V^0 decay. The track parameters are subsequently calculated at the decay point, as opposed to the usual procedure, where the track parameters are calculated at the position of the primary vertex (associated tracks) or at the first measured point (unassociated tracks). This is a very important step, since the direction of the particle momentum vector varies along the particle trajectory due to its curvature.

- The decay plane of the V^0 should not be oriented parallel to the z–direction, since the V^0 reconstruction will suffer from the less precise determination of the current division coordinate. We have established a criterion on the cosine of the dip angle (λ_d) of the vector $\vec{p}_{pos} \times \vec{p}_{neg}$ (normal to the decay plane): $|\lambda_d| > 0.3$, see section 4.4.6.

- Several V^0 masses are tried by assigning π^+/π^-, p/π^-, $\pi^+/\overline{p}$ and e^+/e^- masses to the positive and negative track pairs. The K^0 mass window is within $m(K_S^0) = m_0(K_S^0) \pm$

$20\,MeV/c^2$, the $\Lambda/\bar{\Lambda}$ mass window is within $m(\Lambda/\bar{\Lambda}) = m_0(\Lambda/\bar{\Lambda}) \pm 5\,MeV/c^2$, where $m_0(K^0_S) = 498\,MeV/c^2$ and $m_0(\Lambda/\bar{\Lambda}) = 1116\,MeV/c^2$ [25]. We have rejected events with several hypotheses passing the corresponding mass cuts. Less than 4% of all kaons satisfy the Λ hypotheses simultaneously, see section 4.5.

In the discussion of the V^0 finding algorithm we have indicated our choice for the values of the selection cuts, like $b(V^0) < 3\,mm$ of $\chi^2_i > 4$. These values have been obtained by studying the reconstructed K^0_S mass distribution in real single muon events with relaxed V^0 selection cuts [40]. This study is presented in the next section.

4.3 The analysis procedure.

We calculate the signal to background ratio (S/B) by studying the mass distribution of reconstructed kaons in real single muon events. The mass window in the V^0 finding algorithm has been enlarged up to $m(K^0) \pm 300\ MeV/c^2$. Tracks selected for a V^0 analysis were also allowed to start from secondary vertices, reconstructed from a cluster of ≥ 3 crossing tracks in a space point.

The signal is chosen in the range $m(K^0) \pm 20\,MeV/c^2$ (Signal Band SB). The background is determined from the side bands 340 to $440\,Mev/c^2$ (LSB) and 560 to $660\,MeV/c^2$ (USB). These ranges have been chosen well outside the mass peak, in order not to contain a part of a signal and in order to contain a sufficient linear part of the background. The S/B ratio and the number of signal and background V^0's have been calculated from:

$$\begin{aligned} B &= (number\ of\ V^0\ in\ LSB\ +\ number\ of\ V^0\ in\ USB)/5 \\ S &= number\ of\ V^0\ in\ SB\ -\ B \end{aligned} \tag{4.2}$$

In the first stage, when searching for a K^0, we allow one track to participate in more than one combination with other tracks (ambiguity or track sharing). There are less than 1% ambiguous V^0's in the signal region (SB), however in the background region about 15% of the V^0's share one or both tracks with another V^0. To calculate the signal to background ratio these ambiguities must be resolved. Two methods have been compared to each other: The best track combination has been selected as the one with the best impact parameter, or as the one with the smallest association probability. Triple or higher multiplicity ambiguities are resolved by marking the best track combination; subsequently all combinations are removed, which are ambiguous with the best one. This process is repeated for the remaining V^0's, until no ambiguities are left. The S/B calculation is essentially a counting procedure, therefore the choice of a combination inside the signal or background regions defined above hardly influences the calculated S/B ratio. However, there are about 30% of all ambiguous V^0 candidates, which share a track with a V^0 inside the other mass region. The two methods for the resolution of V^0 ambiguities give similar results within about 10% (or $\simeq 1.5\sigma$) of the calculated S/B ratio. Presumably either of these methods usually selects the correct track combination.

Distributions derived from real data, to be presented in the following section, have been compared to Monte Carlo (M.C.) generated distributions. We have used an ISAJET 5.23 generated $b\bar{b}$ and $c\bar{c}$ sample [41] with full detector simulation, to obtain the shape of the combinatorial background. To obtain an undisturbed mass distribution of kaons in the CD, we have used a M.C. generated single K^0, forced to decay in an otherwise empty detector. This method has the advantage of higher statistics obtainable in an arbitrary momentum range of the kaon.

4.4 Properties of the Signal and the Background bands.

4.4.1 The experimental mass distribution.

The V^0 impact parameter is defined by the shortest distance of the V^0 flight path to the primary vertex in the XY-plane. The χ_i^2 parameter of an individual track is defined by its deviation from the primary vertex, see eq 4.1. The traditional analysis [11] employs a cut on the association probability $P(\chi^2_{ass}) = exp\{-\chi^2_{ass}/2\} < 0.1$ with $\chi^2_{ass} = \chi^2_1 + \chi^2_2$ to reject a large amount of crossing track pairs associated to the primary vertex [11]. This approach tries to optimize the combined association probability. For kaons, however, an improvement in the signal to background ratio can be achieved by a restriction on the individual values of χ_i^2 of the track impact parameter, see table 4.1.

Table 4.1: *S/B ratio for a kaon signal in single muon events for several χ^2 and $b(K^0)$ values. The second number is the corresponding number of kaons after background subtraction (S(K), see eq.2). The V^0 ambiguities have been resolved by taking a combination with the smallest impact parameter. 12020 single muon events from the 1985 data have been processed to obtain the results.*

χ_i^2 / $b(K^0)$	1.5	2.0	2.5	3.0	3.5	4.0	4.5
5mm	1.04 ± 0.03 2452 ± 73	1.25 ± 0.04 2257 ± 66	1.43 ± 0.05 2120 ± 62	1.60 ± 0.06 2033 ± 60	1.74 ± 0.06 1968 ± 58	1.85 ± 0.07 1906 ± 56	1.91 ± 0.07 1821 ± 54
3mm	1.19 ± 0.04 2194 ± 66	1.46 ± 0.05 2036 ± 61	1.69 ± 0.06 1922 ± 57	1.90 ± 0.07 1843 ± 55	2.06 ± 0.08 1775 ± 53	2.22 ± 0.08 1732 ± 52	2.31 ± 0.09 1660 ± 50
2mm	1.28 ± 0.05 1857 ± 60	1.58 ± 0.06 1726 ± 55	1.83 ± 0.07 1620 ± 52	2.08 ± 0.08 1561 ± 50	2.27 ± 0.09 1502 ± 48	2.43 ± 0.10 1459 ± 47	2.56 ± 0.10 1410 ± 46

The S/B values given in table 4.1 should be compared to the values $S/B = 0.38 \pm 0.04$ obtained with $P(\chi^2_{ass}) < 0.1$ and $b(K^0)/\sigma(b) < 1.0$. With $\chi_i^2 > 4$ and $b(K^0) < 3\,mm$ we have $S = 1732 \pm 52$ kaons in the signal band and $B = 780 \pm 13$ in the background side bands. This corresponds to 0.144 ± 0.004 kaons per event, compared to 0.210 ± 0.04 with the previous cuts [42]. The kaon yield dropped by about 35%, but the signal to background ratio is almost 6 times better with the new approach.

An experimental mass distribution corresponding to the cuts $\chi_i^2 > 4.0$ and $b(K^0) < 3\,mm$ is shown in fig. 4.1. The kaon peak at the mass $m(K^0) = 0.497\,GeV/c^2$ is prominent. The background starts at the $\pi^+ + \pi^-$ mass of $0.279\,GeV/c^2$ and falls exponentially, until a slow decreasing background takes over. The side bands given in eq.1 correspond to this slow varying background, which we approximated with a linear function. A flat background distribution is expected from random track combinations, passing the V^0 finding criteria.

Another background source is formed by events with a V^0 like signature , but not representing a kaon coming from the interaction region. These are wrongly assigned Λ or $\bar{\Lambda}$ decays, γ-conversions and secondary interactions in the beam pipe and the CD walls. These background sources do not contribute much in the kaon peak region (Signal Band). From the discussion in section 4.4.3 we estimated this contribution to less than 5% (under the kaon peak).

4.4.2 Random background in the V^0 search.

The largest contribution to the background is provided by a random combination of positive and negative tracks, which pass the V^0 selection cuts. Fig. 4.2 shows a background deduced from M.C. generated $b\bar{b}$ and $c\bar{c}$ events with full detector simulation. This is done by selecting only those of the V^0 candidates, which have prongs not originating from a $K^0_S \to \pi^+\pi^-$ decay.

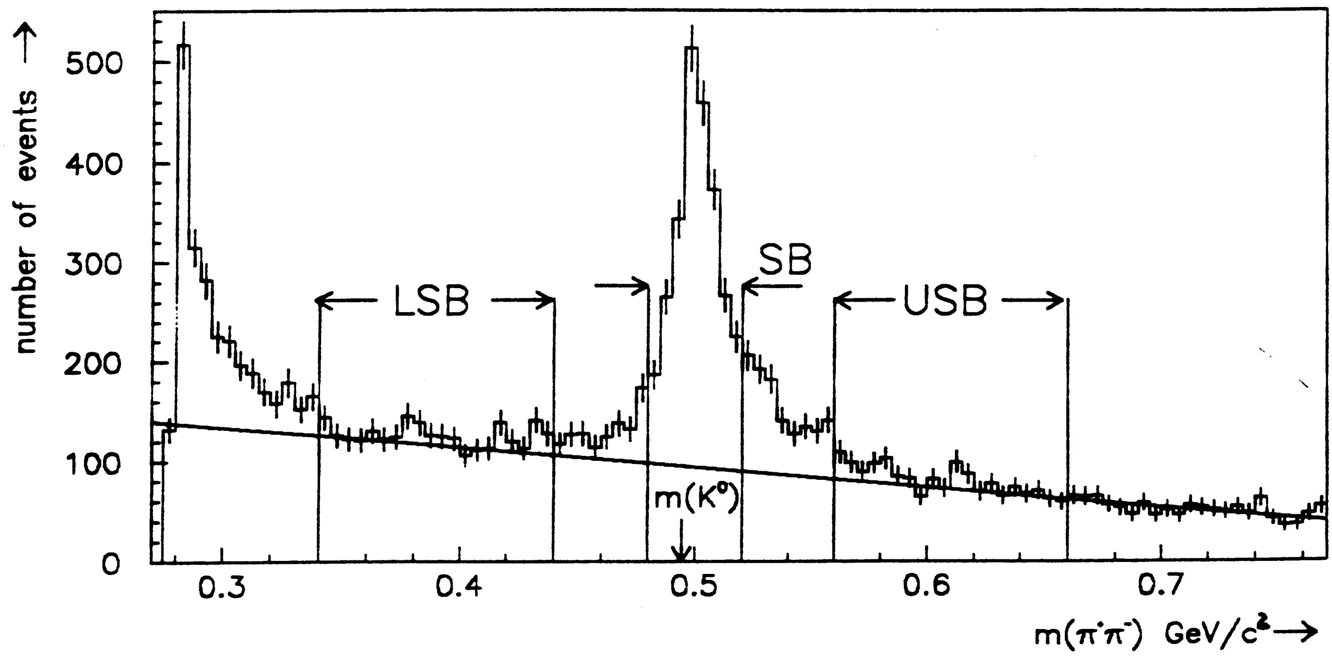

Figure 4.1: *An experimental mass distribution after the cuts* $\chi_i^2 > 4.0$ *and* $b(K^0) < 3\,mm$.

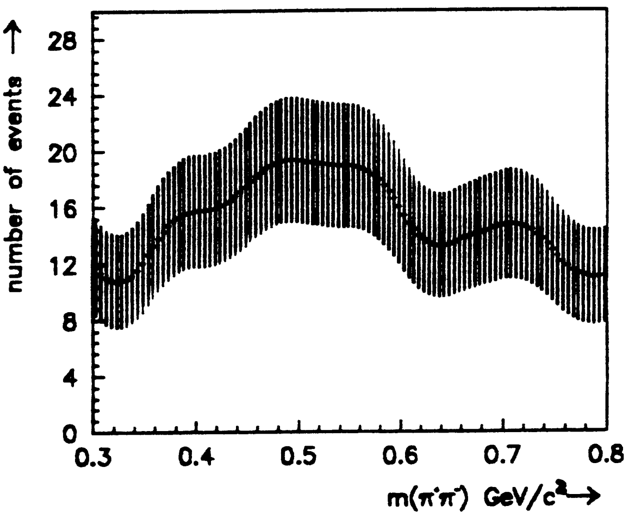

Figure 4.2: V^0 *background form from the* $b\bar{b}$, $c\bar{c}$ *M.C. events.*

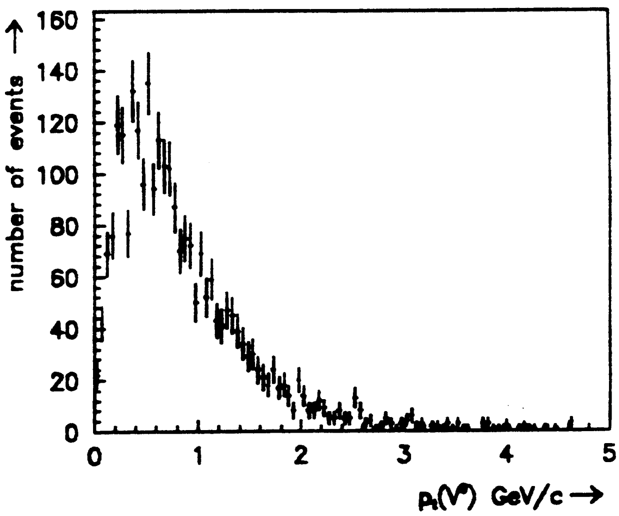

Figure 4.3: *An experimental transverse momentum distribution of* V^0*'s for the mass peak (SB region) shown in fig. 4.1.*

The opening angle between two tracks in a V^0 is important in calculating the random background, because random background grows with increasing opening angle (this can be calculated analytically under the assumption of constant track density). Since a large opening angle corresponds to a lower momentum of a V^0, and thus also to a low transverse momentum, the random background increases at lower transverse momentum values. We consider a transverse momentum, rather than a total momentum, because the transverse momentum is more important for the physics of K^0 production. It can be used, for instance, to separate K^0's in a jet from these from the underlying event.

The kaons with low momentum have rather short lifetime, therefore they decay close to the production vertex. A M.C. study of the K^0_S reconstruction shows a significant drop in efficiency for kaon transverse momenta below $0.2\,GeV/c$ [42]. The reason for this drop might be twofold. First of all the multiple scattering in the beam pipe changes the direction of the slow decay products of low momentum kaons. Therefore the reconstruction of the decay point is uncertain with corresponding uncertainty in the V^0 mass determination. Second, tracks coming from a decay point in the vicinity of the primary vertex are likely to be marked as associated to the primary vertex by the V^0-finding software, i.e. they will not fulfill the $\chi^2_i > 4$ requirement.

An experimental distribution of $p_t(V^0)$ is shown in fig. 4.3. The falling edge below $0.2\,GeV/c$ is steepened by the cut $p_i > 0.1\,GeV/c$ on the individual track momenta of the decay products. The S/B ratio improves with growing $p_t(V^0)$ (see table 4.2). Therefore we tend to cut low p_t V^0's, if they are not required by the physics analysis.

Table 4.2: *S/B ratio and the number of kaons for a signal in single muon events for several $p_t(V^0)$ values. The other cuts are: $b(V) < 3\,mm$ and $\chi^2_i > 4.0$. The V^0 ambiguities have been resolved by taking a combination with the smallest impact parameter. 12020 single muon events from the 1985 data have been processed to obtain the results.*

$p_t(V^0)$	$p_t > 0.2$	$p_t > 0.3$	$p_t > 0.5$	$p_t > 1.0$
S/B	2.55 ± 0.10	2.81 ± 0.11	3.60 ± 0.15	4.01 ± 0.25
S(K)	1757 ± 52	1585 ± 48	1350 ± 42	658 ± 30

4.4.3 Secondary interactions and γ-conversions in the CD walls.

A $K^0 \to \pi^+\pi^-$ hypothesis is used to evaluate all V^0 masses, therefore we assume the two tracks to be pions. A photon converting into a e^+e^- pair would have a mass just above the sum of two pion masses in this calculation. Therefore the left peak at the $\pi^+ + \pi^-$ mass in fig. 4.1 might correspond to γ conversions in the CD chamber walls and the beam pipe material.

In fig. 4.4 we show a distribution of the V^0 decay vertices in the XY-plane of the detector. The points are not distributed randomly: there is a structure visible around +1m and -1m in UA1 x-coordinate. This structure corresponds to the $10\,cm$ thick side walls between the central and forward chambers of the central detector. A correlation of the decay points to other walls and boundaries in the CD is not visible in fig. 4.4.

However, a study of secondary vertices with more than 3 tracks shows, that most of these vertices are lying on the detector boundaries [33]. Their appearance is explained by secondary interactions in the chamber walls and the beam pipe. Since in the present analysis we do not exclude any type of vertices, we have to face a background from these events as well.

An experimental mass spectrum corresponding to V^0's with decay points in the CD chamber walls $(0.91 < |x| < 1.1)$ is shown in fig 4.4. The peak starting at the two pion mass contains only 20% of the leftmost peak below $0.3\,GeV/c^2$ shown in fig. 4.1. However, the general form

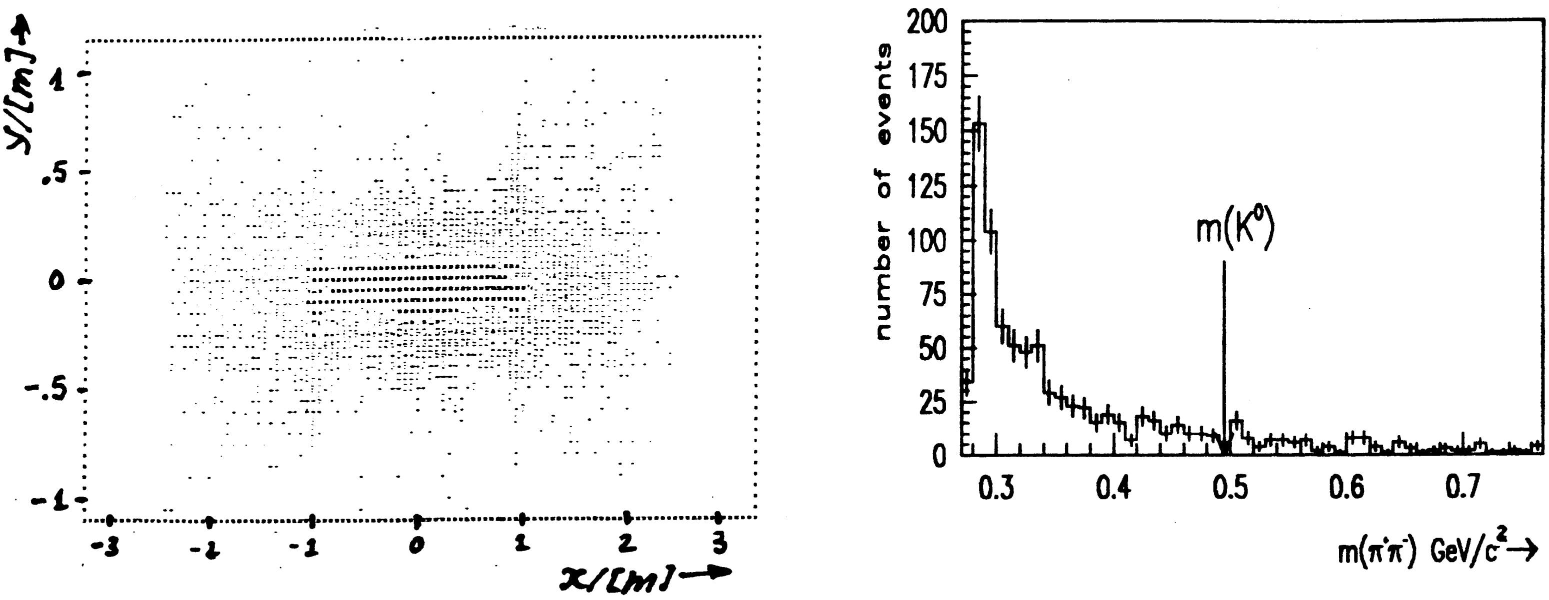

Figure 4.4: *An experimental distribution of* V^0 *decay vertices in the XY-plane (a) and the mass distribution with* V^0 *decay vertices in the CD walls* $0.91 < |x| < 1.1$ *(b).*

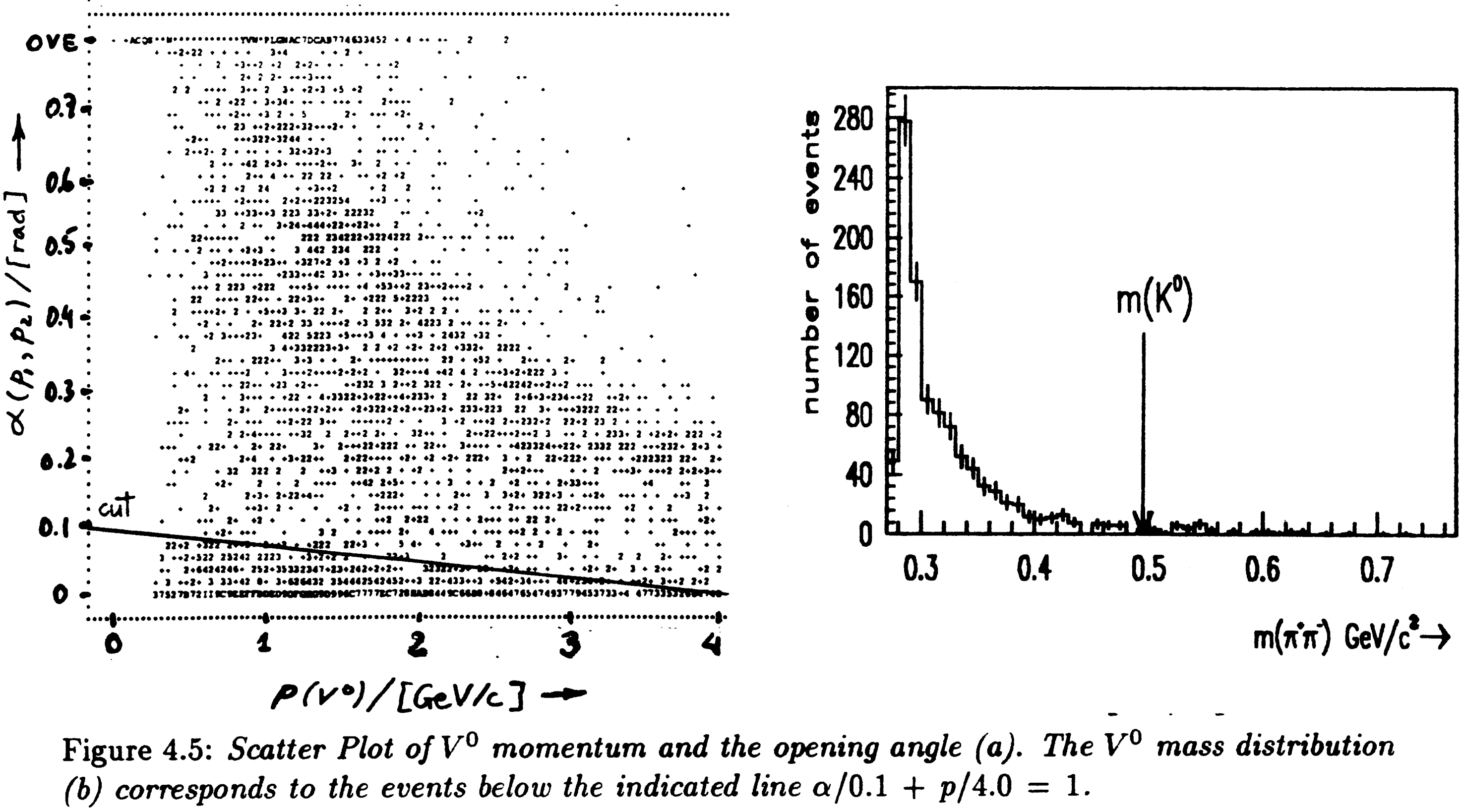

Figure 4.5: *Scatter Plot of* V^0 *momentum and the opening angle (a). The* V^0 *mass distribution (b) corresponds to the events below the indicated line* $\alpha/0.1 + p/4.0 = 1$.

of this background is well reproduced. About 95% of the V^0's entering fig. 4.4 have a very well defined mass with an error less than $40\,MeV/c^2$. There is no peak corresponding to the kaon mass, therefore it is possible to cut on the decays in the chamber walls to reduce this background. A cut on the other detector boundaries is less effective, since it involves the less precise z-coordinate.

There is another possibility to separate secondary processes in the beam pipe and the CD walls. The cross section for radiative energy loss of a charged particle, when traversing a unit of material, is inversely proportional to the momentum of the particle; the opening angle α is also proportional to 1/p (see, e. g. ref [43]). A scatter plot of the V^0 momentum and opening angle between the two tracks is shown in fig. 4.5. An enhancement at small opening angle is apparent in the figure; such an enhancement is absent in M.C. generated data. We have used an 'eye guided' linear cut to separate this enchancement region. A mass plot corresponding to the V^0's with $\alpha/0.1 + p/4.0 < 1$ is also shown in fig. 4.5. The peak contains about 80% of the entries in figure 4.1 below $0.3\,Gev/c^2$.

However, the background from the secondary processes in the CD walls is huge only at the edge of the V^0 mass spectrum and is hardly present under the kaon peak, especially in events with $p_t(V^0) > 0.5\,GeV/c$. Therefore, it is not necessary to cut on the exponential background, if only the kaons from the signal band of $m(K^0) \pm 20\,MeV/c^2$ are used for a physics analysis.

To complete the study, a sample of V^0's from the signal band has to be tested for consistency with the hypothesis of a $K^0 \rightarrow \pi^+\pi^-$ decay. We will consider subsequently the decay probability spectrum, the decay angle distribution, the decay plane orientation and the uncertainties of the mass determination.

4.4.4 Decay Probability of a K^0 for the Signal Band.

The V^0 decay probability P_d can be calculated from the length of the V^0 flight path d and its momentum $p(V^0)$ by

$$P_d = 1 - e^{-\frac{d}{c\tau\beta\gamma}} \qquad \beta\gamma = p(V^0)/m(K^0) \tag{4.3}$$

For a K^0_S $c\tau = 2.675\,cm$ [25]. Equation 4.3 takes into account the time dilatation of an energetic particle, which lives longer in the laboratory system. The relation above is not valid for low momentum V^0's, created in the beam pipe or the CD walls and also not for the random background. The "decay point" of a V^0 from a secondary interaction is reconstructed at a considerable distance from the primary vertex (the beam pipe radius is 8cm and the radius of the CD inner walls is 10cm; other detector boundaries are even at a larger distance). Therefore the calculated lifetime of these V^0's is much longer than the expected one and they have $P_d \approx 1$.

An experimental distribution showing the V^0 decay probability, which should be flat in this representation, is displayed in fig. 4.6. The part of the P_d distribution at $p_d \approx 1$ corresponds to short living 'particles', while small values of the P_d distribution are populated by the particles with a longer life time due to the time dilatation. A decreasing P_d distribution below $P_d \approx 0.4$ is caused by the detector inefficiency for high momentum (long living) particles, since these particles might decay either outside the Central Detector chamber, or so close to the boundary, that no sizable tracks are produced.

If the transverse momentum of the V^0's is not restricted, it is better to cut on the P_d distribution. If the decay probability satisfies $P_d < 0.98$, about 75% of the γ-conversion background is rejected (measured by the number of V^0's with a mass below $0.34\,GeV/c^2$), whereas the number of V^0 in the kaon peak is only 10% less. The background B under the peak, defined by eq. 4.2. is less by about 35%. The signal to background for this cut is summarized in table 4.3. For events with $p_t(V^0) > 0.5\,GeV/c$ this result should be compared to the value of 3.60 ± 0.15. given in table 4.2. A part of the improvement comes from the deformation of the background, since we have used a true kaon mass in eq. 4.3. Therefore, for high momentum V^0's, this cut should not be used to reduce the background.

Table 4.3: *S/B ratio and the number of kaons after the cut $P_d < 0.98$ for several $p_t(V^0)$ values. The other cuts are: $b(V) < 3\,mm$ and $\chi_i^2 > 4.0$. The V^0 ambiguities have been resolved by taking a combination with the smallest impact parameter. 12020 single muon events from the 1985 data have been processed to obtain the results.*

$p_t(V^0)$	$p_t > 0$	$p_t > 0.2$	$p_t > 0.5$
S/B	3.19 ± 0.10	3.33 ± 0.13	3.96 ± 0.17
S(K)	1784 ± 50	1694 ± 48	1344 ± 42

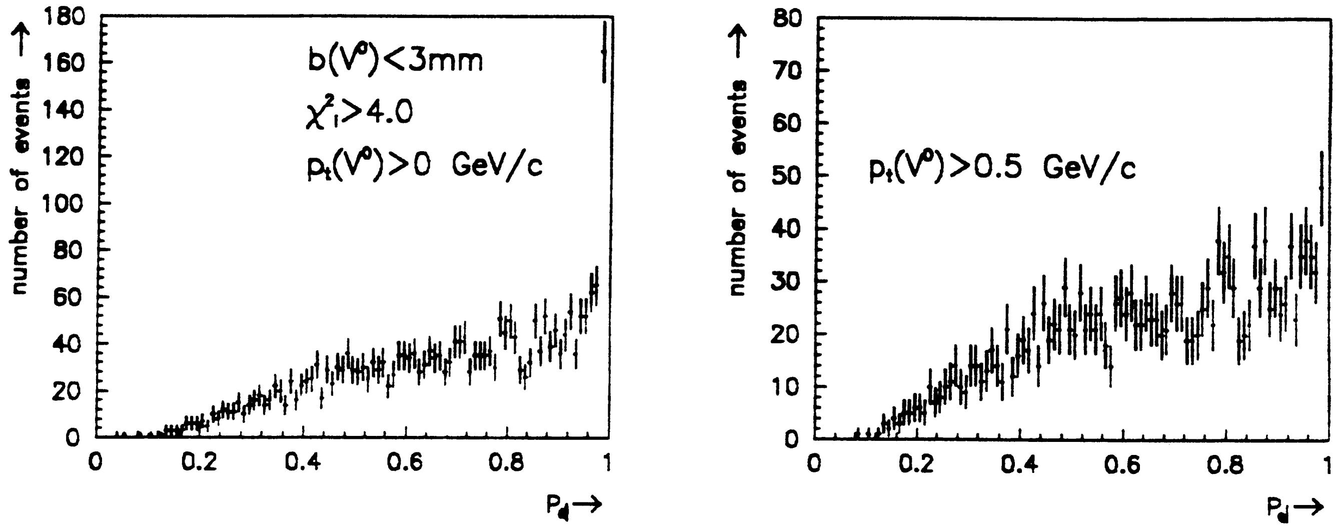

Figure 4.6: *An experimental decay probability distribution for the kaon peak (SB region) shown in fig. 4.1. In the chosen representation this distribution should be flat. The plots are for a) $p_t(V^0) > 0$ and b) $p_t(V^0) > 0.5\,GeV/c$. A spike at $P_d \approx 1$ in the first plot corresponds to the background of V^0's not following the law given by eq. 4.3.*

4.4.5 Decay angle of a K^0 for the Signal Band.

In the center of mass (CM) of a K^0 decay the angle θ^* is defined as an angle between the positive track and the kaon direction of flight in the laboratory. A K_S^0 has spin zero. Therefore it decays isotropically in CM so that the number of decays into the solid angle $d\Omega$ is constant. The number of decays is proportional to $d(cos\theta^*)$ and the $cos\theta^*$ distribution should be flat. An experimental distribution of $cos\theta^*$ for the kaon peak is shown in figure 4.7.

There is an increase in the $cos\theta^*$ spectrum at about ± 0.9. Such an enhancement is typical for a contribution from a wrong assignment of $\Lambda/\bar{\Lambda}$ decay's. We postpone the discussion of decay ambiguities until section 4.5. The results for an additional cut on $cos\theta^*$ are summarized in table 4.4.

4.4.6 Decay plane orientation of a K^0 for the Signal Band.

As the K^0 has spin zero, the orientation of the decay plane around the direction of motion of the K^0 should have a uniform distribution. A fit of the two tracks with a coplanarity constraint,

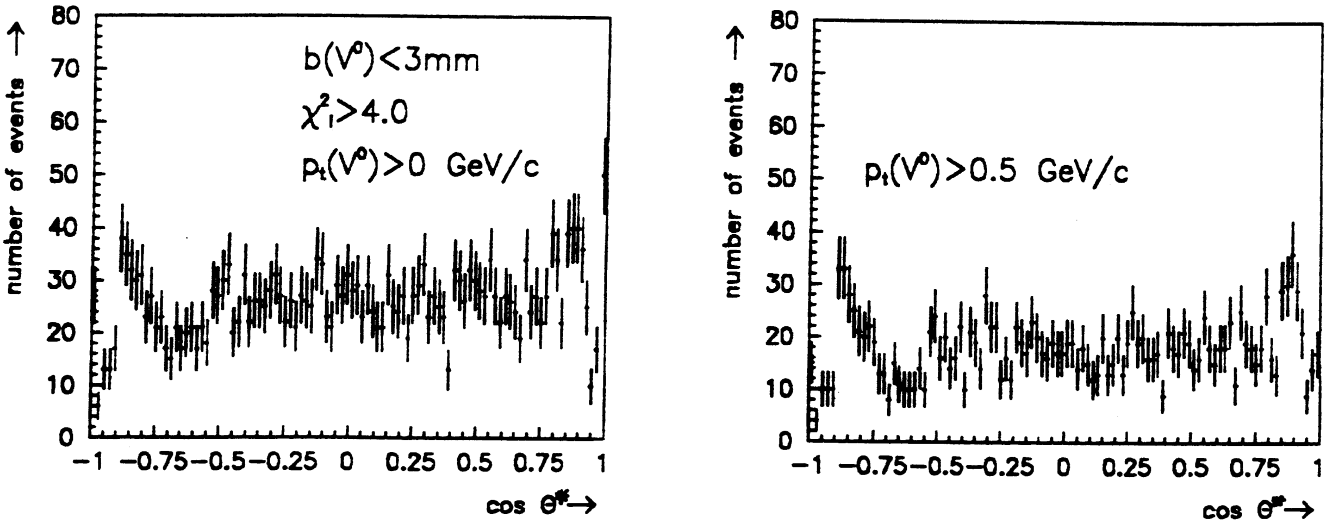

Figure 4.7: *An experimental $cos\theta^*$ distribution for the kaon peak (SB region) shown in fig. 4.1. This distribution must be flat for a $K^0 \rightarrow \pi^+\pi^-$ decay. The plots are for a) $p_t(V^0) > 0$ and b) $p_t(V^0) > 0.5\,GeV/c$.*

Table 4.4: *S/B ratio and the number of kaons for several $cos\theta^*$ values. The other cuts are $b(V) < 3\,mm$ and $\chi_i^2 > 4.0$. The V^0 ambiguities have been resolved by taking a combination with the smallest impact parameter. 12020 single muon events from the 1985 data have been processed to obtain the results.*

	$\|cos\theta^*\| < 1.0$	$\|cos\theta^*\| < 0.9$	$\|cos\theta^*\| < 0.8$	$\|cos\theta^*\| < 0.7$
$p_t > 0\,GeV/c$	2.22 ± 0.10 1732 ± 52	2.85 ± 0.10 1754 ± 50	3.0 ± 0.12 1522 ± 46	3.26 ± 0.14 1358 ± 43
$p_t > 0.2\,GeV/c$	2.55 ± 0.10 1722 ± 50	3.22 ± 0.12 1681 ± 48	3.43 ± 0.14 1452 ± 44	3.74 ± 0.16 1288 ± 41
$p_t > 0.5\,GeV/c$	3.60 ± 0.15 1350 ± 42	4.20 ± 0.18 1317 ± 40	4.60 ± 0.22 1121 ± 38	5.20 ± 0.27 985 ± 35

done by the V^0 finding software, ensures that such a plane exists [11]. The normal to the decay plane is defined by $\vec{n}_d = (\vec{p}_{pos} \times \vec{p}_{neg})/N$, where $\vec{p}_{pos}$ and $\vec{p}_{neg}$ are the momenta of a positive and a negative track respectively, calculated in the K^0 decay point. The normalization factor $N = |\vec{p}_{pos}||\vec{p}_{neg}|$ makes $\vec{n}_d = (n_d^1, n_d^2, n_d^3)$ a unit vector. Figure 4.8 shows a distribution of the angle ϕ between $\vec{n}_d$ and a reference axis perpendicular to the direction of motion of the decaying K^0 and in the plane formed by the K^0 and the z-axis.

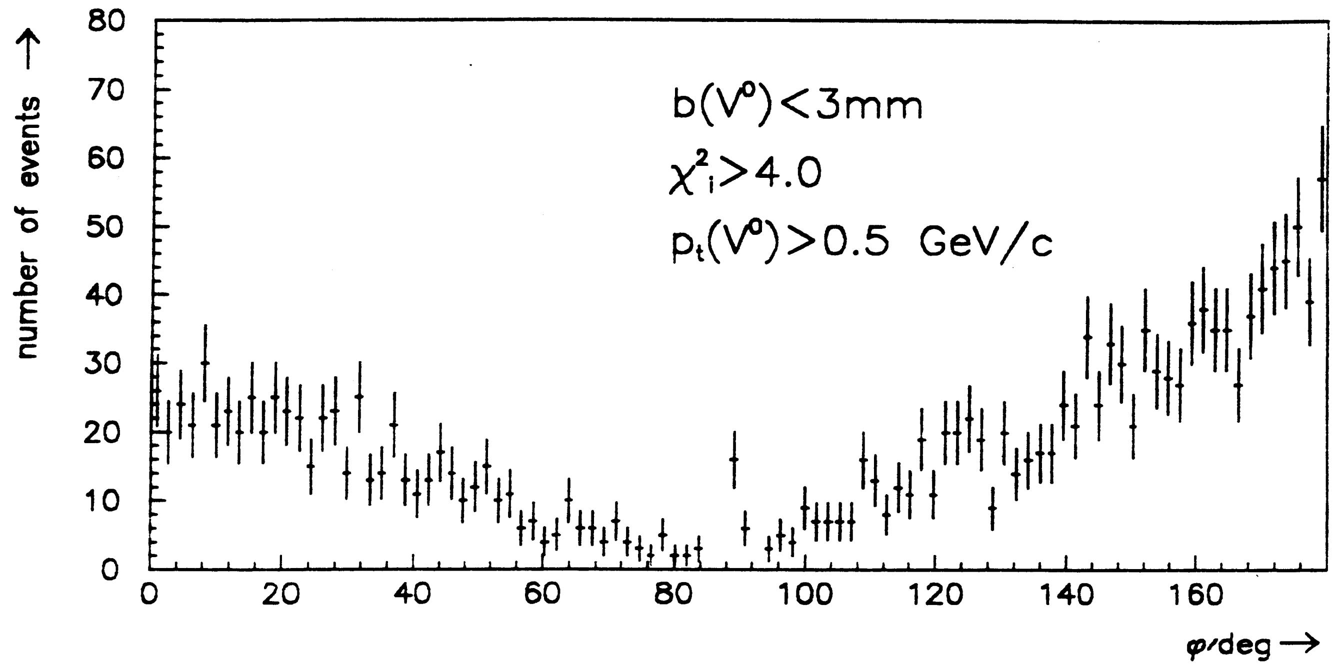

Figure 4.8: *An experimental distribution of the decay plane angle ϕ of V^0's in the Signal Band. The decay plane angle is an angle between the decay plane normal and a reference axis perpendicular to the direction of motion of the K^0.*

The distribution of ϕ is not uniform and is left-right asymmetric (around $\phi = 90°$). For $\phi \approx 90°$ the decay plane contains the z-coordinate. A narrow peak at $\phi = 90°$ is due to V^0's with the track momenta parallel at the decay point, e.g. γ's.

As can be seen in fig. 4.8 the acceptance decreases for the decay plane orientations containing a large contribution from the z-coordinate. This is caused by the less precise determination of the decay point when the tracks are oriented along the magnetic field lines. In addition to the magnetic field effects, there is also an effect of the less precise measurement of the track parameters along the current division coordinate.

A way to study the influence of the inaccurate measurement along the z-coordinate is to plot the V^0 mass as a function of the angle between the decay plane and the z-direction. A decay dip cosine angle λ_d is defined by

$$\lambda_d = n_d^3 \tag{4.4}$$

For small λ_d values the normal to the decay plane is oriented parallel to the magnetic field, whereas for $\lambda_d = \pm 1$ the decay plane coincides with the XY-plane of the central detector. The magnetic field in the UA1 CD points into the positive z-direction (outward SPS).

Fig. 4.9 shows an experimental mass spectrum for the indicated values of the decay plane dip angle. The "γ-peak" at low mass is present below $|\lambda_d| < 0.3$, because we set $\lambda_d = 0$ for a V^0 with a very small opening angle, for which the decay plane normal cannot be defined. The kaon mass peak disappears below $|\lambda_d| < 0.3$. Therefore further reduction of the background is expected from a cut on the orientation of the decay plane at that value. The results are summarized in table 4.5

Table 4.5: *S/B ratio and the number of kaons after the cut* $|\lambda_d| < 0.3$ *for several* $p_t(V^0)$ *values. The other cuts are* $b(V) < 3\,mm$ *and* $\chi_i^2 > 4.0$. *The* V^0 *ambiguities have been resolved by taking a combination with the smallest impact parameter. 12020 single muon events from the 1985 data have been processed to obtain the results.*

$p_t(V^0)$	$p_t > 0$	$p_t > 0.2$	$p_t > 0.5$
S/B	2.75 ± 0.10	3.19 ± 0.12	4.44 ± 0.19
S(K)	1774 ± 51	1708 ± 49	1353 ± 41

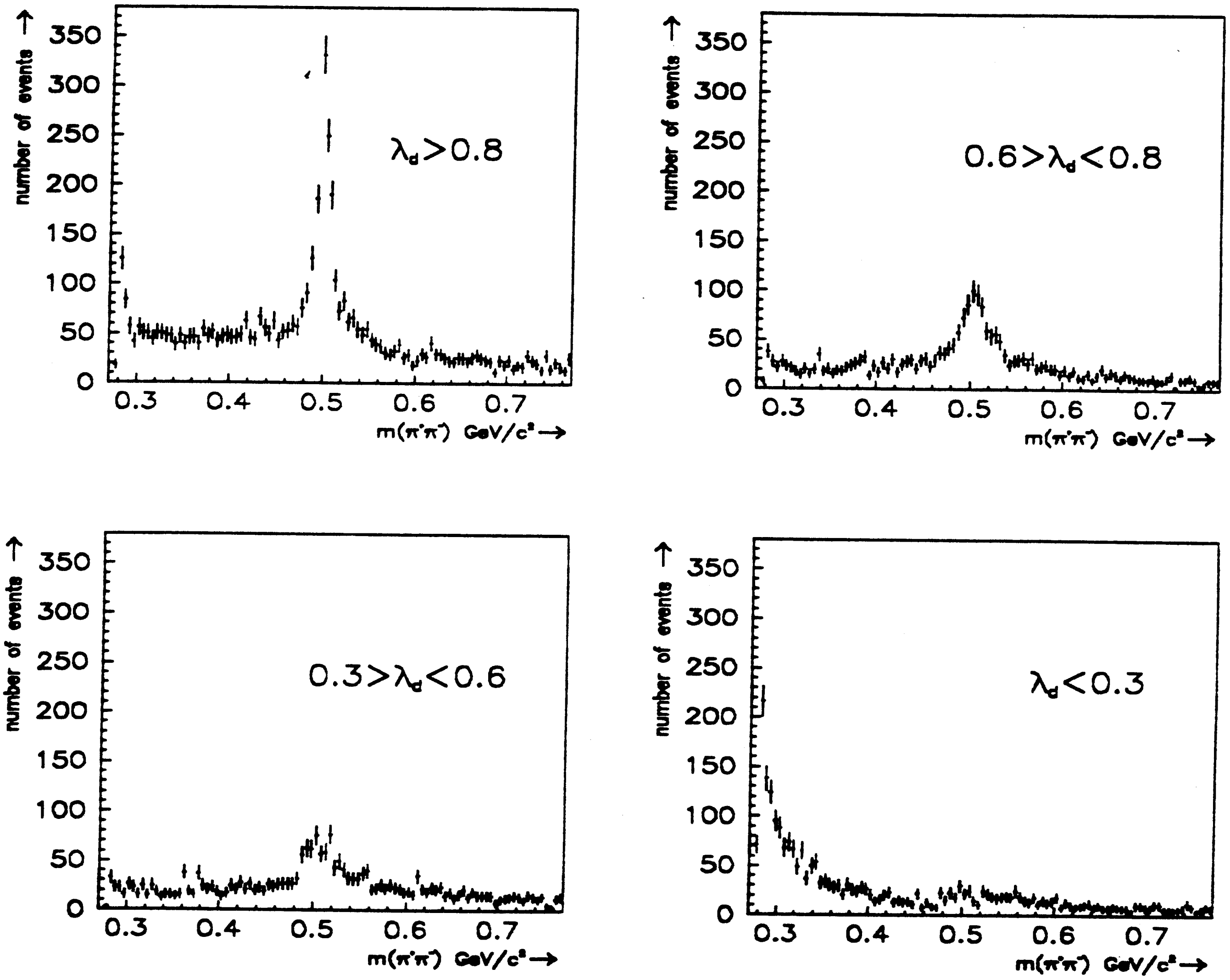

Figure 4.9: *An experimental mass distribution for several decay plane dip angles. The plots are: a)* $|\lambda_d| > 0.8$ *(almost coinciding with the CD XY-plane); b)* $0.6 < |\lambda_d| < 0.8$*; c)* $0.3 < |\lambda_d| < 0.6$*; d)* $|\lambda_d| < 0.3$ *(almost parallel to the z-direction).*

The left-right asymmetry, apparent in figure 4.8 follows from the sign (handness) of the cross product, used to calculate the plane normal. This asymmetry can be explained by noticing, that the V^0 decay point is not unique. The possible K^0 decay points are defined by the track intersections; there are in general two such intersections, with opposite handness of the decay plane normal in these two points. Since a positive track is bend to the right, when looking into the direction of the magnetic field, the first decay point (the closest to the primary vertex) will result in positive handness. If there is a decay point ambiguity, the V^0-finding algorithm takes the most probable decay point at the smallest distance to the primary vertex. Since this point is not necessary the correct one, a left-right asymmetry is created, shown in figure 4.8.

4.4.7 Uncertainties of the mass determination.

The increasing width of the K^0 peak shown in fig. 4.9 emphasizes the inaccuracy of the track parameters measured in the z-direction. However, tracks in the XY-plane can have large errors as well, for instance due to track overlap or insufficient number of digitizings. The best resolution of the K^0_S mass has about $r.m.s. = 5\,MeV/c^2$, which can be determined by looking at the experimental mass distribution (see also [44]).

An experimental mass distribution for several $\sigma(m)$ values is shown in fig. 4.10. The width of the kaon peak estimated at half width half maximum agrees with the calculated mass error. A cut can be defined to accept V^0's with $\sigma(m) < 40\,MeV/c^2$, since the kaon mass is not sharply defined above that limit. The results are summarized in table 4.6.

Table 4.6: *S/B ratio and the number of kaons after the cut $\sigma < 40\,MeV/c^2$ for several $p_t(V^0)$ values. The other cuts are $b(V) < 3\,mm$ and $\chi^2_i > 4.0$. The V^0 ambiguities have been resolved by taking a combination with the smallest impact parameter. 12020 single muon events from the 1985 data have been processed to obtain the results.*

$p_t(V^0)$	$p_t > 0$	$p_t > 0.2$	$p_t > 0.5$
S/B	2.33 ± 0.10	2.69 ± 0.10	3.85 ± 0.16
S(K)	1757 ± 52	1697 ± 50	1351 ± 42

4.4.8 Summary of the study of the mass spectrum.

Table 4.7 summarizes the S/B and the number of V^0's after background subtraction for simultaneous use of several cuts. A minimal sample of the V^0 selection cuts with good kaon resolution corresponds to $b < 3mm$, $\chi^2_i > 4.0$, $p_t > 0.5GeV/c$, $|\lambda_d| > 0.3$ with $S/B = 4.44 \pm 0.19$, which selects about one kaon in ten events.

Table 4.7: *S/B ratio and the number of kaons after background subtraction. From top down, in each row one cut is added to the previous ones. The V^0 ambiguities have been resolved by taking a combination with the smallest impact parameter. 12020 single muon events from the 1985 data have been processed to obtain the results.*

	$p_t > 0\,GeV/c$	$p_t > 0.2\,GeV/c$	$p_t > 0.5\,GeV/c$
$b(V) < 3\,mm$; $\chi^2_i > 4.0$	2.22 ± 0.10 1732 ± 52	2.55 ± 0.10 1757 ± 52	3.60 ± 0.15 1350 ± 42
+			
$\|\lambda_d\| > 0.3$	2.75 ± 0.10 1774 ± 50	3.19 ± 0.12 1708 ± 49	4.44 ± 0.19 1353 ± 41
+			
$\sigma(m) < 40\,MeV/c^2$	2.73 ± 0.10 1797 ± 51	3.27 ± 0.12 1706 ± 48	4.67 ± 0.21 1338 ± 41
+			
$\|cos\theta^*\| < 0.9$	3.17 ± 0.12 1733 ± 49	3.77 ± 0.15 1643 ± 46	5.33 ± 0.25 1267 ± 40
+			
$P_d < 0.98$	3.52 ± 0.13 1727 ± 48	4.24 ± 0.17 1585 ± 45	5.52 ± 0.26 1239 ± 39

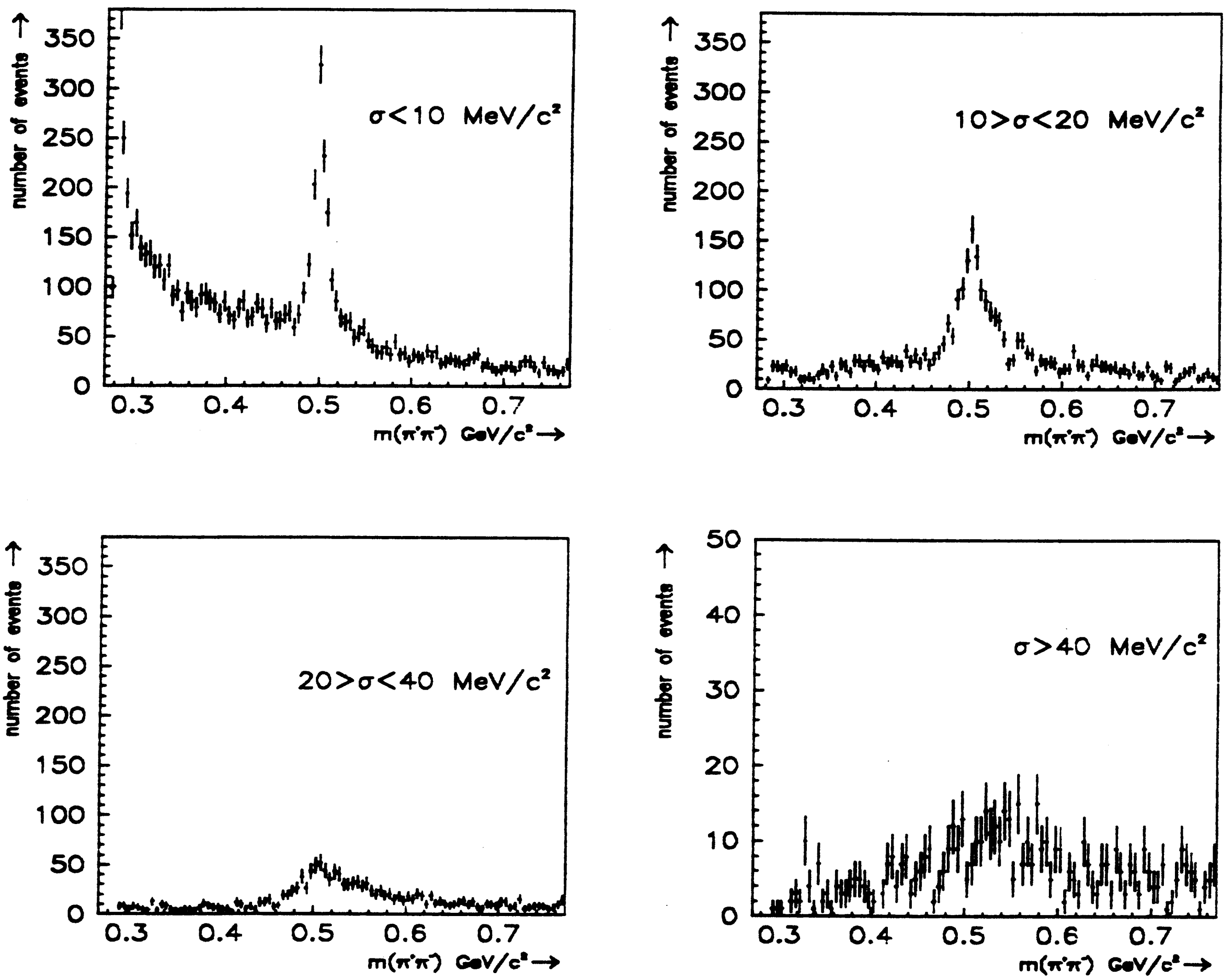

Figure 4.10: *An experimental mass distribution for several values of a mass uncertainty. The plots are: a) $\sigma(m) < 10\,MeV/c^2$; b) $10 < \sigma(m) < 20\,MeV/c^2$; c) $20 < \sigma(m) < 40\,MeV/c^2$; d) $\sigma(m) > 40\,MeV/c^2$.*

4.5 Identification of a V^0 decay.

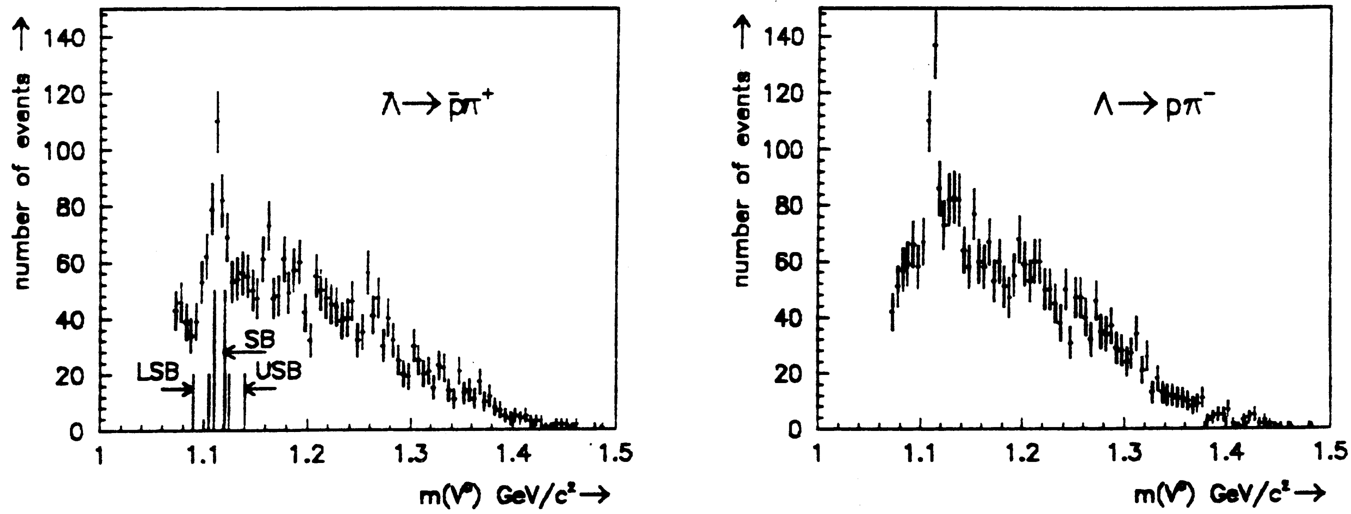

Figure 4.11: *An experimental mass distribution for $\Lambda/\bar{\Lambda}$ decay hypotheses. The V^0 selection cuts are $b(V^0) < 3mm$ and $\chi_i^2 > 4.0$. About 4500 single muon events have been processed.*

A mass spectrum calculated with the hypotheses $\Lambda \to p\pi^-$ or $\bar{\Lambda} \to \bar{p}\pi^+$ is shown in fig. 4.11. Λ and $\bar{\Lambda}$ peaks at $1.1156\,GeV/c^2$ are evident from the picture. Λ's are distinguished from $\bar{\Lambda}$'s by assigning an (anti)proton identity to a track with the highest momentum. For the $\Lambda/\bar{\Lambda}$ hypotheses a signal band has been defined by $m(\Lambda) \pm 5\,MeV/c^2$ and the side bands are 1.09 to $1.105\,GeV/c^2$ (LSB) and 1.125 to $1.14\,GeV/c^2$ (USB). The signal to background ratio for several sets of cuts is summarized in table 4.8. Note, that the fluctuation in the number of $\Lambda/\bar{\Lambda}$'s in table 4.8 is due to a fluctuation in the background, since the assumption of the linearity of the background is not strictly fulfilled.

Table 4.8: *S/B ratio and the number of $\Lambda/\bar{\Lambda}$'s after background subtraction for several cuts. The other cuts are $b(V) < 3\,mm$ and $\chi_i^2 > 4.0$. The V^0 ambiguities have been resolved by taking a combination with the smallest impact parameter. About 4500 single muon events from the 1985 data have been processed to obtain the results.*

$b(V^0) < 3mm$; $\chi_i^2 > 4.0$	Λ	$\bar{\Lambda}$
$p_t > 0\,GeV/c$	0.76 ± 0.14 107 ± 17	0.88 ± 0.17 88 ± 15
$p_t > 0.5\,GeV/c$	1.98 ± 0.22 103 ± 13	1.98 ± 0.36 92 ± 12
$p_t > 0.5\,GeV/c$; $\lvert\lambda_d\rvert > 0.3$	**3.2 ± 0.4 116 ± 13**	**2.47 ± 0.34 84 ± 11**

A question has been raised concerning the use of a high cut $\chi_i^2 > 4.0$ for the selection of $\Lambda/\bar{\Lambda}$ decays, because in a Λ decay the proton carries the main part of the available momentum and the corresponding track is expected to be associated to the main vertex. A calculation shows, however, that for $\chi_i^2 > 1.0$ we have only 50% increase in the number of entries in the Signal Band. Since a large part of the increase is provided by the random background, we expect no improvement in the $\Lambda/\bar{\Lambda}$ signal from a modification of the χ_i^2 cut.

To study the contamination of the kaon mass peak with wrongly assigned $\Lambda/\bar{\Lambda}$ decays, we have to know how often there is an ambiguity in the assignment of a K^0 and a $\Lambda/\bar{\Lambda}$ decay. A $\Lambda \to p\pi^-$ decay produces two tracks in the detector with a momentum imbalance of the order of $\frac{p(proton)}{p(pion)} \simeq \frac{m(p)}{m(\pi)}$. Such a momentum imbalance can in general be reached in a $K_S^0 \to \pi^+\pi^-$

decay at small decay angles, because of the boost the pions are getting from the momentum of the kaon.

A calculation for 4672 single muon events shows, however, that there are 26.6 ± 10.4 V^0's after background subtraction, which satisfy both hypotheses, independent of the transverse momentum of the V^0. Therefore the contamination of the kaon peak with the wrongly assigned $\Lambda/\bar{\Lambda}$'s is less than 4%. Thus the contamination is small for a kaon signal. Note however, that the absolute number of ambiguous identity assignments in the $\Lambda/\bar{\Lambda}$ sample is larger than in the K^0 sample, since in general there are less Λ's in events and the same contamination percentage applies.

4.6 Summary of V^0 reconstruction procedure.

As described in the present chapter the set of V^0 reconstruction cuts discussed in section 4.2 gives a S/B ratio of 4.44 ± 0.19 and selects about one kaon with $p_t > 0.5\,GeV/c$ in seven single muon events. The reconstruction efficiency is calculated in the next chapter.

Chapter 5

The efficiency of K_S^0 reconstruction.

5.1 Introduction.

In chapter 4 we have found a set of V^0 reconstruction cuts which allow K_S^0 detection in the Central Detector with a high signal to background ratio. To use the K_S^0 signal for the cross section measurement we have to estimate the K_S^0 reconstruction efficiency using this set of cuts.

The efficiency of the K_S^0 reconstruction in the UA1 Central Detector has been studied previously by Ciapetti et al. [44] and by Kroll [45]. Both studies were based entirely on Monte Carlo generated events. The efficiency in Monte Carlo generated events can be calculated from $\frac{num.K^0\ found}{num.K^0\ generated}$, since both numbers are known. We emphasize that the above studies used other values for the V^0 reconstruction cuts, different from the values presented in chapter 4.

Ciapetti et al. have generated about 50000 Monte Carlo events with the minimum bias topology and passed them through a complete CD reconstruction [44]. Kroll [45] followed another procedure. In his program a single K_S^0 per event was generated, which decayed in an empty Central Detector. The latter method of the efficiency determination has the advantage of high statistics in an arbitrary momentum range of the kaon. The comparison of the efficiency results from the single kaon program with the efficiency calculated by Ciapetti et al. gives an indication of the track density independence of the K^0 reconstruction. These two results were in agreement with each other within the errors. Apparently, additional tracks in an event do not disturb the reconstruction of a $K^0 \rightarrow \pi^+\pi^-$ decay at least up to the track density of the minimum bias events.

The real single muon data sample, studied in the present analysis has a two to three times higher track density than the minimum bias events, accompanied in addition by high energy jets. The K_S^0 reconstruction problems are more severe in this data sample. A straight forward efficiency estimation method based on the Monte Carlo event generation with subsequent CD reconstruction is too optimistic. For instance Ciapetti et al. obtained a factor 0.89 which was used to correct for the overestimation of the efficiency in the Monte Carlo minimum bias events [44]. The UA5 measurement of the inclusive K^0 cross section at the $p\bar{p}$ Collider [46] has been reproduced with the UA1 minimum bias data [44].

We have developed a novel method of efficiency estimation based on the single K^0 program of Kroll [45]. A decay of a single Monte Carlo K_S^0 into $\pi^+\pi^-$ is generated in the CD and merged subsequently into a real event using a mixing technique. We used real minimum bias events to merge the Monte Carlo K_S^0 for the comparison with the measurements by Ciapetti et al. and dimuon events with $m(\mu,\mu) \geq 6\,GeV/c^2$ to check the effect of a higher track density on the V^0 reconstruction.

We have compared the efficiency calculated with the mixing method to the results of Ciapetti et al. [44] and Kroll [45] in a report to the UA1 Collaboration [42]. We will present this study in the next section. Necessarily, we had to calculate the efficiency for the old set of the V^0 reconstruction cuts for comparison with previous results.

Finally, in section 5.4 the V^0 reconstruction efficiency for the new cuts presented in chapter 4.2 is calculated.

5.2 The merging of Monte Carlo K^0 into real events.

5.2.1 The analysis procedure.

The V^0 reconstruction analysis proceeds in three steps:

- A single K_S^0 is created in the production vertex and subsequently a decay $K_S^0 \rightarrow \pi^+\pi^-$ is generated. Most of the time this decay occurs inside the CD, where the ionization tracks from the two pions are simulated.

- The measured points from these ionization tracks are merged into the CD points of a real event.

- Event reconstruction is done in the usual fashion (see section 3), except that the Monte Carlo tracks from the generated K_S^0 decay were marked and the V^0 reconstruction was done only for these tracks.

To save computer time we merged a single K^0 only if the K^0 has been reconstructed in an empty detector. The efficiency can be easily calculated; the reconstruction problems are close to the problems experienced in real events. We have studied the influence of the track density on the V^0 reconstruction efficiency using this scheme. Also the change of the Monte Carlo track parameters and the shift in the primary vertex position after merging have been analyzed.

We have used the minimum bias real events and a sample of about 300 dimuon events with $m(\mu,\mu) > 6GeV/c^2$ from the 1985 UA1 data. In addition, we have selected some of the dimuon events containing high energy jets and generated a Monte Carlo K^0 decay in the direction of the jet. As far as the V^0 search is concerned, the single muon events have the same properties as the dimuon events, since they have about the same track density and jet multiplicity.

The main draw back of this analysis procedure is the unknown position of the primary interaction vertex in the real event, because the Monte Carlo K_S^0 has to be produced from the primary vertex. We have used the fitted primary vertex position and introduced some smearing with an experimental error distribution. Also multiple scattering of the pions from K_S^0 decay during the passage of the beam pipe has been calculated. This is described in section 5.2.2.

5.2.2 The merging program.

The event reconstruction program has been extended with a feature to merge Monte Carlo K_S^0 with real events. To save computing time only the CD part of an event is reconstructed and the K_S^0 has been forced to decay into $\pi^+\pi^-$ pair. The V^0 finding is performed only on the Monte Carlo generated tracks. The V^0 has been accepted if it has passed all the finding cuts and it's mass was in the window between 0.44 and 0.56 MeV/c^2 (for the old cuts).

The schematic presentation of the modified reconstruction program is given in figure 5.1. A real event is read in first. It is checked, that it contains a correctly reconstructed primary vertex. This vertex is given to the routine GETVTX, that smears its x,y position to obtain the

```
for(#real events)
    read event; {It is checked, that the event contains the necessary vertex information; to generate
              a K^0 in jets, the jet finding is done }
    for(#K^0 per event)
        GRSE; { Monte Carlo K^0 generated in the given p_t, y, φ interval.}
              → GETVTX; { is called from GRSE; it obtains the real event vertex and smears it
                          with the experimental distribution (see text)}
        SERC; { decays the K^0 in the CD. The time slewing correction needed for real events is not
              used for the Monte Carlo digitizings.}
              → MULTSC; { is called from SERC. It calculates the multiple scattering of the decay
                          products in the beam pipe material. }
        status = SINGLE;
    10 continue;
        CALC; { the digitizings are combined in tracks }
        IMRE; { track fitting and V^0 finding. For the track fit with the Monte Carlo digitizings the
              time slewing correction for those digitizings is set to zero. The Monte Carlo digitizings
              are recognized by their special ionization information (see comments to RIME). The
              fitted tracks are considered to be Monte Carlo tracks if the majority of the points are
              coming from a Monte Carlo track (routine TMCODE).}
              → if(status = SINGLE) TKVFIL; { obtains the primary vertex from the real event
                                              and associates the tracks with it. The track errors
                                              are propagated to the vertex position; the vertex
                                              errors are included }
              → if(status = MERGED) VEFI; { vertex finding and fitting processor }
              → V0FI; { the V^0 finding is attempted on the Monte Carlo tracks only }
        CHKV0; { analysis of the V^0 reconstruction and histogram filling }
        if(status = SINGLE) then
              RIME; { mix the Monte Carlo and real event digitizings. Bits 19-28 of the first data
                    word of each digitizing in the database contain the ionization information for
                    the real digitizings; they contain the Monte Carlo track numbers for the Monte
                    Carlo digitizings. }
              status = MERGED;
              goto 10; { repeat the analysis chain for the merged events }
        endif
        DROP; { delete the mixed event, before a new K^0_S will be generated and mixed with the same
              real event}
    end
end
```

Figure 5.1: *Skeleton of the main program for the V^0 reconstruction analysis using the mixing technique. No mixing is performed if the single K^0 has not been reconstructed (output flag of the subroutine CHKV0 is zero). Note, that in the mixed events the V^0 reconstruction is attempted only on the Monte Carlo tracks. A track is a Monte Carlo track by definition, if the majority of digitizings in the track fit are originating from the Monte Carlo.*

Monte Carlo generated K_S^0 production vertex. The smearing is done in the x and y coordinates:

$$\begin{aligned} x_{smeared} &= x_{real} + \sigma_x * G_x \\ y_{smeared} &= y_{real} + \sigma_y * G_y \end{aligned}$$

where $\sigma_y = 0.1\,mm$ and G_x, G_y are the random numbers generated from a Gaussian distribution with $\sigma = 1$. For the x-position, σ_x is selected from the measured distribution of errors in the x-position of the primary vertex in the real events. We have used the primary vertex error distribution from the minimum bias events and from the single muon events. In the minimum bias events the distribution of the difference between the smeared x-position and the real x-position has a r.m.s. value of about 1mm [45]. In the single muon events this distribution has a r.m.s value of about 0.25mm (see fig 3.3 in chapter 3).

The multiple scattering in the beam pipe material changes the track direction in the CD. For a part it has a similar effect on the V^0 reconstruction efficiency as the vertex smearing. We calculated the multiple scattering in the beam pipe from a gaussian distribution with the r.m.s deviation given by [25]

$$\sigma(\theta_0) = 14.1\,MeV/c\frac{E}{p^2}\sqrt{\frac{L}{L_R}}\,[radians]$$

Here p, E are the momentum and energy of the traversing particle; $\frac{L}{L_R}$ is the thickness of the traversed material in radiation lengths. For pion tracks with $p = 0.5GeV/c$ traversing a corrugated beam pipe with relative radiation length 0.025 the r.m.s. of angle distribution is $\sigma(\theta_0) \approx 5mrad$. For a beam pipe radius of $6\,cm$ and the CD inner walls, total distance $10\,cm$, multiple scattering gives an uncertainty in the vertex position of about $0.5\,mm$.

The tracks are reconstructed in the routine IMRE. In real events the primary interaction point is reconstructed from the clusters of tracks gathering at the position of the beam. However, when we calculate a single K_S^0 reconstruction efficiency, there is no possibility to fit the primary vertex. Therefore we copy the vertex parameters of a real event to stand for the new vertex. The Monte Carlo generated K_S^0 production vertex is smeared around this position.

The mixing of the digitizings is done by the routine RIME. A new primary vertex position has been determined and fitted using all tracks, including the new Monte Carlo tracks.

We have also calculated the K_S^0 reconstruction efficiency, when the Monte Carlo K_S^0 is generated in the direction of a jet. A jet search is done immediately after a new dimuon event has been read in. A CD jet has been required with track multiplicity ≥ 4 and $p_t(jet) > 6\,GeV/c$. If there are several jets in the event, the jet with highest p_t is used. Next, a Monte Carlo K_S^0 is generated in a small cone $\Delta y = \pm 0.1$, $\Delta\phi = \pm 5°$ around the direction of the jet-axis in the momentum range given by the input parameters. We proceed then with the event reconstruction as described before.

5.2.3 Deviation of the vertex and the track parameters after mixing.

The mixing of the Monte Carlo CD digitizings from the $K^0 \to \pi^+\pi^-$ decay with the digitizings from a real event influences the track reconstruction properties. We have studied the resulting shift in momentum of the Monte Carlo tracks and the shift in the number of points used in the track fit after the mixing. The results are summarized in table 5.1. After the merging of the Monte Carlo generated digitizings in a real minimum bias or dimuon event the Monte Carlo tracks contain about 20 CD points less than before the mixing. The distribution of $\delta p = p^{new} - p^{old}$ has a sharp peak at zero for all the tracks with a correctly reconstructed momentum. There is a long tail of values that deviate strongly after mixing. The shift in the track momentum is correlated to the fit error on the momentum. Large deviations can be

Table 5.1: *Deviation of the Monte Carlo track parameters after the reconstruction in merged events from the values obtained in the reconstruction of single K^0 events. The figures give the fraction of events with the deviation smaller then the indicated limits. Tracks are the $\pi^+\pi^-$ pairs from the Monte Carlo K^0 decay with $1 < p_t(K^0) < 3GeV/c$, $-2.5 < y(K^0) < 2.5$ and $0 < \phi(K^0) < 2\pi$ or $\Delta y = \pm 0.1$, $\Delta\phi = \pm 5°$ around the Jet direction. About 4000 tracks have been mixed, the errors are statistical.*

deviation in track parameter	deviation limits	percentage of events within the deviation limits minimum bias (%)	dimuon (%)	dimuon Jet (%)
δp	$\pm 50\,MeV$	90 ± 2	86 ± 2	77 ± 2
δp_t	$\pm 50\,MeV$	90 ± 2	84 ± 2	76 ± 2
$\delta\chi^2_{fit}$	± 1.0	87 ± 2	82 ± 2	68 ± 2
(track fit)	± 2.0	96 ± 2	95 ± 2	90 ± 3
δl	$\pm 6\,cm$	76 ± 2	64 ± 2	37 ± 1
(track length)	$-30 < \delta l < +6cm$	89 ± 2	82 ± 2	62 ± 2
$\delta\,(num.\ of\ points)$	< 10	55 ± 1	37 ± 1	13 ± 1
	< 20	71 ± 1	57 ± 2	29 ± 1
	< 30	81 ± 2	70 ± 2	44 ± 2
$\delta\,(non\ m.c.\ points)$	0	36 ± 1	31 ± 1	21 ± 1
	< 5	71 ± 2	69 ± 2	63 ± 2
	< 10	86 ± 2	87 ± 2	86 ± 2

reduced by taking the cut $\frac{\delta p^{new}}{p^{new}} < 20\%$, see fig 5.2. In jets the number of points used for the track fit is reduced considerably after merging in a jet.

The efficiency of a single K^0 reconstruction is independent of the primary vertex smearing distribution. The efficiency in the whole range of $0.2 < p_t(K^0) < 5.0GeV/c$ has been calculated using a) no primary vertex smearing; b) smearing with the error distribution of the minimum bias and c) smearing with the error distribution of the single muon events. At the statistical level of 2% no differences in a single K^0 reconstruction efficiency have been found between these smearing methods. Note, that for the Monte Carlo production of a single K^0 we use position and errors of the primary vertex from a real event. In addition a variation caused by the multiple scattering in the beam pipe is more important than the primary vertex smearing and the resulting shift in the primary vertex position after the reconstruction in the mixed events is larger than the smearing of the K^0 production vertex. Nevertheless, we have always smeared for convenience the Monte Carlo production vertex in our program.

We have studied the shift in the vertex x-position ($\delta x = x_{new} - x_{old}$) after the inserted Monte Carlo tracks are allowed to participate in the primary vertex fitting. In the minimum bias events the shift δx distribution has zero mean and r.m.s = $1.2\,mm$. About $13 \pm 1\%$ events have been found outside the $3\,mm$ range. The vertex shift distribution in the dimuon events has zero mean and $r.m.s = 0.7\,mm$. About $97 \pm 3\%$ of the dimuon events are within the limits $|\,\delta x\,| < 1mm$.

Due to the variation of the primary vertex position the V^0 reconstruction efficiency decreases by $9.8 \pm 2.5\%$ in the minimum bias events and only by $3.4 \pm 2.8\%$ in the dimuon events. On the other hand the efficiency in the dimuon mixed events can be affected by the secondary vertex search. In the secondary vertex search we look for a cluster of ≥ 3 tracks originating from approximately the same space point. Strictly speaking, the secondary vertices of this type do not have the V^0 pattern and should be excluded from the V^0 analysis. On the average the V^0 decay products have tracks not associated to the primary vertex. Therefore one additional track in the neighborhood of the K^0 can easily simulate the pattern of the secondary vertices.

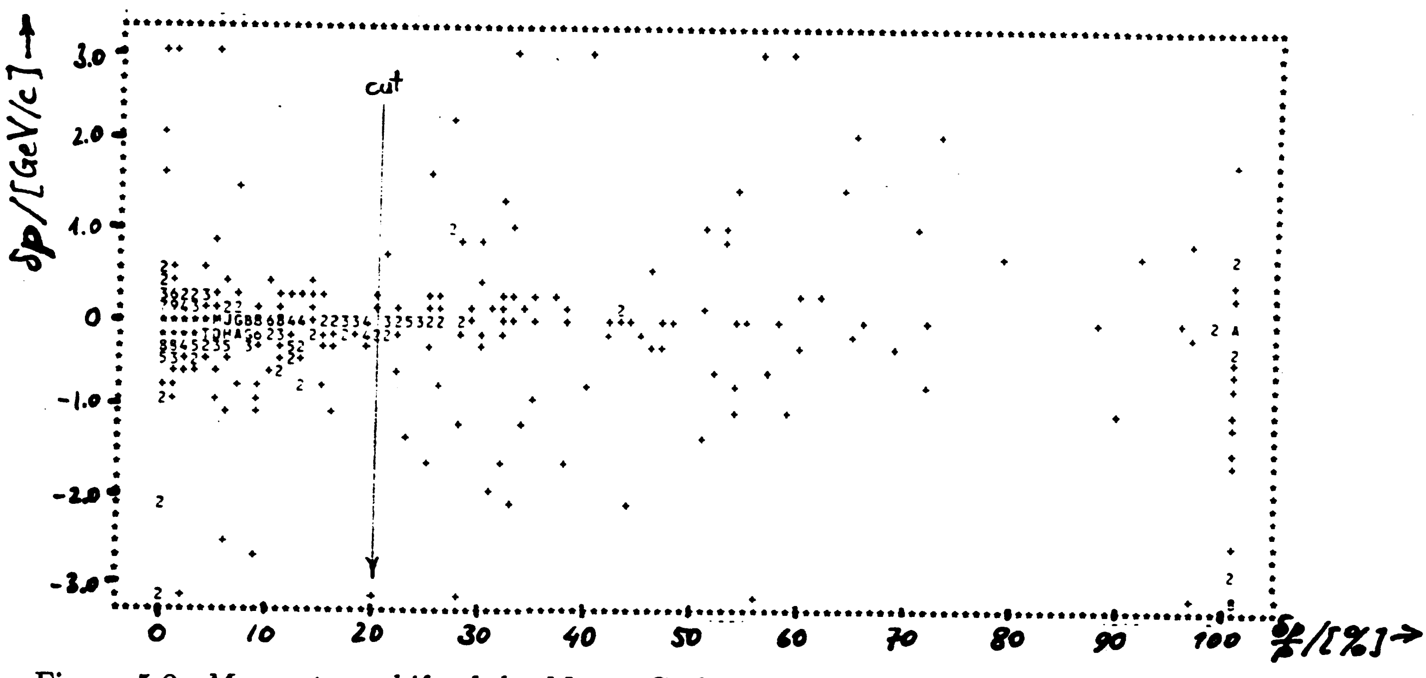

Figure 5.2: *Momentum shift of the Monte Carlo tracks after mixing with dimuon events (ordinate[GeV/c]) as function of the relative error on the momentum of the tracks $\delta p/p$ [%].*

The kaon decay in the minimum bias events is misinterpreted as a secondary vertex in 4% of the cases and in up to 10% of the dimuon events due to the higher track density. Therefore tracks coming from secondary vertices of the discussed type are allowed to participate in the V^0 reconstruction.

5.3 The V^0 reconstruction analysis for the old cuts.

5.3.1 The V^0 reconstruction for the single K^0 Monte Carlo events

To understand the V^0 reconstruction in the mixed events, it is helpful to consider the losses in the single K^0 Monte Carlo, before mixing with a real event. The causes of the losses of the K^0_S are different for the lower and higher momentum kaons.

The largest decrease of the V^0 reconstruction efficiency for the low momentum kaons is caused by the track reconstruction difficulties in the CD. The probability to find both tracks from the decay of a $0.2\,GeV/c$ kaon is only 75%, as compared to almost 90% for the higher momentum tracks. The track reconstruction acceptance in the CD is shown in table 5.2. The

Table 5.2: *Track acceptance in the UA1 CD as function of K^0 transverse momentum for the single K^0 Monte Carlo events in [%]. The acceptance has been averaged over $-2.5 < y(K^0) < 2.5$, $0 < \phi < 2\pi$; the errors are statistical.*

$p_t(K^0)$ range [GeV/c]:	$0.2 \div 0.3$	$0.3 \div 0.5$	$0.5 \div 1.0$	$1.0 \div 3.0$	$3.0 \div 5.0$
num. of K^0 decayed in CD	1816	1708	1408	1474	1373
Probability 0 track reconstr.				1.4 ± 3.0	3.7 ± 0.5
Probability 1 track reconstr.	15.0 ± 1.0	13.6 ± 0.9	13.0 ± 1.0	8.2 ± 0.8	7.4 ± 0.8
Probability 2 track reconstr.	75.0 ± 3.0	78.0 ± 3.0	83.0 ± 3.0	89.0 ± 3.0	88.0 ± 3.0
Probability 3 track reconstr.	7.3 ± 0.6	6.7 ± 0.6	3.6 ± 0.5	1.6 ± 3.0	

track reconstruction algorithm can easily split the low momentum tracks into several parts, since they curl over several CD chambers and suffer from multiple scattering in the chamber walls. More over, if these track segments cross the xz-plane in CD, they are assigned a wrong charge, see fig.5.3.

An improvement of the V^0 reconstruction efficiency is expected at higher K^0_S momentum, since the multiple scattering in the beam pipe is lower. The multiple scattering of pions of $1\,GeV/c$ is about half of that of pions of $0.5\,GeV/c$. Moreover, at $p_t(K^0) = 1\,GeV/c$ about 16% of the kaons are likely to decay after the passage through the beam pipe and avoid multiple scattering all together. However the kaons with higher momentum are lost owing to a less precise determination of the track parameters. The K^0 decay point is difficult to determine for small curvature tracks, an example of which is shown in fig. 5.4. This leads to the losses by the cuts for the decay distance and for the Causality Condition (see section 4.2). It should be noted, that an uncertainty in the K^0 decay point causes an uncertainty in the K^0 mass measurement, since the track parameters must be calculated at the decay point for the K^0 mass determination. This problem is more severe for low momentum, curved tracks, although the decay point can be determined more reliably for the low momentum tracks. The uncertainty of the track momentum leads also to the broadening of the mass spectrum; the mass peak width calculation is summarized in table 5.3.

Table 5.3: *The (estimated) r.m.s. width of the Monte Carlo* $K^0 \rightarrow \pi^+\pi^-$ *mass spectrum as function of* $p_t(K^0)$ *in single* K^0 *events. The events have been generated in the range* $-2.5 < y(K^0) < 2.5$ *and* $0 < \phi(K^0) < 2\pi$.

$p_t(K^0)$ range [GeV/c]:	$0.2 \div 0.3$	$0.3 \div 0.5$	$0.5 \div 1.0$	$1.0 \div 3.0$	$3.0 \div 5.0$
width of the mass peak $[MeV/c^2]$	9 ± 3	10 ± 3	12 ± 3	20 ± 3	30 ± 3

Finally, some reduction in the V^0 reconstruction efficiency at the higher momentum part of the spectrum is caused by kaons with a large flight path $\beta\gamma c\tau$, because they are likely to decay outside the CD.

In summary, the losses of the Monte Carlo generated K^0_S decays by the reconstruction cuts sum up to 50-60%. These losses cannot be attributed to a single cut, but they are accumulated from all the cuts used in the V^0 reconstruction in about equal amounts [42]. The resulting K^0_S reconstruction efficiencies will be shown in fig. 5.5, together with the results from the K^0_S reconstruction in mixed events.

5.3.2 The V^0 reconstruction in mixed events.

The efficiency for K^0 reconstruction in mixed or merged events is lower than the efficiency in single K^0 events. There are additional difficulties of the primary vertex reconstruction and track fitting after merging. The difficulties of the track reconstruction increase somewhat by going from minimum bias to the more complicated jet events. The probability to find both tracks from the $K^0_S \rightarrow \pi^+\pi^-$ decay in the CD after mixing (A_2^m) has been calculated relative to the acceptance before mixing (A_2^s) (see table 5.2) in the three types of events for the $p_t(K^0_S)$ range 1 to 3 GeV/c:

$$\frac{A_2^m}{A_2^s}(1 < p_t(K^0) < 3GeV/c) = \begin{cases} 0.96 \pm 0.02 & \text{mixing in minimum bias events} \\ 0.94 \pm 0.02 & \text{mixing in dimuon events} \\ 0.93 \pm 0.02 & \text{mixing in dimuon jet events} \end{cases}$$

Similar acceptance ratios for merged/single K^0 hold for the other K^0 momentum ranges. Thus the acceptance of the tracks results in some extra losses in mixed events. The deterioration of

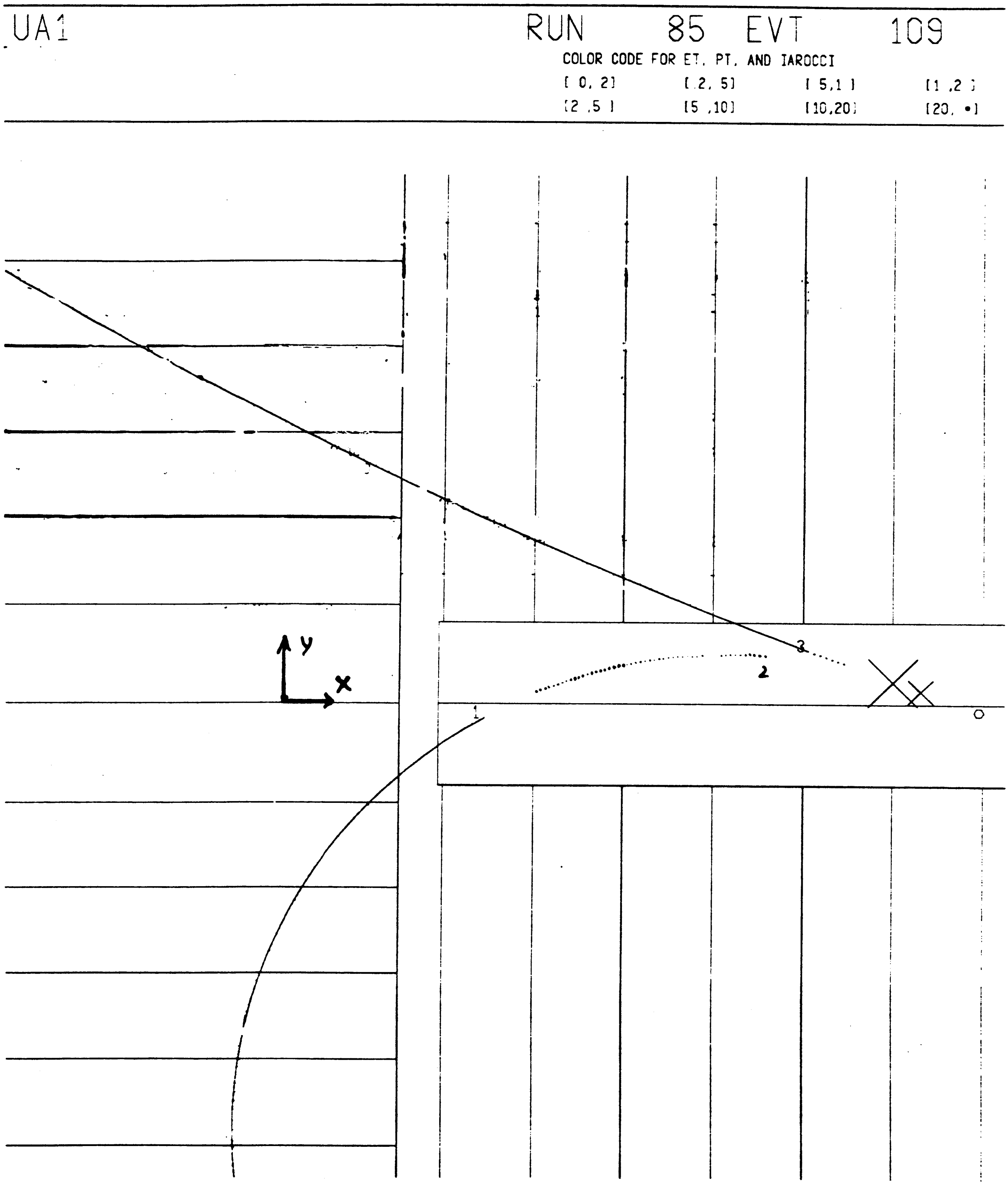

Figure 5.3: *Track splitting in CD. The Monte Carlo K^0 decay vertex is shown by a small cross, the calculated decay vertex by a large cross. Tracks 1 and 2 come from the same pion, but have been split and given opposite charges, because the start of a track is defined by the closest approach to the horizontal plane Y=0.*

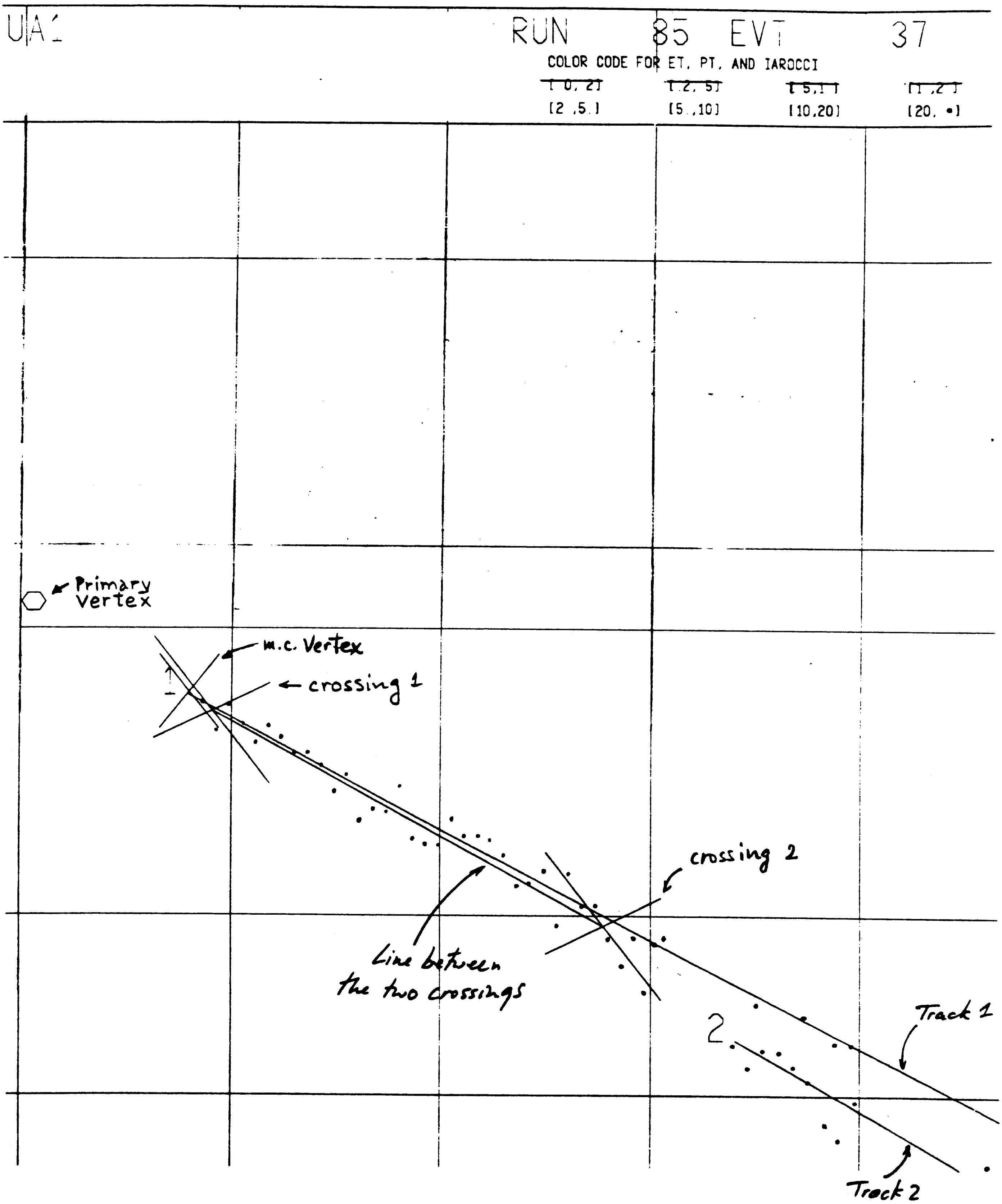

Figure 5.4: ***Track crossing uncertainty in the CD. The detector has been rotated out of the XY-plane to show separately the position of the second crossing in projection. Note, that the crossings are calculated only in the XY-plane (their z coordinate is zero). The track digitizings have a large spread in this picture, because the less accurate current division coordinate is visible after the rotation. The Monte Carlo decay vertex is shown by the small cross, the calculated decay vertices by large crosses. The digitizings start before crossing 1, therefore this K^0_S fails the cuts for the Causality Condition.***

the track quality after mixing is a larger effect, resulting in 10 to 30% lower V^0 reconstruction efficiency after mixing.

This has been studied with the Monte Carlo correction factor C_{mc}:

$$C_{mc} = \frac{E_{ff}\ mixed}{E_{ff}\ single\ K^0\ Monte\ Carlo} = \frac{E^m_{ff}}{E^s_{ff}} \tag{5.1}$$

$$\Delta C_{mc} = C_{mc} \cdot \sqrt{\frac{var(E^s_{ff})}{(E^s_{ff})^2} + \frac{var(E^m_{ff})}{(E^m_{ff})^2} - \frac{2 \cdot cov(E^s_{ff}, E^m_{ff})}{E^s_{ff} \cdot E^m_{ff}}} \tag{5.2}$$

$$cov(E^s_{ff}, E^m_{ff}) = \sqrt{var(E^s_{ff})}\sqrt{var(E^m_{ff})} \cdot r \quad \text{with } r \approx 0.8 \tag{5.3}$$

The Monte Carlo correction factor is approximately constant for $0.3GeV/c < p_t(K^0) < 5.0GeV/c$ in the minimum bias and dimuon events and has about the same value (see table 5.4). The formulae for the uncertainty of the correction factor take into account the correlation between the 'single' and 'merged' efficiencies, because we compare the same Monte Carlo $K^0_S \to \pi^+\pi^-$ event reconstruction before and after merging. The correlation coefficient $r \approx 0.8$, because after mixing the efficiency drops by about 10–30%. The E^s_{ff}, E^m_{ff} correlation reduces the independent statistical error by about 40%.

Table 5.4: *The Monte Carlo efficiency correction factor as a function of kaon transverse momentum. The errors are statistical with the correlation of 80% taken into account.*

$p_t(K^0)$ range [GeV/c]:	$0.2 \div 0.3$	$0.3 \div 0.5$	$0.5 \div 1.0$	$1.0 \div 3.0$	$3.0 \div 5.0$
minimum bias events	0.81 ± 0.02	0.80 ± 0.02	0.75 ± 0.02	0.75 ± 0.02	0.73 ± 0.02
dimuon events	0.82 ± 0.02	0.75 ± 0.02	0.74 ± 0.02	0.74 ± 0.02	0.70 ± 0.02
dimuon events, K^0 in Jet	0.76 ± 0.04	0.72 ± 0.03	0.70 ± 0.02	0.63 ± 0.02	0.56 ± 0.02

The calculation of the Monte Carlo correction factor is summarized in table 5.4. This way of presentation shows, that there is some dependence of the Monte Carlo correction factor on the event topology. This is especially true for the higher K^0 momenta. The Monte Carlo correction factor for the reconstruction of kaons in jets is more important for increasing transverse momentum of the kaon.

Although the K^0 reconstruction suffers more in jets, the reconstructed jets themselves are oriented in a more favourable direction. Therefore the K^0 reconstruction efficiency with a kaon in a jet has about the same value, within 2%, as the efficiency in minimum bias or in dimuon events with a kaon outside a jet, see fig. 5.5. Consequently, after merging of single K^0 into a real event, the K^0 reconstruction efficiency does not depend on the topology of the event within 2% accuracy. The losses of the V^0 finding cuts balance each other such, that at the end of the K^0 reconstruction chain we get the same efficiency for all types of events. The efficiency is, of course smaller in mixed events than in the single K^0 Monte Carlo.

We conclude, that the Monte Carlo results for the single K^0 reconstruction efficiency can be used to calculate the cross sections. The single K^0 Monte Carlo efficiency has to be multiplied by a factor of about 0.75 to correct for the systematic overestimation. If the K^0 appears in a CD jet and $p_t(K^0) > 1Gev/c$, the single K^0 efficiency has to be multiplied by a factor of about 0.60.

5.3.3 Comparison of the V^0 reconstruction efficiency with previous results.

We have plotted the single K^0 reconstruction efficiency and our mixing results (minimum bias, dimuon and jet dimuon) as a function of the K^0 transverse momentum in fig. 5.5. These values can be compared to the efficiency obtained by Ciapetti et al. [44] for the minimum bias events.

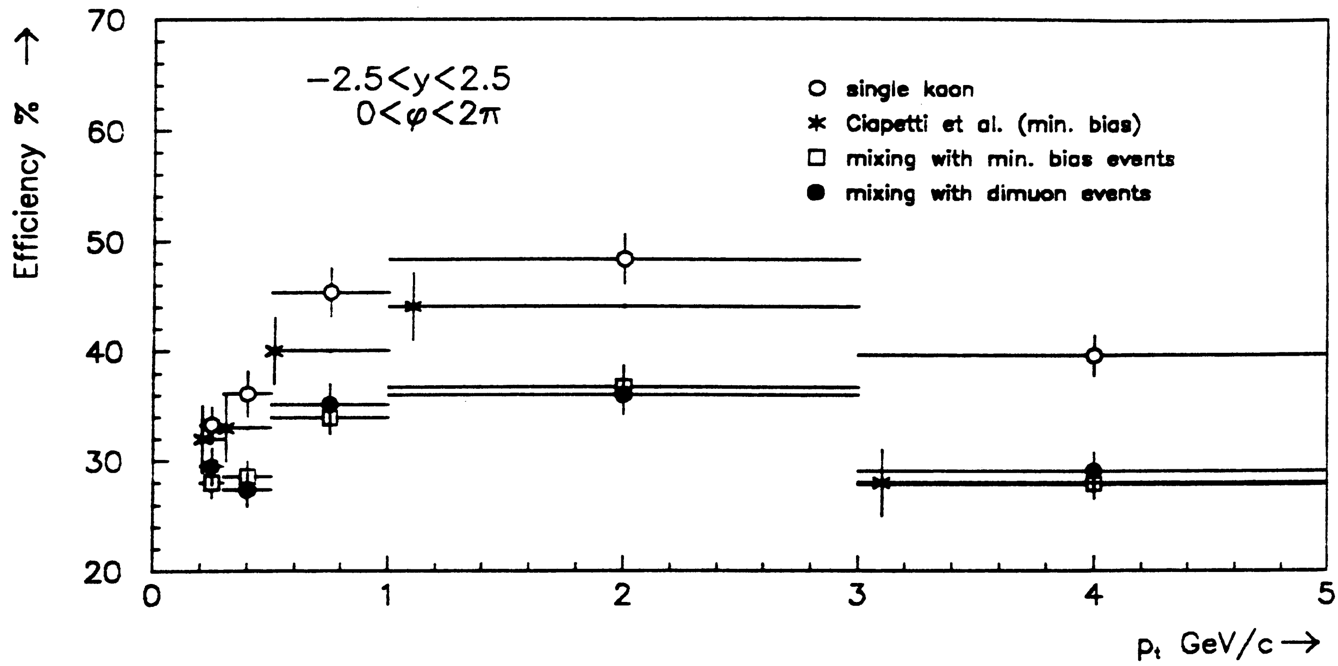

Figure 5.5: *The K^0 reconstruction efficiency ([%]) as function of $p_t(K^0)$ ([GeV/c]). The values have been integrated over $-2.5 < y(K^0) < 2.5$ and $0 < \phi < 2\pi$. Single K^0 efficiencies and the Ciapetti et al. [44] results for minimum bias are shown for comparison. The data points from Ciapetti et al. corresponding to the efficiency in the minimum bias events are plotted at the beginning of the p_t interval to emphasize the not uniform $p_t(K^0)$ distribution in this measurement.*

In general, the single K^0 and the Ciapetti et al. efficiency agree with each other, although our mixing results are systematically lower. The Ciapetti et al. results agree better with our calculations when their Monte Carlo overestimation factor of 0.89 is applied.

The Ciapetti et al. efficiency calculation deviates significantly only in the point $3 < p_t(K_S^0) < 5\,GeV/c$ from the single K^0 efficiency value. This deviation is due to a steeply falling transverse momentum spectrum of neutral kaons in the minimum bias events, especially in this high p_t region. The efficiency of the minimum bias kaons at $3 < p_t < 5\,GeV/c$ is close to the efficiency at $p_t \approx 3\,GeV/c$, because most kaons are produced at the beginning of the p_t interval. In conclusion, the systematically lower reconstruction efficiency obtained in the present work is explained by the track reconstruction difficulties, which are more severe in the real events than in the Monte Carlo generated events.

The agreement between the various efficiency calculation methods gives confidence in the mixing technique used in the present analysis. We have found no statistically significant differences in the K^0 reconstruction efficiency between the minimum bias and the dimuon events, see table 5.4. As can be judged from table 5.4 the same efficiency applies roughly for K^0's generated in jets. In conclusion, the K^0 reconstruction efficiency is rather independent of the event topology.

5.4 Efficiency of K_S^0 reconstruction with the new cuts.

To use the new V^0 selection cuts we have to recalculate the V^0 reconstruction efficiency. The efficiency for the reconstruction of a $K_S^0 \rightarrow \pi^+\pi^-$ decay in the UA1 CD has been calculated using the mixing technique. A single $K_S^0 \to \pi^+\pi^-$ decay is generated in the CD and subsequently merged into a real dimuon event. We present the K^0 reconstruction efficiency calculated under the following conditions:

- A Monte Carlo K_S^0 has been generated with a transverse momentum distribution deduced from real single muon events (a p_t distribution in real events is shown in fig 4.3). The K^0 rapidity distribution is generated uniformly in the range $-3 < y < 3$ and the azimuthal angle is also uniform in the full range $0 < \phi < 2\pi$.
- The production vertex of a Monte Carlo generated K^0 has been smeared around a primary vertex obtained from a real event with the vertex error distribution obtained from real single muon events.
- The new primary vertex has been fitted with the Monte Carlo generated tracks included.
- A Monte Carlo generated kaon has been merged into a real event only if it has been found by the V^0-finding software in an otherwise empty detector.

The results of the efficiency calculation are summarized in table 5.5.

Table 5.5: *Efficiency of the $K_S^0 \to \pi^+\pi^-$ reconstruction in % for an experimental $p_t(K^0) > 0.2\,GeV/c$ distribution, the V^0 impact parameter $b < 3mm$, decay plain orientation $|\lambda_d| > 0.3$ and several χ_i^2 values, defined in eq. 4.1. The signal is in the window $m(K^0) \pm 20\,MeV/c^2$. The errors are statistical.*

$\chi_i^2 > 1.5$	$\chi_i^2 > 2.0$	$\chi_i^2 > 2.5$	$\chi_i^2 > 3.0$	$\chi_i^2 > 3.5$	$\chi_i^2 > 4.0$	$\chi_i^2 > 4.5$
19.0 ± 1.8	17.9 ± 1.7	17.1 ± 1.7	16.3 ± 1.6	15.3 ± 1.5	14.7 ± 1.5	13.9 ± 1.4

The results of table 5.5 cannot be compared directly to the K_S^0 reconstruction efficiency calculated with the old set of the V^0 selection cuts, because the efficiencies in table 5.5 have been calculated for an experimental $p_t(K^0) > 0.2\,GeV/c$ distribution. For this comparison we calculated the efficiency (E_{ff}) for a flat distribution $p_t(K^0) = 1 - 3GeV/c$ and a rapidity range $-2.5 < y < 2.5$. Then for $b < 3mm$, $|\lambda_d| > 0.3$ and $\chi_i^2 > 4.0$ we obtain $E_{ff} = 23.8 \pm 2.4\%$ for a signal in $m(K^0) \pm 60\,MeV/c^2$ and S/B value of about 4. A larger mass window has been retained to show the effect of the other cuts (mainly the $\chi_i^2 > 4$ cut). This efficiency and S/B ratio can be compared to the value $E_{ff} = 36.0 \pm 1.8\%$ (see fig. 5.5) and S/B ratio of less than 1 for the previous set of the V^0-finding cuts [42].

Including the $K_S^0 \to \pi^+\pi^-$ branching ratio of 68.6% [25], we arrive at the reconstruction efficiency for K_S^0 mesons in the ranges $-2.5 < y < 2.5$ and $0 < \phi < \frac{\pi}{2}$ (with the cuts $b < 3\,mm$, $|\lambda_d| > 3$ and $\chi_i^2 > 4$) of:

$$\begin{aligned} E_{ff}(p_t(K_S^0) > 0.2\,GeV/c) &= (10.1 \pm 1.0)\% \\ E_{ff}(p_t(K_S^0) > 0.5\,GeV/c) &= (14.6 \pm 0.6)\% \end{aligned} \quad (5.4)$$

One might in addition use cuts on $cos\theta^*$ and P_d (see chapter 4). The efficiency for these cuts can be calculated analytically, since these distributions are uniform. Note, that to obtain a total efficiency for a K^0 reconstruction, the value in eq 5.4 has to be divided by 2 for the $K^0 \to K_S^0 + K_L^0$ process. For a detailed calculation of the K_S^0 cross section we calculated the reconstruction efficiency ($E(p_t, y, \phi)$) as function of flat $p_t(K^0)$, rapidity, and ϕ intervals. The results are summarized in the Appendix A.

Chapter 6

The inclusive K^0_S cross section.

For the calculation of the inclusive K^0_S cross section the 'single K^0' tables $A(p_t, y, \phi)$ have been used as described in Appendix A. The efficiency of K^0_S reconstruction E_{ff} is given by

$$E_{ff}(p_t, y, \phi) = A(p_t, y, \phi) \cdot C_{mc} \tag{6.1}$$

where the Monte Carlo correction factor (C_{mc}) has been defined in eq. 5.1 and tabulated in table 5.4. As discussed in chapter 5.3.2 the Monte Carlo correction factor is slightly dependent on the kaon momentum and on the track density in the event. We have used $C_{mc} = 0.75 \pm 0.02$ and $C_{mc} = 0.70 \pm 0.02$ for kaons with transverse momentum bellow 1 Gev/c and above that value respectively and we used the same correction for kaons in jets. The systematic bias in the cross section due to the choice of C_{mc} is less than the systematic uncertainty due to the variation in the integrated luminosity (15%, see chapter 3) and it will be discussed below.

The kaon background has been subtracted assuming the S/B ratio of 4.44 ± 0.19 for all values of transverse momentum. Although the background is somewhat higher for low momentum K^0_S's (i.e. below 0.5 GeV/c, see chapter 4.4.2) we have neglected this difference for the cross section calculation.

The inclusive K^0_S cross section in single muon events with $p_t(\mu) > 6\, GeV/c$ has been calculated by summing up all reconstructed neutral kaons in a given (p_t, y, ϕ) interval. Then

$$\frac{d\sigma}{dp_t dy d\phi} = \frac{\Delta N(p_t, y, \phi)/(\Delta p_t \Delta y \Delta\phi)}{L \cdot E_{ff}(p_t, y, \phi)} \cdot \frac{S/B}{S/B + 1} \tag{6.2}$$

where L is the integrated luminosity, ($L = 556 nb^{-1}$). The statistical errors due to the uncertainties in the efficiency and S/B ratio contribute about 7% to the error in cross section in each ΔN bin.

As described in section 3.6, the single muon event sample consists of events with stringent cuts on the muon acceptance. The total sample with $p_t(\mu) > 6\, GeV/c$ has up to 30% muons produced in a heavy quark (b or c quarks) decay. Up to about 70% of the events contain muons produced in the decay of pions and kaons. The inclusive kaon cross section has been evaluated in this single muon sample with $p_t(\mu) > 6\, GeV/c$ and $|\eta(\mu)| < 1.5$.

The total inclusive K^0_S cross section in single muon events with $p_t(\mu) > 6\, GeV/c$ and $|\eta(\mu)| < 1.5$ has been calculated by integrating over the transverse momentum, rapidity and azimuthal angle of the kaons in the ranges $0.2 < p_t < 5.0\, GeV/c$, $-2.5 < y < 2.5$ and $0 < \phi < 2\pi$. There are (uncorrected) 4380 (unique) neutral kaons in this sample giving:

$$\sigma_{tot}(p\bar{p} \to K^0_S + \mu + X) = 164 \pm 17 \pm 25\, nb \tag{6.3}$$

Where the first error is statistical and the second is systematical. The total muon acceptance of 0.29 ± 0.03 (see chapter 3.6) has been taken into account. In the statistical error we summed up the errors from the efficiency calculation (see Appendix A) and the uncertainty of the muon acceptance in quadrature. This procedure is justified by an approximate independence of the errors in the adjacent entries of the efficiency tables. The largest contribution to the systematic error is coming from the uncertainty in the integrated luminosity. The efficiency correction contributes to the systematic error mainly by the uncertainty in the Monte Carlo correction factor at $p_t(K^0) < 1\,GeV/c$. The half maximal difference between the entries of the C_{mc} table 5.4 for $p_t < 1\,GeV/c$ is (0.82-0.7)/2=0.06, therefore the systematic error due to the efficiency correction is estimated 0.06/0.75=8%. The total systematic error is obtained by quadratical sum of the efficiency and integrated luminosity errors.

The differential cross section $d\sigma/dp_t$ is obtained by integrating eq. 6.2 over $-2.5 < y < 2.5$ and $0 < \phi < 2\pi$, dividing by the size of the p_t interval. The results are given in table 6.1 and plotted in fig. 6.1a. The differential cross section $d\sigma/dy$ has been obtained by integrating eq. 6.2 over $0.2 < p_t < 5\,GeV/c$ and $0 < \phi < 2\pi$, dividing by the size of the rapidity interval ($\Delta y = 0.05$); it is plotted in fig 6.1b.

Table 6.1: *The inclusive differential $d\sigma/dp_t$ K^0_S production cross section in single muon events. Kaon rapidity and ϕ intervals are $-2.5 < y < 2.5$ and $0 < \phi < 2\pi$. Single muon events contain muons with $p_t(\mu) > 6\,GeV/c$ and $|\eta| < 1.5$. The muon acceptance factor of* 0.29 ± 0.03 *(see chapter 3.6) has been taken into account.*

p_t $[GeV/c]$	$\frac{d\sigma}{dp_t}$ $\left[\frac{nb}{GeV/c}\right]$	p_t $[GeV/c]$	$\frac{d\sigma}{dp_t}$ $\left[\frac{nb}{GeV/c}\right]$	p_t $[GeV/c]$	$\frac{d\sigma}{dp_t}$ $\left[\frac{nb}{GeV/c}\right]$
0.2-0.3	208 ± 24	1.1-1.2	52 ± 7	2.0-2.2	14.8 ± 2.6
0.3-0.4	219 ± 25	1.2-1.3	53 ± 7	2.2-2.4	10.0 ± 1.7
0.4-0.5	162 ± 19	1.3-1.4	46 ± 6	2.4-2.6	9.0 ± 1.7
0.5-0.6	138 ± 16	1.4-1.5	40 ± 6	2.6-2.8	4.8 ± 1.1
0.6-0.7	122 ± 14	1.5-1.6	33 ± 5	2.8-3.0	5.2 ± 1.2
0.7-0.8	97 ± 12	1.6-1.7	26 ± 4	3.0-3.2	5.9 ± 1.2
0.8-0.9	81 ± 10	1.7-1.8	26 ± 4	3.2-3.4	5.9 ± 1.8
0.9-1.0	68 ± 8	1.8-1.9	19 ± 3	3.4-3.8	2.4 ± 0.7
1.0-1.1	73 ± 9	1.9-2.0	18 ± 3	3.8-4.2	2.4 ± 0.7
				4.2-4.8	1.4 ± 0.4

A comparison will be made with the inclusive K^0_S production in the minimum bias events. For that aim we transformed the $d\sigma/dp_t$ differential cross section into an invariant form $E\frac{d^3\sigma}{dp^3}$ [47] (E, p are the kaon energy and momentum) by using an approximate constancy of the $d\sigma/dy$ spectrum.

$$E\frac{d^3\sigma}{dp^3} = \frac{1}{2\pi}\frac{d^2\sigma}{p_t\,dp_t\,dy} \approx \frac{1}{10\pi}\frac{d\sigma}{p_t dp_t} = \frac{1}{5\pi}\frac{d\sigma}{dp_t^2} \tag{6.4}$$

In this equation after the $\approx$ sign we integrated and averaged over $-2.5 < y < 2.5$ and $0 < \phi < 2\pi$.

For the comparison of the inclusive K^0_S production in single muon events (1μ) with the inclusive K^0_S production in minimum bias events (m.b.) we normalized the invariant cross section (eq. 6.4) to the total inclusive single muon cross section of 124 nb discussed in section 3.6. The quantity $\frac{1}{5\pi\sigma_{tot}}\frac{d\sigma}{dp_t^2}(1\mu)$ has been plotted together with the quantity $\frac{1}{5\pi\sigma_{NSD}}\frac{d\sigma}{dp_t^2}(m.b.)$ from ref. [44] in fig. 6.2, where σ_{NSD} is the total non-single diffractive cross section: $\sigma_{NSD} = 42 \pm 1\,mb$ [48].

Note that the value for σ_{NSD} has been derived for $p_t \to 0$, whereas the inclusive K^0_S cross section has been normalized to the inclusive single muon cross section with $p_t(\mu) > 6\,GeV/c$.

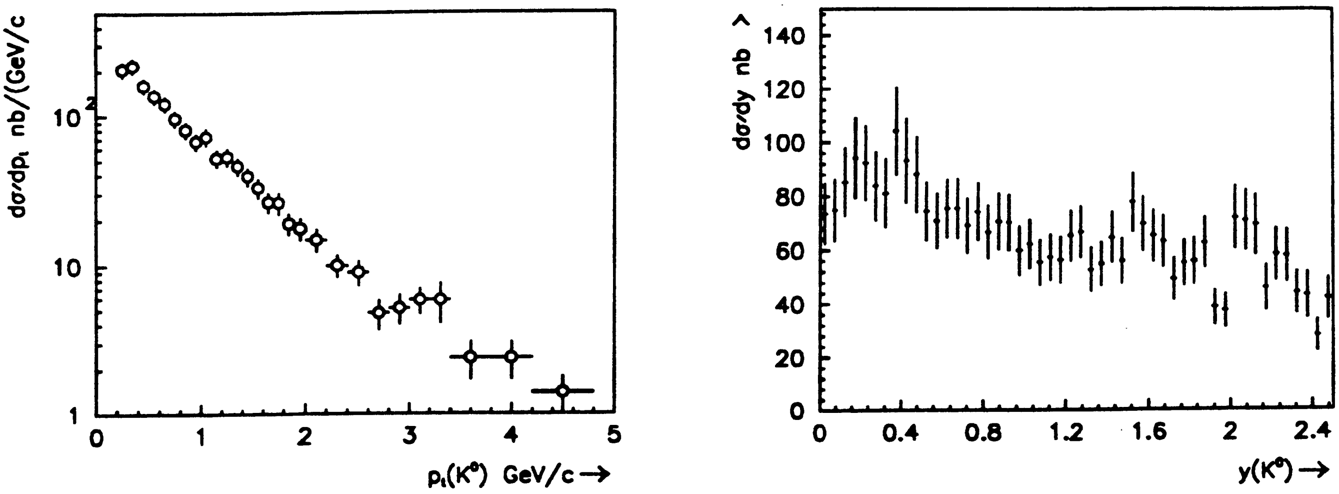

Figure 6.1: *The inclusive differential $d\sigma/dp_t$ (a) and $d\sigma/dy$ (b) K^0_S production cross section in single muon events. The kaon rapidity and azimuthal angle intervals are $-2.5 < y < 2.5$ and $0 < \phi < 2\pi$. The kaon transverse momentum interval is $0.2 < p_t < 5.0\,GeV/c$. Single muon events contain muons with $p_t(\mu) > 6\,GeV/c$ and $|\eta(\mu)| < 1.5$.*

This difference is explicit in the comparison of the K^0_S multiplicity in the minimum bias and in the single muon events. The K^0_S multiplicity $< n_{K^0_S} >$ is the number of kaons per event after the efficiency correction. In single muon events we have

$$< n_{K^0_S} > = \ 1.31 \pm 0.02 \pm 0.1 \qquad p_t(K^0_S) > 0.2\,GeV/c \quad |y| < 2.5 \tag{6.5}$$

where the first error is statistical and the second is systematical, taking in account the uncertainty of the Monte Carlo correction factor.

In minimum bias events the kaon multiplicity is $< n_{K^0_S} >= 0.64 \pm 0.06$ ($|y| < 2.5$) [44], this value is extrapolated to $p_t \rightarrow 0$. It is not possible to compare our result at $p_t(K^0_S) > 0.2\,GeV/c$ (eq. 6.5) directly with the K^0_S multiplicity in minimum bias events. However the differential K^0_S cross section in single muon events falls less steeply than the differential K^0_S cross section in the minimum bias events. Since the main contribution to the kaon multiplicity comes from low energy kaons we conclude, that low energy kaon production in the single muon events is compatible (within a factor of order unity) with the kaon production in the minimum bias events.

There is a difference in production of high energy kaons, however. The single muon data presented in fig. 6.2 allow for a conclusion, that in the single muon events there is an additional source of high energy kaons, compared to the minimum bias events. In general, the kaon production in single muon events is expected to be higher, because the track density in single muon events is larger than in minimum bias events. The K^0_S/π^0 ratio has been found to be about constant (about 0.1) over a wide range of the Collider energies [49]. The high momentum particles in single muon events are produced in jets. Therefore the less steep fall of the K^0_S cross section observed in fig 6.2 can be attributed to kaon production in jets.

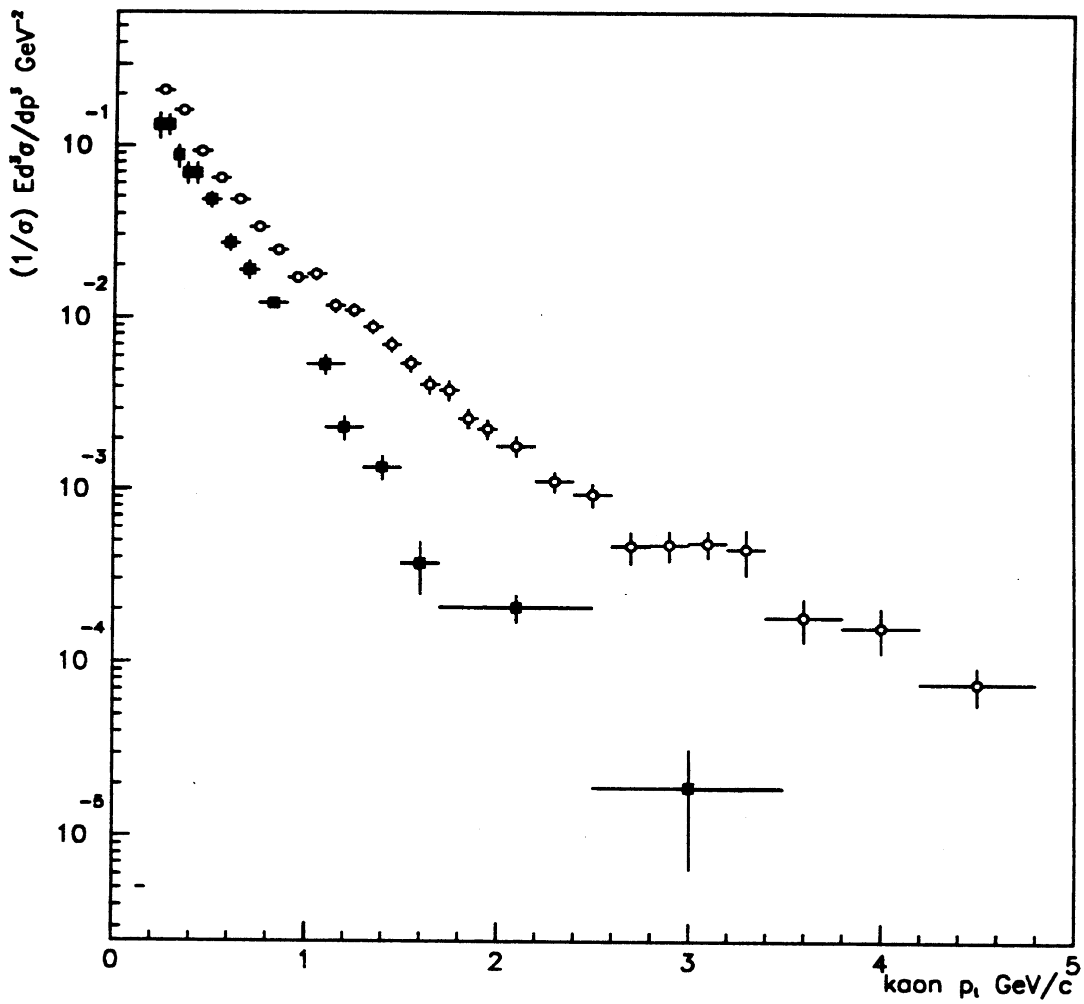

Figure 6.2: *Comparison of the K_S^0 production in minimum bias (black squares) and single muon (open circles) events. The differential cross section $d\sigma/dp_t^2$ has been normalized to $\sigma_{tot}(1\mu)$ (see chapter 3.6) for the single muon events and to the total non-single diffractive cross section σ_{NSD} for the minimum bias events.*

Chapter 7

K_S^0 production in jets.

7.1 Introduction

It has been concluded in chapter 6 that high energy kaons are produced in jets. In this chapter a study of the topological and kinematical properties of kaons in jets is presented. The aim of this study is to identify the quark producing the jet with neutral kaons, in particular to establish a signature for heavy quark production with kaons, as it is done presently with the muons.

It has been found in previous studies that if a muon with a high transverse momentum appears inside a jet of particles, i.e. not isolated, it is likely to come from a semi-leptonic decay of a heavy quark [10] [39]. A Monte Carlo study of the heavy quark production reveals that this jet contains particles from the initial fragmentation of the heavy quark and the subsequent heavy quark meson decay. A statistical separation of the events with the $b\bar{b}$ and $c\bar{c}$ quarks is then possible, using the transverse momentum of the muon relative to the jet axis (p_t^{rel}) in the Central Detector (CD) [10]. As compared to the jets detected in the calorimeter, the CD provides a better measurement of the jet axis. The event separation is based on the mass difference of the b and c quarks. Heavy flavour separation from decay background is also possible with this technique, because the background muons from light quarks will have a rather low $p_t^{rel}(\mu)$ value.

Heavy quarks are created in pairs. Since the data selection requires only one muon, the other quark is expected to decay mainly hadronically. If the heavy quarks are produced in the QCD process of flavour creation, this second jet will balance the first muon jet in the CM system of the hard scattering process. Therefore in this case the balancing jet (j_{op}) from another heavy quark can be identified in the real data by applying the topological condition $\phi(j_{op}) \approx \phi(j_\mu) \pm 180°$, where ϕ is the azimuthal angle with respect to the direction of the beam.

Two kaon properties have been considered for use to identify the quark producing the jet: the multiplicity of neutral kaons in the jets and the $p_t^{rel}(K_S^0)$ of neutral kaons with respect to their jets in the CD. A special study is devoted to the $p_t^{rel}(K_S^0)$ in events selected with a leading kaon in the jet. Selection of leading kaons should minimize dilution of p_t^{rel} in chain decays of the heavy quarks. After the selection of events with a leading kaon in a jet we have studied again the muon $p_t^{rel}(\mu)$ distribution in these events. Larger value of $p_t^{rel}(\mu)$ after this selection would imply a smaller decay background contribution in these events.

This chapter is subdivided in three main sections. In section 7.2 we start with a summary of the data selection. We have chosen a real data sample with $p_t(\mu) > 7\,GeV/c$ and $p_t(K_S^0) > 0.5\,GeV/c$, because the statistics did not allow to use a cleaner sample with $p_t(\mu) > 10\,GeV/c$ and $p_t(K_S^0) > 1\,GeV/c$. The full data sample with $p_t(\mu) > 6\,GeV/c$ has also been used to study the heavy flavour production. A larger value of kaon transverse momentum is favourable for selection of a kaon produced in a jet. Nevertheless, section 7.2.5 contains a comparison of the absolute numbers of selected events with the expectations from the heavy flavour production. Then, the analysis of kaon properties in jets containing a muon and their balancing jets proceeds along two main lines.

First, in section 7.3 the kaon production is studied in Monte Carlo generated data. The Monte Carlo program (ISAJET 5.23) is tuned to reproduce the real single muon data [10], therefore we expect it to give a realistic description also for kaon production. The same selections as in the real data have been applied in the Monte Carlo generated events; then the K_S^0 multiplicity in jets (section 7.3.3) and the $p_t^{rel}(K_S^0)$ in jets (section 7.3.4, 7.3.5) are studied for jets of different origin.

Second, in section 7.4 the K_S^0 properties acquired in the study of the Monte Carlo generated events have been compared to K_S^0 properties measured in real single muon events. In particular we compare the muon $p_t^{rel}(\mu)$ with respect to the muon jet containing also a K_S^0 in it with the Monte Carlo predictions (section 7.4.2). Finally, the kaon selection is attempted in a real event sample with more background, containing muons with $p_t(\mu) > 6\,GeV/c$ (section 7.4.5).

7.2 Selection of the data sample.

7.2.1 The μ and the calorimeter jet selection cuts.

The inclusive muon data used in the present analysis consists of about 20000 events with $p_t(\mu) > 6\,GeV/c$, $|\eta(\mu)| < 1.5$ and with tight cuts on the muon track reconstruction, see chapter 3.6. We have used mainly μ events with $p_t(\mu) > 7\,GeV/c$; this sample contains $(55 \pm 10)\%$ background, mainly from the $\pi/K^{\pm}$ decays [39].

Calorimeter jets (j_{CA}) in the single muon events have been selected with the requirement $E_t(j_{CA}) > 10\,GeV$. All jets have been validated with a CD track or a neutral kaon, both with $p_t > 0.5\,GeV/c$ and within a cone around j_{CA} of $\Delta R < 0.4$. There are approximately 3% of jets above $E_t > 10\,GeV$ validated by a K_S^0 only, without any other suitable track within the $\Delta R = 0.4$ cone. The jets are defined using the standard UA1 jet algorithm; the E_t value of the jet is the uncorrected value from the jet algorithm.

7.2.2 Selection of the non-isolated muons.

To measure the muon $p_t^{rel}(\mu)$ with respect to its jet, it is important to define the proper jet axis. The CD jets are used in this case since they have better spatial resolution than the calorimeter jets. Spatial resolution is measured by $\Delta R = \sqrt{\Delta y^2 + \Delta\phi^2}$, where Δy and $\Delta\phi$ are the differences in rapidity and azimuthal angle, respectively, between the jet initiator and the other tracks.

The muon jet should have at least one track (t) with $p_t(t) > 1\,GeV/c$, otherwise the jet axis will not be determined properly and the $p_t^{rel}(\mu)$ will anyway be low. This jet should also not be too wide, since the muon will have a large $p_t^{rel}(\mu)$ in a wide jet. To incorporate jet features properly the CD jets in single muon events have been recalculated.

A standard UA1 algorithm for CD jet finding has been employed with two modifications: a) the muon tracks are skipped in the initial jet definition, b) the neutral kaons are accepted as jet particles and their secondaries are not used. The CD jet parameters are then chosen as follows:

- jet initiator is a CD track or a K_S^0 with rapidity $|y| < 2.5$ and $p_t > 1\,GeV/c$, which defines the initial jet axis j_{CD}
- additional tracks or K_S^0's are added to the initiator vector, if they are within a cone around j_{CD} of $\Delta R < 0.4$. Moreover, $p_t(track) > 0.1\,GeV/c$ and $p_t(K_S^0) > 0.2\,GeV/c$.

The higher p_t threshold for the kaons ($0.2\,GeV/c$, as compared to $0.1\,GeV/c$) is introduced to obtain a reliable K_S^0 reconstruction [42].

Only those single muon events are selected, for which there is a CD jet defined as above within a cone of $\Delta R = 0.7$ to the muon. This selection follows a study by Jimack [39] who shows that the distance between the muon and its jet in the R-space larger than 0.4 is due to a side kick of the muon in the heavy flavour (semi-leptonic) decays. The cone of $\Delta R = 0.7$ is large enough to contain the muon with $p_t > 7\,GeV$ and the other charged particles of the jet; for $p_t(\mu) > 10\,GeV/c$ this cone size could even be reduced to $\Delta R = 0.6$. The initial quark direction is represented by the vector sum of the j_{CD} and the muon: $\vec{j_\mu} = \vec{j_{CD}} + \vec{\mu}$. The muon p_t^{rel} is measured with respect to this new axis.

Furthermore, the transverse mass m_t of the jet j_{CD} is calculated. The transverse mass is defined by $m_t c = \Sigma p_t^{rel}(t_i)$, where p_t^{rel} for each track i in the jet is measured with respect to j_μ. Only events with $m_t < 2\,GeV/c^2$ are selected for the present analysis, since large transverse mass is an indication for mixing of two jets. Two jets close to each other can be created in higher order QCD processes, like gluon splitting. Gluon splitting may distort the muon-jet measurement, when the second jet is close to the muon [10]. Also a jet from final state gluon bremsstralung might merge into the heavy flavour jet and distort the measurement of p_t^{rel}. Also the measurement of K_S^0 multiplicity in such jets is biased.

Muons inside the j_μ described above, passing the $m_t < 2\,GeV/c^2$ cut, are called non-isolated.

We stress at this point, that the inclusion of the neutral kaons in jets is important for our data analysis. About 6% of the non-isolated muons in our data sample (564 events, see table 7.1) are not isolated due to a neutral kaon. This number is low, but the contribution from the events with a muon not isolated due to a high momentum kaon near to it is significant for the present analysis. We will discuss these jets in section 7.4.2.

7.2.3 Selection of the muon balancing jet.

As mentioned in the introduction to this chapter, heavy quarks are produced in pairs, creating a special topology of the events. In our event sample one heavy flavour jet is tagged by a muon, the other one may be found by other means.

Events with one or more jets outside $\Delta R = 1$ from the muon should have jets arranged in a way to balance the muon jet in the CM system of the hard scattering process. For first order QCD process of flavour creation the balancing jet is initiated by the other heavy quark. For higher order QCD processes more jets are created in addition to the muon jet. For instance in gluon splitting processes, two jets correspond to the heavy quarks and the third one is the recoil gluon. The selection of the other heavy flavour jet is difficult in this case. Therefore we are interested primarily in the first order QCD processes. Moreover, the selection of muons with $p_t > 7\,GeV/c$ (instead of $p_t > 10\,GeV/c$ as used by Albajar et al. [10]) favours the first order processes (see section 7.3).

The μ-balancing jet (j_{op}) has been selected among the calorimeter jets with the azimuthal angle $\phi(j_{op}) \approx \phi(j_\mu) \pm 180°$. We allow an uncertainty of 30° in the azimuthal angle definition. If several calorimeter jets satisfy these requirements, we select the jet with the transverse energy that best matches the transverse momentum of the muon: $E_t(j_{op}) \sim p_t(\mu)$.

Albajar et al. [10] used another selection of the opposite jets in the $b\bar{b}/c\bar{c}$ analysis with muons of $p_t > 10\,GeV/c$. In that study the balancing jet is the one with $E_t(j_{CA}) = max$ for all jets outside the cone $\Delta R(\mu, j_{CA}) = 1$. The balancing jets selected with the $E_t = max$ criterion tends to have $\Delta\phi(\mu, j_{CA}) = max \to 180°$, compatible with the calculation for the first order QCD process of flavour creation.

A deviation from the $\Delta\phi = max$ rule is expected for the higher order QCD processes, which are less important for the events with the low energy muons (lower than $10\,GeV/c$). In only 3% of events a different decision has been taken by the present algorithm. Our selection is slightly tighter, we loose about 10% of the events compared to the Albajar et al. algorithm. Requiring a fast topological condition $\phi(j_{op}) \approx \phi(j_\mu) + 180°$ rejects more background events than heavy flavour events, whereas the selection with $E_t(j_{CA}) = max$ is always satisfied in jet events. There is of course more background in the sample with muons of $7 < p_t < 10\,GeV/c$. A calorimeter jet with the required properties could be found in nearly 40% of the single muon events.

In summary, about 40% of the events have the required j_{op} topology; nearly 40% had no calorimeter jet with the required energy and 20% of the events had no recoil jet topology, as measured in the data sample with the non-isolated muons.

7.2.4 The K_S^0 selection cuts.

The present study uses a set of selection criteria for kaons, which give a high S/B ratio for the K_S^0 reconstruction, see chapter 4. In summary the selection is:

- Impact parameter: $(b/\Delta b)^2 > 4$ for an individual track and $b(V^0) < 3\,mm$ for a V^0
- The cosine of the $\pi^+\pi^-$ decay plane angle with respect to the z-axis: $|\lambda_d| > 0.3$
- Mass window: $m(K_S^0) = 498 \pm 20\,MeV/c^2$
- Kinematics: $p_t(K_S^0) > 0.5\,GeV/c$ and $|y(K_S^0)| < 2.5$ (see fig. 7.1)

With the above selection criteria for the kaon signal we obtained in the single muon events a signal to background ratio (S/B) and an efficiency (E_{ff}) for the K_S^0 reconstruction (see chapters 4 and 5):

$$S/B(p_t > 0.5\,GeV/c) = 4.4 \pm 0.2 \tag{7.1}$$
$$E_{ff}(p_t > 0.5\,GeV/c;\ |y| < 2.5) = (14.6 \pm 0.6)\% \tag{7.2}$$

The above cuts allow for about 18% background from random track combinations satisfying the V^0 selection criteria. The quoted efficiency includes the $K_S^0 \to \pi^+\pi^-$ branching fraction. (It does not include the $K^0 \to K_S^0 + K_L^0$ branching fraction). Only unique K_S^0's have been selected. The fraction of ambiguous K_S^0 is less than 3%. These efficiencies have been determined for an inclusive experimental $p_t(K_S^0) > 0.5\,GeV/c$ spectrum and a flat rapidity and azimuthal angle range: $|y(K_S^0)| < 2.5$, $0 < \phi < 180°$.

7.2.5 Data selection summary and expectations for a $b\bar{b}/c\bar{c}$ signal.

The initial data sample consists of $\approx$ 20000 single muon events. Table 7.1 summarizes the individual steps in the selection. After the selection of K_S^0 with $p_t > 0.5\,GeV/c$ and rapidity $|y| < 2.5$ we are left with 2187 events. Some events contain more than one neutral kaon, the total number of neutral kaons, unambiguously defined is 2433. Further restriction to events with non-isolated muons of $p_t(\mu) > 7\,GeV/c$ leaves us with 564 events. The recoil jet topology with $E_t(j_{CA}) > 10\,GeV$ exists in 282 of these events.

The 282 events with j_μ, j_{op} and K_S^0 might still have approximately 50% of muon background, as before the kaon selection. The kaon background is about 20%. About 120 events are expected to be left after this background subtraction. The kaons in these events are not necessarily

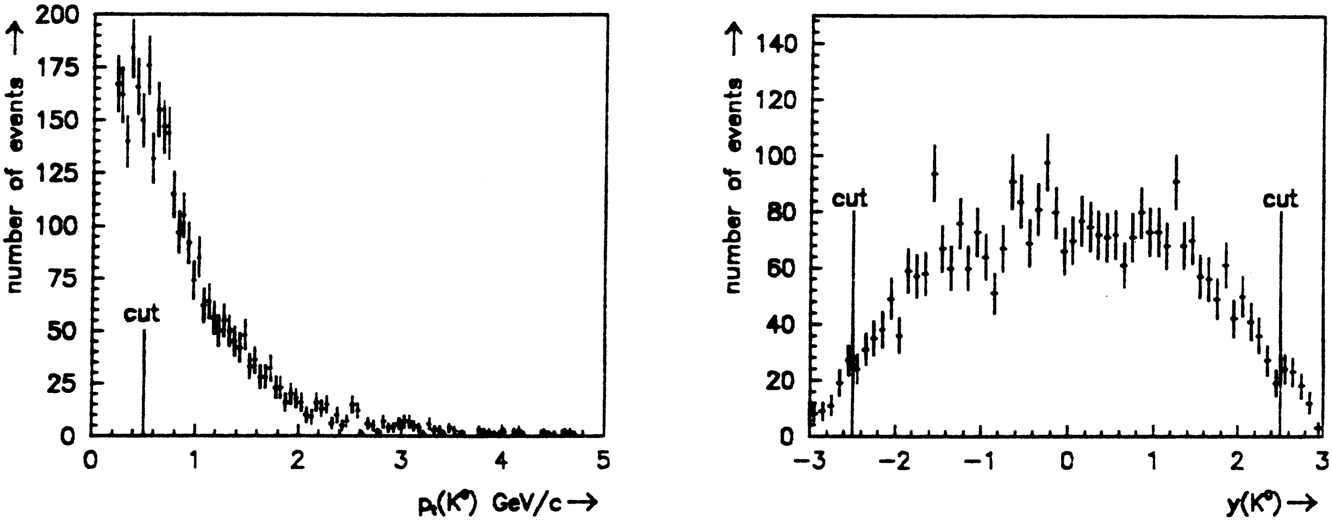

Figure 7.1: *The inclusive p_t and rapidity spectra of kaons in the single muon events.*

Table 7.1: *Selection of events. The cuts are cumulative.*

selection	number of events
initial sample $p_t(\mu) > 6\,GeV/c$; tight μ cuts	19724
Kaons $p_t(K^0_S) > 0.5\,GeV/c$ $\lvert y(K^0_S)\rvert < 2.5$	2187
muons $p_t(\mu) > 7\,GeV/c$ non-isolated	564
Jet $E_t(j_{CA}) > 10\,GeV$	388
Recoil Jet $E_t(j_{CA}) > 10\,GeV$	282

Table 7.2: *Estimation of the number of neutral kaons in the heavy flavour events.*

reduction factor	number of events
initial sample	≈ 20000
muons $p_t(\mu) > 7\,GeV/c$ non-isolated	≈ 5000
Background 55% subtracted	≈ 2250
fraction of K^0_S per event 0.3	≈ 675
K^0_S reconstr. Efficiency 14%	≈ 100

produced in jets, however. The Monte Carlo study shows, that about 30% of kaons are made in the underlying event, see section 7.3. Thus about 85 K^0_S in jets are expected in the real data.

On the other hand we can calculate the expected number of neutral kaons from the $b\bar{b}/c\bar{c}$ signal. The number of heavy flavour events is obtained after the muon background subtraction (2250 events). A $b\bar{b}$ or a $c\bar{c}$ initiated jet produces (at a certain jet energy) a K^0_S with probability about 0.15 per quark, see section 7.3, table 7.6. Heavy quarks are produced in pairs, therefore we expect 0.3 K^0_S's per event.

The calculation of the expected number of events is summarized in table 7.2. From the initial sample and after background subtraction we are left with about 2250 single muon events with $p_t(\mu) > 7\,GeV/c$. The reconstruction efficiency for K^0_S with $p_t > 0.5\,GeV/c$ is about 14%. Therefore we are left with about 100 events with a K^0_S from the $b\bar{b}/c\bar{c}$ sample.

The expectations for the $b\bar{b}/c\bar{c}$ production are thus compatible with the measured number of events. However, as mentioned before not all kaons in the real data sample have to come from the heavy quarks. An other uncertainty is the muon background. In the $\mu + K^0_S$ sample it could be less than the assumed 55%. On the other hand the probability of K^0_S production in the heavy flavour jets depends on the energy of the jet. In conclusion, the expected number of the events and the measured number of the events are compatible within a factor of 2 or better.

For the calculation of the K^0_S multiplicity in the next sections we used a normalization on the number of jets in a sample with $|y(K^0_S)| < 2.5$, $p_t(\mu) > 7\,GeV/c$ non-isolated, $E_t(j_{CA}) > 10\,GeV$ and $p_t(K^0_S) > 0.2\,GeV/c$, instead of $p_t(K^0_S) > 0.5\,GeV/c$. This was done to avoid a possible bias of the jet distribution, which would occur if neutral kaons would be predominantly produced in certain jets and not produced in the others. Therefore the transverse momentum cut has been lowered to allow for a larger fraction of neutral kaons from the underlying event in the sample. There are 525 events in a sample with $p_t(K^0) > 0.2\,GeV/c$, as compared to 388 events with $p_t(K^0_S) > 0.5\,GeV/c$.

7.3 Monte Carlo study of K^0_S properties in jets.

7.3.1 Monte Carlo event generation.

In the present analysis we used the ISAJET 5.23 $b\bar{b}$ and $c\bar{c}$ production [41]. The generation of the heavy quarks was performed via direct $Q\bar{Q}$ creation, through flavour excitation and by gluon splitting.

The events have been generated with the p_t of the $2 \rightarrow 2$ hard scattering process (p_t^{hard}) in the range between 8 and 70 GeV/c. Below $p_t^{hard} = 10\,GeV/c$ the contribution from the gluon splitting process tends to be low. In the Monte Carlo sample used for $p_t^{hard} > 10\,GeV/c$, the heavy quarks have been generated for 1/3 by the process of flavour creation, for 1/3 by the process of flavour excitation and for 1/3 by the process of gluon splitting.

About $10\,pb^{-1}$ of data has been generated and passed through a complete detector simulation. In the Monte Carlo study we used events with a muon $p_t(\mu) > 10\,GeV/c$. For the real data we used all events with $p_t(\mu) > 7\,GeV/c$ to improve the statistics. We do not expect large deviations in the conclusions due to this difference. The K^0_S and the jet selection in the Monte Carlo data is identical to the selection in the real data. Since the $p_t(\mu)$ is higher in the Monte Carlo data, we used a cone size of $\Delta R(\mu, j_{CD}) < 0.6$ to select events with the non-isolated muons (instead of $\Delta R < 0.7$ as was used in the real data).

In the Monte Carlo data the calorimeter and the CD jets have been associated to their initiator quark by choosing the quark with the minimal angle α between the quark momentum and the momentum vector of the jet: in any case $\alpha < 30°$ was required. We remark, that it also possible to search for the nearest quark with the ΔR variable, with compatible results. This procedure of attributing a jet to a quark, by selecting the closest quark, has been chosen to approximate the selection of jets in real events as much as possible. In real events particles are assigned to a jet if they appear close enough to a jet initiator — a high momentum particle. In real events and in the Monte Carlo data after the detector simulation, some of the jets might be created as a detector effect, bearing no relation to a quark. For $E_t(jc_A) > 10\,GeV$ and validated (see section 7.2) about 85% of the calorimeter jets correspond to a quark [39].

Thus, in 15% of the jets reconstructed in the calorimeter, no quark within $\alpha < 30°$ was found; therefore we have not assigned any identity to such jets. Table 7.3 summarizes the distribution of jets in this Monte Carlo data. The entry named q(uds) consists of 61% u-quark, 30% d-quark and 9% s-quark. The contribution from s-quark is low in this Monte Carlo.

Table 7.3: *Jet-parton association in the $b\bar{b}/c\bar{c}$ ISAJET Monte Carlo after reconstruction in the detector. The entry q(uds) consists of 61% u-quark, 30% d-quark and 9% s-quark.*

quark	q(uds)	$c\bar{c}$	$b\bar{b}$	gluon	no assignment
fraction	$18.1 \pm 0.8\%$	$13.3 \pm 0.7\%$	$22.9 \pm 0.9\%$	$30.5 \pm 1.0\%$	$15.2 \pm 0.7\%$

The jet balancing a muon jet has been selected the same way as in the real data. In about 61% of events the balancing jet was initiated by a light quark or a gluon (26% light quark and 37% gluon jet) and not by a heavy quark.

In the Monte Carlo data it is, of course, possible to identify all particles coming from one and the same quark and assign them in one jet. This is an ideal case of a jet selection, which we performed using the Eurojet Monte Carlo program. The Eurojet program was necessary to study the production of kaons in an s-quark initiated jet, see section 7.3.3.

7.3.2 General properties of the Monte Carlo data.

We enriched the sample with $b\bar{b}$ or $c\bar{c}$ events in the Monte Carlo data using $p_t^{rel}(\mu)$. Table 7.4 gives the results. On the average, the $b\bar{b}$ initiated muons will have a larger p_t^{rel} value ($< p_t^{rel}(\mu) >= 0.78\,GeV/c$), than the $c\bar{c}$ initiated muons ($< p_t^{rel}(\mu) >= 0.51\,GeV/c$). Note that the real data will contain also a large portion of the muon background in the sample with $p_t^{rel}(\mu) < 0.6\,GeV/c$, because the background muons, which are produced in π/K decays, will also have rather small p_t^{rel} values ($< p_t^{rel}(\mu) >\approx 0.5\,GeV/c$).

Table 7.4: *Heavy Flavour separation in the Monte Carlo data using $p_t^{rel}(\mu)$.*

selection	$c\bar{c}$	$b\bar{b}$
$p_t^{rel}(\mu) > 0.6\,GeV/c$	$14.8 \pm 1.4\%$	$85.2 \pm 4.2\%$
$p_t^{rel}(\mu) < 0.6\,GeV/c$	$40.3 \pm 2.5\%$	$59.7 \pm 3.3\%$

There is no contribution from the muon background sources in this Monte Carlo data, unlike in the real data. The K_S^0 production probability is not significantly different for the b and c-quarks, see section 7.3.3. Therefore the p_t^{rel} of the muon does not change after the K_S^0 selection:

$$< p_t^{rel}(\mu) > \; = \; 0.655 \pm 0.008\,GeV/c \tag{7.3}$$

$$\Delta R(\mu, K_S^0) < 0.7 \qquad < p_t^{rel}(\mu) > \; = \; 0.66 \pm 0.02\,GeV/c \tag{7.4}$$

Kaons in an event are expected to come from three main sources. In the first place kaons are produced in the fragmentation process of the spectator partons, which did not take part in the hard scattering process (underlying event). These kaons are expected to be soft and tend to have rather large rapidity, therefore the majority of kaons from the underlying event will remain inside the beam pipe. The reconstruction efficiency for kaons with rapidity above 3 is rather low. Nevertheless, the multiplicity of kaons from this source in an event is so high that it is the main background in the study of the kaons produced in the hard scattering process.

The second source of kaons is the fragmentation of gluons and quarks produced in the hard scattering process. The third source is the decay of heavy quarks. The kaons from the last two sources are expected to be aligned to the jets created by the outgoing quarks. To study the hard scattering processes with the kaon signal it is necessary to separate the underlying event kaons from the kaons produced in the hard scattering via quark decay and fragmentation. Table 7.5 lists the contribution from the underlying event and from the different quarks in the $b\bar{b}/c\bar{c}$ Monte Carlo data. In conclusion, as much as 95% of the kaons in a (calorimeter) jet are produced by the gluon or quark that creates the jet as is shown in the last row of table 7.5. The reduction of the background kaons from the underlying event is achieved mainly by applying the ΔR cut.

Table 7.5: *K^0_S sources for several cuts for the ISAJET Monte Carlo after the detector simulation.*

selection	underl.event	gluon	u,d,s-quarks	$c\bar{c}$	$b\bar{b}$
$p_t(K^0_S) > 0.2\,GeV/c$	$37.5 \pm 1.0\%$	$25.9 \pm 0.8\%$	$8.5 \pm 0.4\%$	$6.5 \pm 0.4\%$	$21.6 \pm 0.7\%$
$p_t(K^0_S) > 0.5\,GeV/c$	$32.5 \pm 1.1\%$	$24.5 \pm 1.0\%$	$8.3 \pm 0.5\%$	$7.9 \pm 0.5\%$	$26.8 \pm 1.0\%$
$p_t(K^0_S) > 0.5,\ \|y\| < 2.5$	$29.2 \pm 1.6\%$	$25.8 \pm 1.5\%$	$9.1 \pm 0.8\%$	$8.9 \pm 0.8\%$	$27.0 \pm 1.6\%$
$p_t(K^0_S) > 0.5,\ \|y\| < 2.5$ and $\Delta R(K^0_S, j_{CA}) < 0.7$	$5.1 \pm 1.2\%$	$23.7 \pm 2.9\%$	$14.7 \pm 2.2\%$	$15.6 \pm 2.3\%$	$40.9 \pm 4.1\%$

7.3.3 K^0_S multiplicity in the Monte Carlo data.

Exact first order calculation using the Eurojet Monte Carlo program has been performed to compare the K^0_S production probabilities for different types of quarks. No detector simulation has been done in this case. In the Eurojet program we traced the particles to their parent quark, therefore the jet was very well defined as a bunch of particles from one quark only. The K^0_S production probability per quark type is summarized in table 7.6. The jet width was $\Delta R = 0.7$; particles from the same quark outside this cone were rejected.

Table 7.6: *The probability of K^0_S production ($\frac{num.\ K^0_S\ in\ \Delta R(K^0_S, q)}{num.\ quarks}$) for jets originating from different quarks (q). Data has been generated with the Eurojet Monte Carlo program. No detector simulation has been applied.*

gluon	u-quark	d-quark	s-quark	c-quark	b-quark
0.21 ± 0.01	0.13 ± 0.01	0.15 ± 0.02	0.28 ± 0.03	0.15 ± 0.01	0.16 ± 0.01

The probability to create a kaon in the s-quark initiated jet is larger than for all other quarks. The probability for the $c\bar{c}$ and $b\bar{b}$ is about the same as for the u and d-quarks. Note, that no distinction has been made for heavy quarks decaying semileptonically.

The calculated probability for the K^0 production in jets depends on the fragmentation scheme used in the Monte Carlo program. For the fragmentation of the heavy quarks Eurojet and ISAJET use both the Peterson et al. function [24]. The fragmentation of a gluon is treated differently, however. In Eurojet the gluon is split in a quark–antiquark pair and these two quarks are fragmented in one jet [22]. Therefore the probability of K^0 production in the gluon jets is higher than in an u-quark or a d-quark jet. The ISAJET Monte Carlo program fragments instead the gluon like a light quark of random flavour [10]. Therefore ISAJET produces kaons in the gluon jets with lower probability, compared to the Eurojet calculations.

The exact probabilities for kaon production in jets will depend also on the energy of the quarks producing the jets. Since quarks with a higher energy will have in general a longer fragmentation chain, they can produce also more neutral kaons. Jets from higher energy quarks are also more collimated, therefore more particles will find themselves inside the ΔR cone and the probability to find a kaon in the jet is higher. Therefore we do not rely heavely on the Eurojet predictions for comparison with the real data. ISAJET predictions are used instead, where the energy of the processes has been tuned to reproduce the real data (see section 7.3.1).

For the ISAJET Monte Carlo data and the real data we used a more practical definition of the kaon multiplicity. The K_S^0 multiplicity in the jet initiated by a quark q ($\alpha < 30°$) is defined by

$$K_S^0\ multiplicity = \frac{number\ of\ K_S^0\ with\ \Delta R(K_S^0, j_q) < 0.7}{number\ of\ j_q} \tag{7.5}$$

For technical reasons we used the number of jets after the selection of kaons with $p_t(K_S^0) > 0.2\,GeV/c$, instead of $p_t(K_S^0) > 0.5\,GeV/c$. It is assumed, that the jet distribution is not changed by the presence of a kaon somewhere in the event.

The ISAJET multiplicity of the K_S^0 production in the muon jets and the recoil jets originating from the indicated quarks is summarized in table 7.7.

Table 7.7: *The K_S^0 multiplicity in the ISAJET Monte Carlo data for jets of different origin.*

selection	multiplicity muon jet j_μ	multiplicity recoil jet j_{op}
$b\bar{b}$	0.20 ± 0.01	0.15 ± 0.02
$c\bar{c}$	0.17 ± 0.02	0.09 ± 0.04
gluon		0.10 ± 0.01
q(uds)		0.08 ± 0.01

In table 7.7, it seems that the K_S^0 multiplicity in the recoil jets is lower than in the muon jets. The K_S^0 multiplicity in the gluon jets is a factor 2 lower than in the muon jet initiated by a b-quark. The K_S^0 multiplicity in the u-quark jet is the same as in the gluon jet. The k_S^0 multiplicity in the $b\bar{b}$ and the $c\bar{c}$ jets is about the same.

In table 7.6 the probability to obtain a kaon in a gluon jet is higher than in a $b\bar{b}$ jet. All other probabilities, except for the s-quark are about the same. The differences between table 7.6 and table 7.7 can be explained by the differences in the fragmentation model as mentioned before. We have used also a different normalization procedure in both tables and the different selection procedures to obtain the data. As explained before, ISAJET data selection is closer to the experimental situation. Therefore we prefer to use the ISAJET simulation for the analysis.

In summary, we expect up to factor 2 difference in the K_S^0 multiplicity between the muon initiated heavy flavour jet and an u-quark or a gluon jet. The differences in the jets not tagged by a muon are less certain and, within the statistics, we expect about the same multiplicity for all types of jets.

7.3.4 $p_t^{rel}(K_S^0)$ in the Monte Carlo data.

We have analyzed the relative p_t of a neutral kaon with respect to the calorimeter jet axis. The $< p_t^{rel}(K_S^0) >$ measured with respect to the calorimeter jet axis has been compared to the $< p_t^{rel}(K_S^0) >$ measured with respect to the axis build from the calorimeter jet and the closest CD-jet. The CD-jet has been selected the same way as for the non-isolated muons with the separation $\Delta R(j_{CA}, j_{CD}) < 1$. The jet axis is then $\vec{j} = \vec{j}_{CA} + \vec{j}_{CD}$. The required CD-jet could not always be found, however. The $p_t^{rel}(K_S^0)$ was about the same within the errors.

The results from the ISAJET Monte Carlo after the detector simulation are shown in table 7.8. Recall, that j_μ is a CD-jet containing a muon, whereas j_{op} is a calorimeter jet.

Table 7.8: *The $p_t^{rel}(K_S^0)$ in the ISAJET Monte Carlo data for jets of different origin. Number of events is given in the parenthesis.*

selection	muon jet j_μ $< p_t^{rel}(K_S^0) > [GeV/c]$	recoil jet j_{op} $< p_t^{rel}(K_S^0) > [GeV/c]$
$b\bar{b}$	0.51 ± 0.02 (204)	0.53 ± 0.04 (53)
$c\bar{c}$	0.38 ± 0.04 (65)	0.53 ± 0.11 (12)
gluon		0.55 ± 0.04 (106)
q(uds)		0.46 ± 0.03 (58)

There is no difference between the relative transverse momentum of a neutral kaon in a gluon or a $b\bar{b}$ jet and in general not between the recoil jets of the heavy flavour decay. There is a difference in the muon jets between the $< p_t^{rel}(K_S^0) >$ in the $b\bar{b}$ and the $c\bar{c}$ initiated jets. The errors in the averaged p_t^{rel} have been calculated from the formula $\sigma = (r.m.s.)/\sqrt{N}$, where N is the number of events in the sample. Since this formula is rather inaccurate for low statistics, we give the number of events in parenthesis. Note, that the figure for p_t^{rel} in the $c\bar{c}$ recoil jets is not very representative, since there are only 12 events in this sample. The Eurojet program without the detector simulation gives $< p_t^{rel}(K_S^0) >= 0.43 \pm 0.005\, GeV/c$ for the $c\bar{c}$ events, the other Eurojet results for the p_t^{rel} are compatible with table 7.8.

7.3.5 $p_t^{rel}(K_S^0)$ for a leading K_S^0 in the Monte Carlo data.

As mentioned in the introduction, the $p_t^{rel}(\mu)$ has been successfully used to separate the heavy flavours [10]. With kaons, however, the differences in $p_t^{rel}(K_S^0)$ are masked by a long decay chain. A K_S^0 is likely to appear after several other decays, which dilutes the effect of the $p_t^{rel}(K_S^0)$ selection. Selection of events with a leading kaon in a jet might improve on this situation.

A leading kaon is determined by the comparison of its p_t with the transverse momenta of other particles in the CD-jet. A kaon belongs to a jet if $\Delta R(K_S^0, j) < 0.7$. For kaons in the muon jets j_μ, we compare the kaon p_t to all tracks except the muon. For the calorimeter jets we select j_{CD} closest to the j_{CA}-axis, but not outside the $\Delta R = 1$ cone.

In a muon jet, we call a kaon leading, if it has a p_t larger than all other particles in the jet, excluding the muon. In the other jets we count all the particles, and a kaon is less likely to be leading.

Leading neutral kaons are created in less than 5% of the jets in the Monte Carlo data. We calculate the probability to obtain a leading kaon, normalized to the number of kaons in a jet. Table 7.9 summarizes these probabilities in the muon jet and in the recoil jet. Almost 50% of kaons in the muon jet are leading, whereas in the recoil jet (or in jets in general) this percentage drops to less than 30%. Especially the u-jets are not likely to produce a leading neutral kaon, probably because the leading neutral kaon in u-jet must come from a K^* decay (see entry q(uds) in table 7.9, which contains for 61% an u-quark contribution). Hence, for the recoil jets the percentage of the 'next to leading' kaons has been calculated. We call a kaon 'next to leading', if there is exactly one track in the jet with p_t larger than the transverse momentum of the kaon. The 'next to leading' kaon kinematics in jets without a muon corresponds to the kinematics of a leading kaon in the muon jets, where we do not count the muon when determining the kaon leadership. As summarized in table 7.9 the percentage of the 'next to leading' kaons is about the same as the leading kaons, except for the u-quark jet, where the increase is factor 3. In total, the percentage of the leading+'next to leading' kaons in the recoil jets are about 50% for the $b\bar{b}$ and the gluon jets. This is compatible with the percentage of leading kaons obtained in the muon tagged jets. This percentage is lower for the u-quark jets (a total of 34%) and perhaps also in the c-quark jets ($22 \pm 14\%$).

Table 7.9: *Percentage of the Monte Carlo generated kaons that are leading and 'next to leading' in different types of jets.*

selection	muon jet j_μ leading K_S^0	recoil jet j_{op} leading K_S^0	recoil jet j_{op} 'next to leading' K_S^0
$b\bar{b}$	48 ± 6	24 ± 7	32 ± 9
$c\bar{c}$	46 ± 10	7 ± 8	15 ± 12
gluon		28 ± 6	26 ± 6
q(uds)		9 ± 4	25 ± 7

We have calculated the $p_t^{rel}(K_S^0)$ for the leading kaons in the muon jets. In view of the low statistics we have combined the leading and the 'next to leading' kaons for the calculation of $p_t^{rel}(K_S^0)$ in the recoil jets. The results are presented in the table 7.10.

Table 7.10: *The mean $p_t^{rel}(K_S^0)$ for leading and 'next to leading' kaons in the ISAJET Monte Carlo data for jets of different origin. Number of events is given in the parenthesis.*

selection	muon jet j_μ leading kaon $< p_t^{rel}(K_S^0) > [GeV/c]$	recoil jet j_{op} leading + 'next to leading' kaon $< p_t^{rel}(K_S^0) > [GeV/c]$
$b\bar{b}$	0.61 ± 0.04 (99)	0.56 ± 0.11 (27)
$c\bar{c}$	0.35 ± 0.05 (33)	0.40 ± 0.60 (3)
gluon		0.34 ± 0.06 (53)
q(uds)		0.54 ± 0.13 (18)

There is a clear difference in the mean $p_t^{rel}(K_S^0)$ between the $b\bar{b}$ and the $c\bar{c}$ $\mu - tagged$ jets. In the recoil jets, gluon jets seem to have lower $< p_t^{rel}(K_S^0) >$ than the $b\bar{b}$ jets.

We expect that the selective power of the $p_t^{rel}(K_S^0)$ variable is higher in the $\mu - tagged$ jets than in the recoil jets, because the latter are calorimeter jets and the jet axis is not very well defined. For the muon jets in the Central Detector, there is a high p_t muon track, which approximates closely the original quark direction. A calorimeter jet defines this direction with less precision. The CD–jets supporting a calorimeter jet are unlikely to define a proper jet axis either, because in the absence of a high momentum track this jet might contain a substantial contribution from neutral particles, not seen in the Central Detector. In addition to the difficult jet axis determination in the recoil jets, we have quite low statistics available for the present analysis. In conclusion, the leading kaons can be used for the event study only in the muon jets, where they might complement the information obtained from the $p_t^{rel}(\mu)$.

We have checked the effect of the selection of the leading kaons in the $b\bar{b}/c\bar{c}$ jets on the $p_t^{rel}(\mu)$ in these jets. We obtained $< p_t^{rel}(\mu) >= 0.58 \pm 0.03\, GeV/c$ in the sample with leading kaons and $< p_t^{rel}(\mu) >= 0.70 \pm 0.04\, GeV/c$ in the sample with non leading kaons. This unexpected decrease in the average $p_t^{rel}(\mu)$ in the sample with a leading kaon in the muon jet is caused by the change in jet profile after the selection of a leading K_S^0. In general, K^0's are produced at the end of the decay chain of a B–meson. If a K^0 from heavy quark decay is leading, then either the K^0 has been produced directly, or the contribution from the intermediary decaying particles to the jet p_t is small. The $c\bar{c}$ jets with a leading K_S^0 appear to be more collimated (as measured by the ΔR distribution of the jet particles with respect to the jet axis). In the $b\bar{b}$ data sample with leading kaons in the muon jet, these muon jets appear to be as wide (in ΔR) as before, however the jet axis is shifted towards the muon direction. Therefore the mean $< p_t^{rel}(\mu) >$ drops below the average of $0.66 \pm 0.02\, GeV/c$ (see eq. 7.4) in the data sample with leading kaons in the muon jet. We have remeasured the $p_t^{rel}(\mu)$ for the leading kaon selection for the $b\bar{b}$ and the $c\bar{c}$, see table 7.11.

Table 7.11: *The mean $p_t^{rel}(\mu)$ in events with leading kaons, compared to other selections, in the ISAJET Monte Carlo data.*

selection	$c\bar{c}$ $< p_t^{rel}(\mu) > [GeV/c]$	$b\bar{b}$ $< p_t^{rel}(\mu) > [GeV/c]$	$b\bar{b}+c\bar{c}$ $< p_t^{rel}(\mu) > [GeV/c]$
initial sample	0.51 ± 0.01	0.78 ± 0.01	0.655 ± 0.008
$\Delta R(K_S^0, j_\mu) < 0.7$	0.46 ± 0.02	0.73 ± 0.02	0.66 ± 0.02
Leading K_S^0 in j_μ	0.44 ± 0.03	0.68 ± 0.03	0.58 ± 0.03

In the event sample with leading kaons in the muon jet the $p_t^{rel}(\mu)$ is lower than in the initial sample. It is lower by about the same amount for the $b\bar{b}$ and the $c\bar{c}$ jets. This means, that although the jet profile is affected in both cases, the differences between the $b\bar{b}$ and the $c\bar{c}$ jets are preserved. It can be concluded also from table 7.9, that the ratio $b\bar{b}/c\bar{c}$ should remain the same after the leading K_S^0 selection, since the percentage of the leading kaons in the $b\bar{b}$ and the $c\bar{c}$ samples is about the same. An explicit calculation gives the ratio $b\bar{b}/c\bar{c}$ of 2.3 ± 0.3, independent of the presence of a leading kaon in the muon jet.

We have checked, that the sample with large $< p_t^{rel}(\mu) >$ (for instance in the $b\bar{b}$ sample or after the selection $p_t^{rel}(\mu) > 0.6\, GeV/c$) has also large $< p_t^{rel}(K_S^0) >$. This correlation is expected, since all particles from a heavy quark decay should have on the average a larger transverse momentum relative to the jet axis, compared to the p_t^{rel} of the decay products from a light quark. In any jet it is $\sum p_t^{rel} = 0$ for all particles in the jet, irrespective the value of $p_t^{rel}(\mu)$. Therefore $p_t^{rel}(\mu)$ and $p_t^{rel}(K^0)$ will tend to balance each other as a consequence of particle kinematics. The information we get from the $p_t^{rel}(K_S^0)$ of a neutral kaon on the heavy flavour production is therefore correlated to the information from the $p_t^{rel}(\mu)$ of the muon.

To prove this statement, we have calculated the azimuthal angle between the $\vec{p}_t^{rel}(\mu)$ and $\vec{p}_t^{rel}(K_S^0)$ around the jet axis. This distribution peaks at 180°, therefore the $\vec{p}_t^{rel}(\mu)$ and $\vec{p}_t^{rel}(K_S^0)$ balance each other relative to the jet axis. In section 7.4.3 this distribution will be demonstrated for real data.

In summary, the $p_t^{rel}(K_S^0)$ of a leading kaon in $\mu - tagged$ jets can be used the same way the $p_t^{rel}(\mu)$ is used to separate the heavy flavours.

7.3.6 Summary of the Monte Carlo study.

We have calculated the K_S^0 multiplicity and the mean $p_t^{rel}(K_S^0)$ in the $\mu-$*tagged* jets from heavy flavours and in the jets from heavy flavours not containing a muon. The same calculation has been done for gluon jets and for the mixture of the u,d,s jets in ratio 61/30/9. The $b\bar{b}$ and the $c\bar{c}$ $\mu-$ *tagged* jets have a rather large K_S^0 multiplicity, compared to gluon or light quark jets (table 7.7). The $b\bar{b}$ $\mu-$ *tagged* jets have a rather distinct $< p_t^{rel}(K_S^0) >$ (tables 7.8, 7.10), as compared to the $c\bar{c}$ jets. Differences between jets not containing a muon are smaller. Although the K_S^0 multiplicity and the $p_t^{rel}(K_S^0)$ in the latter jets follow the same trend as the muon tagged jets, our present statistics does not allow to draw any practical conclusions.

The ISAJET Monte Carlo data contains about 20 times the statistics of our real data. However, there are 10 times more single muon events with $p_t(\mu) > 7\,GeV/c$, as compared to the number of single muon events with $p_t(\mu) > 10\,GeV/c$. Therefore there is only a factor 2 difference in statistics between the real data and the Monte Carlo data. Nevertheless, the differences in the K_S^0 multiplicity and the mean $p_t^{rel}(K_S^0)$ between the jets, as presented in this section, will be even smaller in the real data, not only because of the lower statistics, but also because of the background contribution in real events.

In the present Monte Carlo data no muon background has been generated. Real data has the additional difficulty of background from the muons produced in the $K/\pi^{\pm}$ decays. Although the probability for a kaon in an u or a d jet might be lower than in a b or $\bar{b}$ jet (see table 7.7), the presence of a kaon does not guarantee a background free sample. As the Eurojet data shows, the probability to obtain a K_S^0 in an s-quark jet is higher than for all other quarks. Since the difference is quite big, this property might be present also in real data. The events selected with a leading K_S^0 in the jet might contain an $s\bar{s}$-system, which gives a high momentum muon from a $K/\pi^{\pm}$ decay in one jet and a leading kaon in the other jet. The $p_t^{rel}(\mu)$ should be lower in jets from light quarks, however. In section 7.4.2 we will check the $p_t^{rel}(\mu)$ for several K_S^0 selections.

In conclusion, there is little hope to separate the jets from different origin in the real data, unless they are tagged by a muon. In the $\mu-$ *tagged* jets we can try to use the kaon instead of the muon in the study of the heavy flavour production. For instance we can try to select events with a muon jet containing a leading neutral kaon with a high $p_t^{rel}(K_S^0)$. This is a signature for a $b\bar{b}$ event.

7.4 The K_S^0 properties in real data.

7.4.1 K_S^0 multiplicity in real data.

The selection of the muons and the calorimeter jets has been described in section 7.2. In summary, there are 282 events with a μ, K_S^0 and j_{op} topology, where $p_t(\mu) > 7\,GeV/c$, $p_t(K_S^0) > 0.5\,GeV/c$ and $E_t(j_{op}) > 10\,GeV$ (validated).

A statistical separation of the $b\bar{b}$ and $c\bar{c}$ events in the single muon sample has been performed using the $p_t^{rel}(\mu)$ of the muon. The $p_t^{rel}(\mu)$ distribution in real data containing a kaon in the muon jet will be shown in fig. 7.7. A $b\bar{b}$ enriched data sample is obtained by requiring $p_t^{rel}(\mu) > 0.6\,GeV/c$. A Monte Carlo study shows that $c\bar{c}$ contribution to muons with $p_t^{rel} > 0.6\,GeV/c$ is reduced to 15%, whereas for the $p_t^{rel} < 0.6\,GeV/c$ the contribution from $c\bar{c}$ events has increased to 40%, see table 7.4.

The distribution of neutral kaons in the cone around the muon jet and its opposite jet is shown in fig. 7.2 – 7.5. There is a clustering of kaons in the direction of the jets, which can be observed in the ΔR^2 plot. Table 7.12 summarizes the K_S^0 multiplicity for the $b\bar{b}/c\bar{c}$ enhanced jets and their recoil jets respectively. In general, the ISAJET Monte Carlo described in section 7.3

predicts correctly the K_S^0 multiplicity in the real data. The K_S^0 multiplicity is lower than expected in the opposite jet in the sample with $p_t^{rel}(\mu) > 0.6\,GeV/c$. The size of the effect is apparent from the comparison of fig. 7.2 and 7.3. However at the present level of statistics we conclude, that the measured multiplicities are compatible with the predictions from the Monte Carlo.

Table 7.12: *K_S^0 multiplicity for the muon jets, selected according to their p_t^{rel} and their recoil jets, compared to the Monte Carlo data.*

selection	num. jets real data	num. kaons in $\Delta R < 0.7$	multiplicity real data	multiplicity Monte Carlo
j_{op} not required				
j_μ	761	118	0.15 ± 0.01	
j_μ with $p_t^{rel}(\mu) > 0.6\,GeV/c$	322	60	0.19 ± 0.03	
j_μ with $p_t^{rel}(\mu) < 0.6\,GeV/c$	439	58	0.13 ± 0.02	
j_{op} required				
j_μ	367	49	0.13 ± 0.02	
j_{op}		42	0.11 ± 0.02	
j_μ with $p_t^{rel}(\mu) > 0.6\,GeV/c$	151	24	0.16 ± 0.03	0.14 ± 0.01
j_{op} with $p_t^{rel}(\mu) > 0.6\,GeV/c$		11	0.07 ± 0.02	0.11 ± 0.01
j_μ with $p_t^{rel}(\mu) < 0.6\,GeV/c$	216	25	0.12 ± 0.02	0.17 ± 0.02
j_{op} with $p_t^{rel}(\mu) < 0.6\,GeV/c$		31	0.14 ± 0.03	0.11 ± 0.01

The K_S^0 multiplicity is rather difficult to study, because the normalization cannot be handled easily. There is no 'natural' normalization for the K_S^0 multiplicity. The multiplicity has been normalized on the number of jets in the present analysis. It could be normalized, for instance on the number of tracks in the jet. The K^0 multiplicity depends in each case on the relative activity of the background, which is difficult to model in a Monte Carlo program.

In comparing the real data with ISAJET predictions it should be remembered, that the selection of events in the Monte Carlo data contains muons with $p_t(\mu) > 10\,GeV/c$, compared to $p_t(\mu) > 7\,GeV/c$ in real data. Although we do not expect large deviations in the conclusions due to this difference, the exact multiplicity figures can suffer from the effect of the dependence of the quark fragmentation on quark energy, mentioned in section 7.3.3. The p_t^{rel} variable depends less on the jet energy.

7.4.2 The $p_t^{rel}(\mu)$ after the K_S^0 selection in the real data.

Neutral kaons are selected with $p_t(K_S^0) > 0.5\,GeV/c$ and $|y(K_S^0)| < 2.5$. The Monte Carlo study shows, that these two cuts reduce the background of kaons from the spectator quarks (underlying event) to 30% in our sample. In summary, events are selected with:

- $p_t(\mu) > 7\,GeV/c$ - $p_t(K_S^0) > 0.5\,GeV/c$
- μ non-isolated   - $y(K_S^0)| < 2.5$

After this selection we are left with 564 events, see table 7.1.

Fig 7.6 shows the distribution of neutral kaons as function of $\Delta R^2(K_S^0, j_\mu)$ and the corresponding $\Delta y \times \Delta\phi$ scatter plot with the original muon direction. There is an enhancement in the number of kaons close to the muon.

We have seen in the Monte Carlo study that the kaon multiplicity in heavy quark jets (tagged by a muon) is higher than in gluon or light quark jets (see table 7.7). If the muons from $K/\pi^\pm$ decays (decay background) are produced in the gluon or u,d–quark jets, we expect a larger content of heavy quark muon jets after K_S^0 selection. Then the mean $< p_t^{rel}(\mu) >$ should

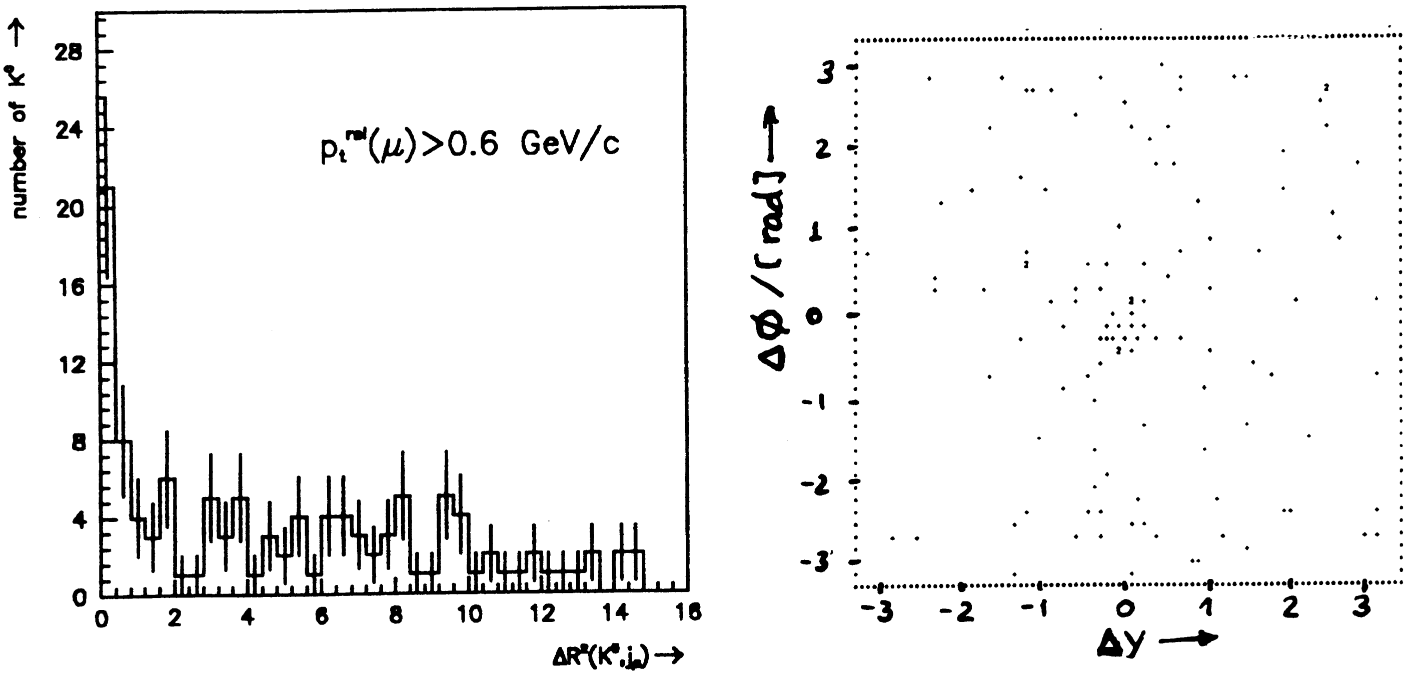

Figure 7.2: *Distribution of neutral kaons relative to a muon jet for* $p_t^{rel}(\mu) > 0.6$. *a)* $\Delta R^2(K_S^0, j_\mu)$*; b)* $\Delta y \times \Delta\phi(K_S^0, j_\mu)$.

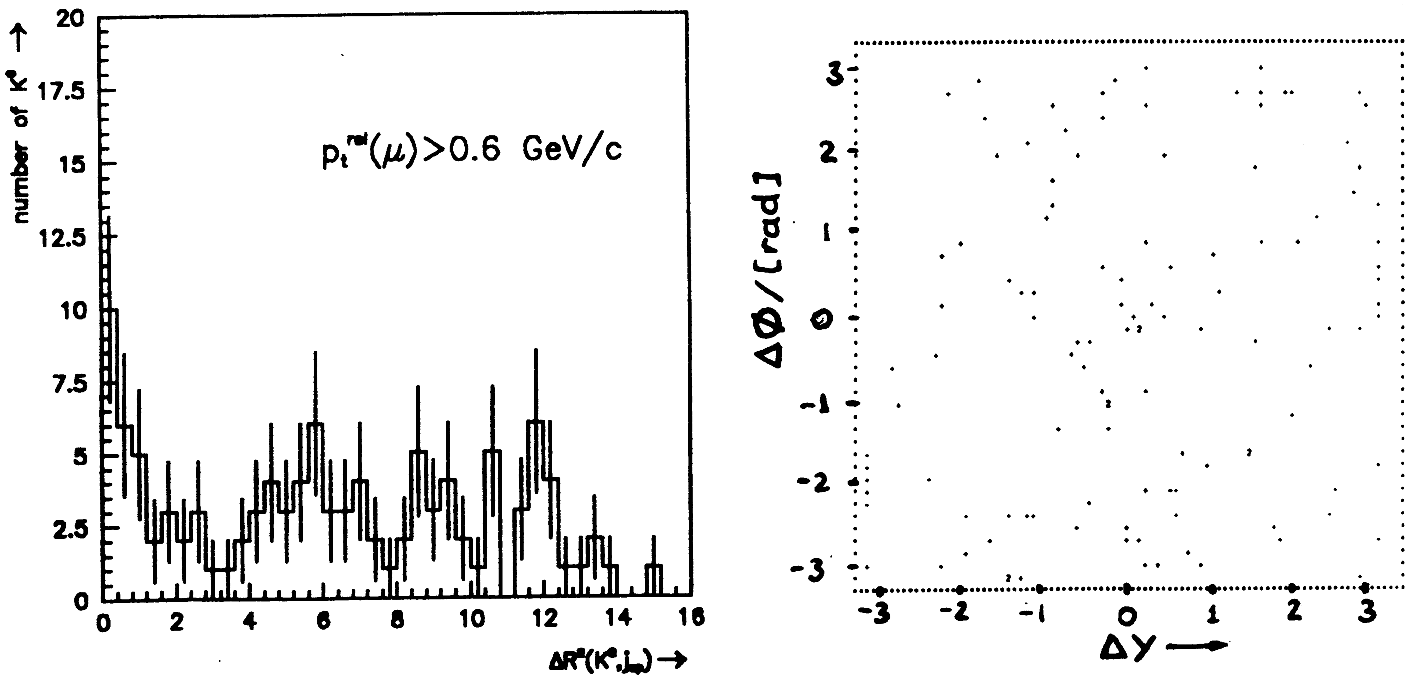

Figure 7.3: *Distribution of neutral kaons relative to a muon balancing jet for* $p_t^{rel}(\mu) > 0.6$. *a)* $\Delta R^2(K_S^0, j_{op})$*; b)* $\Delta y \times \Delta\phi(K_S^0, j_{op})$.

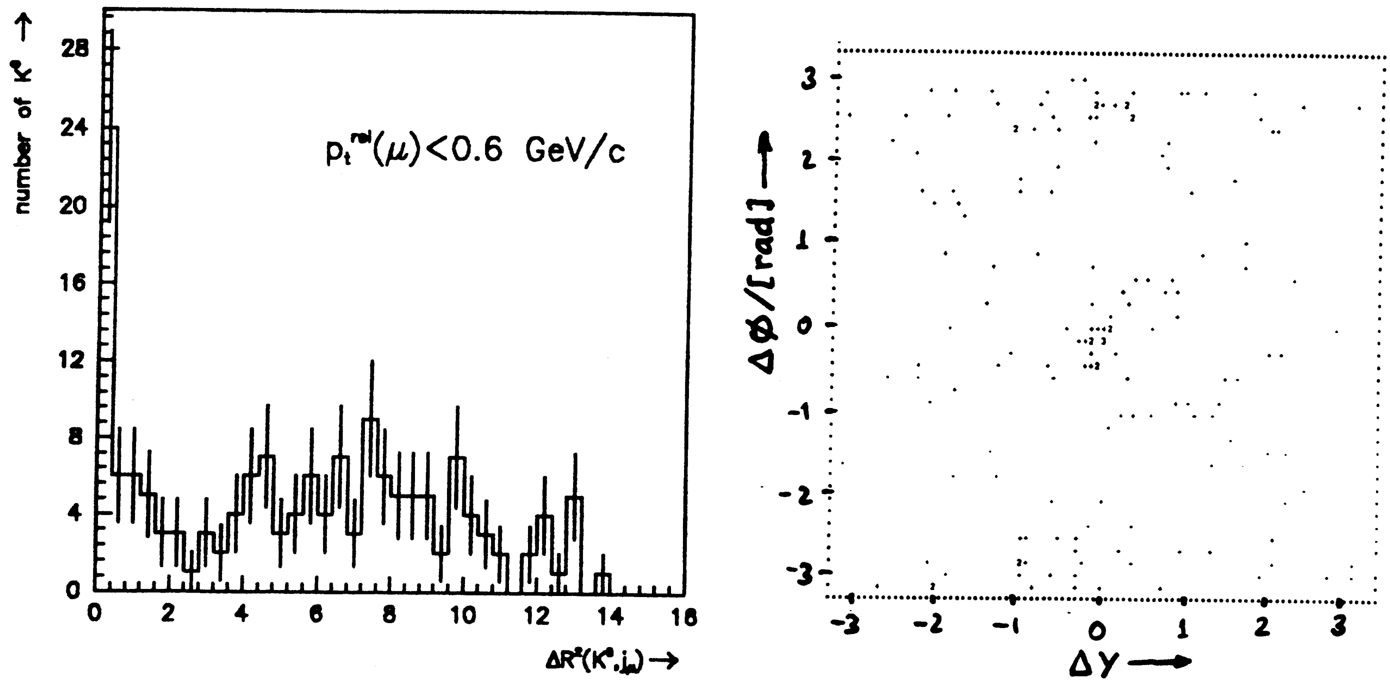

Figure 7.4: *Distribution of neutral kaons relative to a muon jet for* $p_t^{rel}(\mu) < 0.6$. *a)* $\Delta R^2(K_S^0, j_\mu)$*; b)* $\Delta y \times \Delta\phi(K_S^0, j_\mu)$.

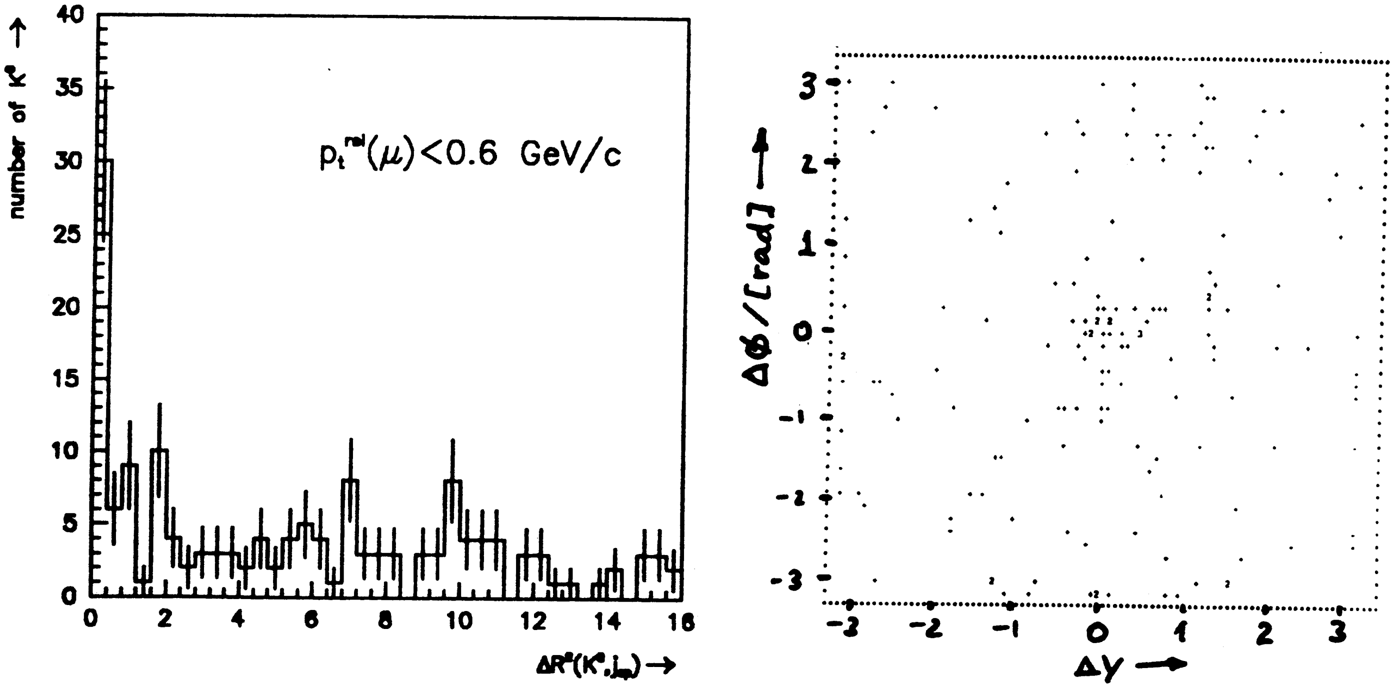

Figure 7.5: *Distribution of neutral kaons relative to a muon balancing jet for* $p_t^{rel}(\mu) < 0.6$. *a)* $\Delta R^2(K_S^0, j_{op})$*; b)* $\Delta y \times \Delta\phi(K_S^0, j_{op})$.

increase after the kaon selection in the jets. However, as explained in section 7.3.6 the decay background has not been modeled in this Monte Carlo program, in particular the contribution from s–quark is unknown.

We have measured the $p_t^{rel}(\mu)$ before and after the kaon selection within the $\Delta R < 0.7$ cone. Note that the balancing jet topology was not required. After the selection $\Delta R(K_S^0, j_\mu) < 0.7$ the sample is reduced to 118 events, see fig 7.7.

$$< p_t^{rel}(\mu) > \; = \; 0.60 \pm 0.01\, GeV/c \tag{7.6}$$

$$\Delta R(j_\mu, K_S^0) < 0.7 \qquad < p_t^{rel}(\mu) > \; = \; 0.64 \pm 0.05\, GeV/c \tag{7.7}$$

Thus, after the selection of events, containing a K_S^0 in the muon jet, the $< p_t^{rel} >$ of the muon with respect to that jet is barely affected. The mean p_t^{rel} after the kaon selection is as expected from the $b\bar{b}/c\bar{c}$ Monte Carlo (see equations 7.3, 7.4).

7.4.3 The $p_t^{rel}(\mu)$ in jets with leading K_S^0.

The ISAJET Monte Carlo program predicts about 50% of leading kaons in the $b\bar{b}/c\bar{c}$ sample. Recall, that we do not include the muon track when determining the leadership of the kaon in muon jets; in jets without a muon all tracks are counted. In the real data we find 75 events with a leading kaon in the muon jet. It is $(64 \pm 9)\%$ of the sample with a kaon within $\Delta R < 0.7$ (118 events).

We have measured the $p_t^{rel}(\mu)$ in events with a leading kaon in the j_μ jet, see table 7.13. For the calculation of the mean $p_t^{rel}(\mu)$ in the table 7.13, no balancing jet structure was required. If we require the opposite jet topology the numbers do not change significantly.

Table 7.13: *The mean $p_t^{rel}(\mu)$ for leading kaons in the muon jet in real data. The expected values from the ISAJET $b\bar{b}/c\bar{c}$ are given in the second column. The numbers in parenthesis are the number of events in the sample.*

selection	$< p_t^{rel}(\mu) > [GeV/c]$ real data	$< p_t^{rel}(\mu) > [GeV/c]$ Monte Carlo data
leading kaon in j_μ	0.59 ± 0.04 (75)	0.58 ± 0.03 (132)
kaon not leading in j_μ	0.78 ± 0.07 (43)	0.70 ± 0.04 (137)

In table 7.13 we see a slightly lower value of $p_t^{rel}(\mu)$ in the sample with leading kaons, as compared to the value given in eq. 7.7. The $p_t^{rel}(\mu)$ for the sample of the non-leading kaons increases, as compared to the average in eq. 7.7. This effect is reproduced in the Monte Carlo; it is the change in the jet profile, explained in section 7.3.5.

As discussed in section 7.3.5, the information on heavy flavour production obtained from $p_t^{rel}(\mu)$ is identical to the information obtained from $p_t^{rel}(K_S^0)$ of a leading kaon in the muon jet. This point is illustrated in figure 7.8, where the difference in azimuthal angle around the jet axis between a kaon and a muon has been plotted. Similarly to the distribution obtained in the Monte Carlo generated data, the angle between the muon and the kaon tends to 180°. Therefore $p_t^{rel}(\mu)$ and $p_t^{rel}(K_S^0)$ balance each other relative to the jet axis.

7.4.4 The $p_t^{rel}(K_S^0)$ for a leading kaon in real data.

The percentage of the leading kaons in the muon jets and their recoil jets is shown in table 7.14. In general, the percentages of the leading kaons are reproduced with the Monte Carlo, see

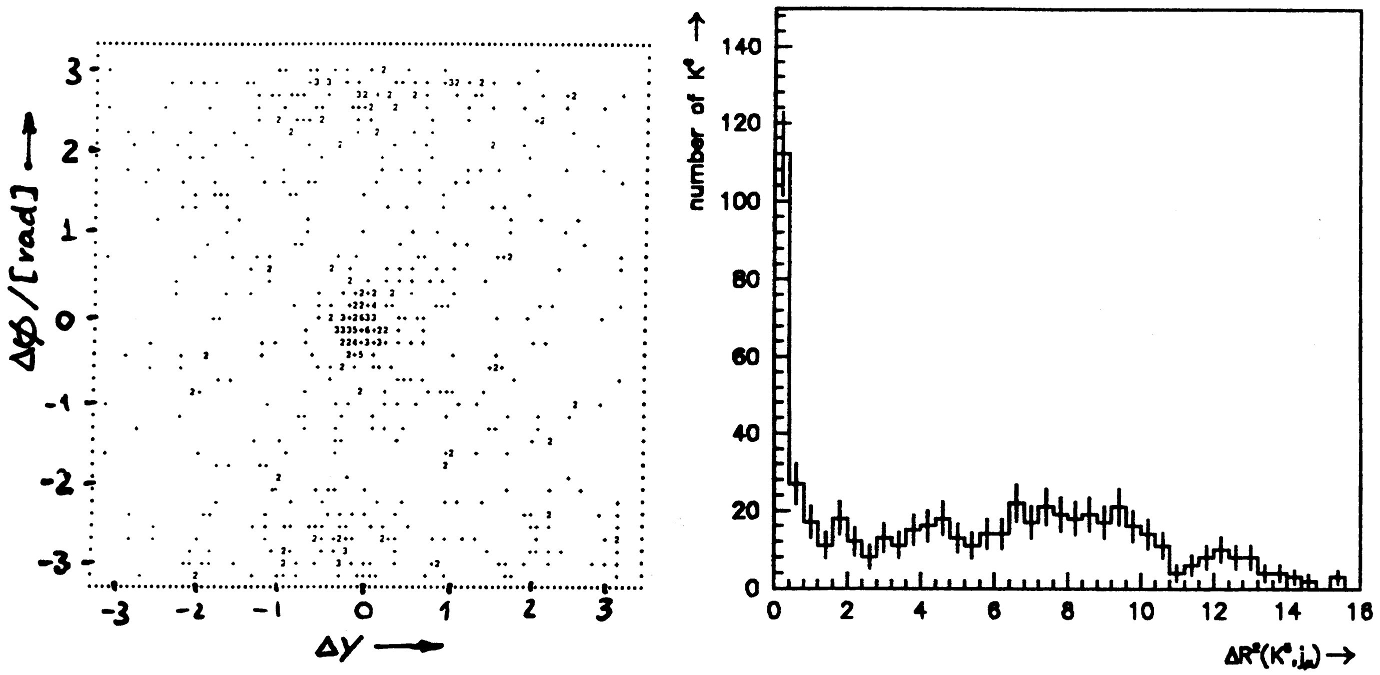

Figure 7.6: *Spatial separation between a kaon and a muon within a jet.*

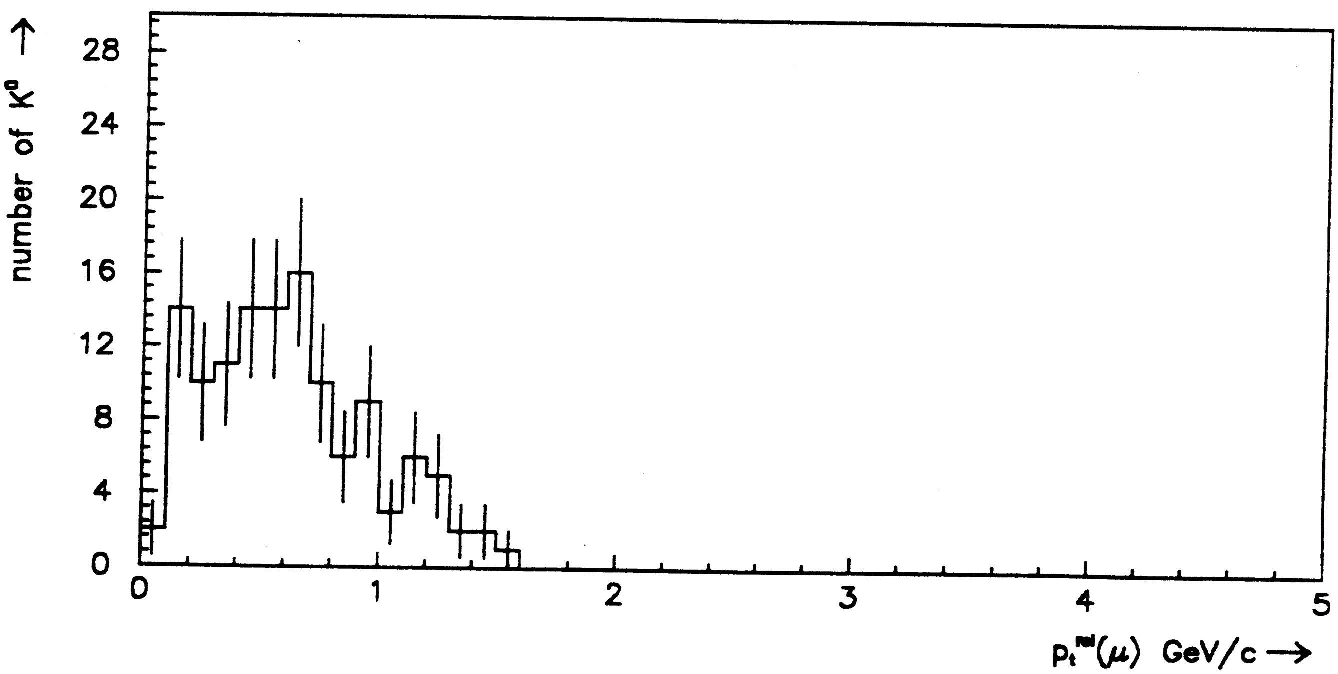

Figure 7.7: *The muon p_t relative to its jet containing a kaon.*

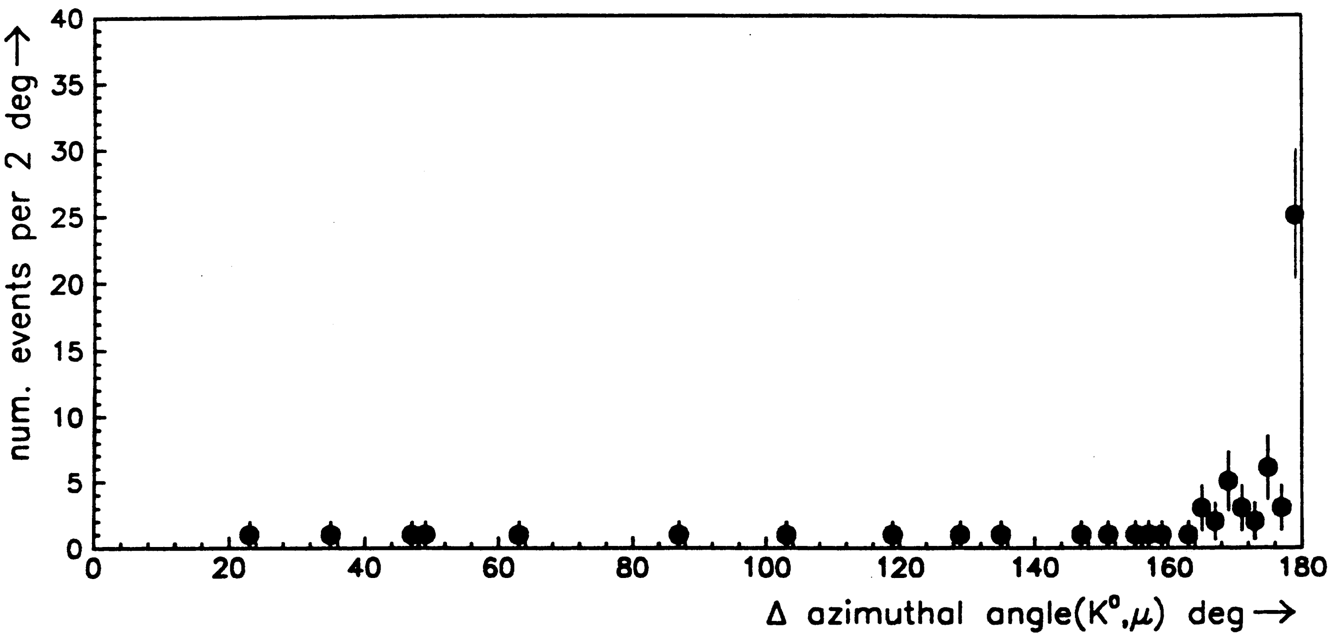

Figure 7.8: *The difference in azimuthal angle between K_S^0 and a muon relative to jet axis.*

table 7.9. The number of the leading kaons in the recoil jets is quite low, therefore the analysis of the $p_t^{rel}(K_S^0)$ in these jets has not been attempted (errors are nearly 100%).

Table 7.14: *Percentage of leading K_S^0 for the muon jets and their recoil jets.*

selection	percentage of K_S^0 leading [%]	percentage of K_S^0 leading+'next to leading' [%]
j_{op} not required		
j_μ	63 ± 9	
j_μ with $p_t^{rel}(\mu) > 0.6\,GeV/c$	55 ± 12	
j_μ with $p_t^{rel}(\mu) < 0.6\,GeV/c$	72 ± 15	
j_{op} required		
j_μ	53 ± 13	
j_{op}	24 ± 8	57 ± 15
j_μ with $p_t^{rel}(\mu) > 0.6\,GeV/c$	42 ± 16	
j_{op} with $p_t^{rel}(\mu) > 0.6\,GeV/c$	18 ± 14	54 ± 28
j_μ with $p_t^{rel}(\mu) < 0.6\,GeV/c$	64 ± 20	
j_{op} with $p_t^{rel}(\mu) < 0.6\,GeV/c$	26 ± 10	58 ± 17

In the muon jets we have obtained the averaged $< p_t^{rel}(K_S^0) >$ for the 75 leading neutral kaons in the cone $\Delta R(K_S^0, j_\mu) < 0.7$:

$$< p_t^{rel}(K_S^0) > = 0.52 \pm 0.04\,GeV/c \qquad (7.8)$$

The data has been compared to the predictions from the ISAJET Monte Carlo in fig. 7.9. Note that the ISAJET predictions have been normalized to the number of events in the real data sample with $p_t(\mu) > 7\,GeV/c$.

To estimate the $b\bar{b}$ fraction from equation 7.8 we assume the same $p_t^{rel}(K^0)$ for the background, as for the $c\bar{c}$ sample. It has been found in the analysis of the muon $p_t^{rel}(\mu)$, that the background $p_t^{rel}(\mu)$ distribution is close to the $c\bar{c}$ distribution [39]. Using table 7.10 we solve for

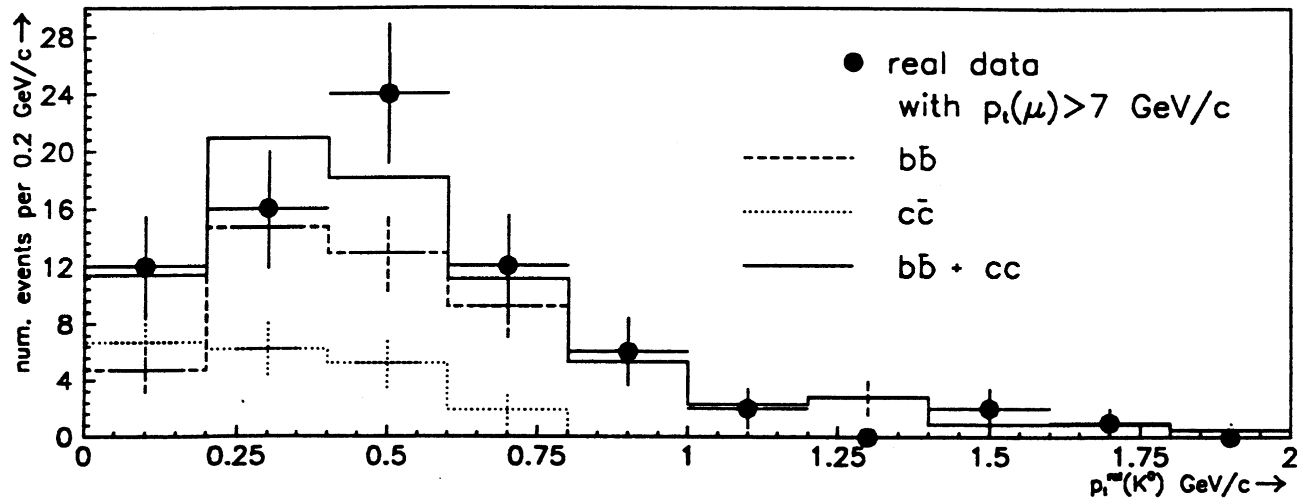

Figure 7.9: *The $p_t^{rel}(K_S^0)$ in real data with $p_t(\mu) > 7\,GeV/c$ compared to ISAJET predictions for the $b\bar{b}$ and the $c\bar{c}$ contributions. The Monte Carlo predictions have been normalized to the number of events in real data.*

the fraction x of the $b\bar{b}$ events the equation 0.61x+0.35(1-x)=0.52:

$$fraction\ of\ b\bar{b}\ =\ 0.7 \pm 0.3 \tag{7.9}$$

The error is statistical. This result can be compared to $(35 \pm 4^{+2}_{-1})$% calculated from the fit of the muon background distribution and the ISAJET predictions for $b\bar{b}/c\bar{c}$ to the muon $p_t^{rel}(\mu)$ [39]. There is no reason for these two results to be the same, since we have a different data selection with a leading neutral kaon in the muon jet.

7.4.5 The K_S^0 selection in the data sample with $p_t(\mu) > 6\,GeV/c$.

In section 7.4.2 we have studied the K_S^0 production in the single muon sample with $p_t(\mu) > 7\,GeV/c$, non-isolated. Certain selections for K_S^0 have been applied to create a cleaner sample with less muon background. The criterion for a cleaner sample is a large value of the $p_t^{rel}(\mu)$, typically above $0.6\,GeV/c$. The following conclusions have been reached:

- Selection of a K_S^0 in a $\Delta R < 0.7$ cone around the muon jet does not change the mean $p_t^{rel}(\mu)$ significantly. See eq. 7.6, 7.7 for the real data and eq. 7.3, 7.4 for the Monte Carlo data.

- Selection of a leading K_S^0 decreases the average $p_t^{rel}(\mu)$ due to a change in the muon jet profile, but it preserves the differences between the average $p_t^{rel}(\mu)$ in the $b\bar{b}$ and the $c\bar{c}$ Monte Carlo samples. See table 7.11.

- Since the $p_t^{rel}(K_S^0)$ is higher for the $b\bar{b}$ events than for the muon background, it is possible to select a cleaner $b\bar{b}$ sample by requiring a kaon of high $p_t^{rel}(K_S^0)$ near to the muon (see section 7.3.4.

- The $p_t^{rel}(K_S^0)$ can be used for the heavy flavour separation the same way as the $p_t^{rel}(\mu)$ is used, see section 7.3.4 and 7.3.5.

- A data sample with leading kaons and with a high $p_t^{rel}(K_S^0)$ value will contain muons with a large $p_t^{rel}(\mu)$, because of the correlation between $p_t^{rel}(K_S^0)$ and $p_t^{rel}(\mu)$ discussed in section 7.3.5.

The selection criteria according to these conclusions have been applied to the much larger data sample with $p_t(\mu) > 6\,GeV/c$. The background in this data sample is about 70% [39]. The kaons and the jets have been selected as described in section 7.2. The results of the kaon selection are summarized in table 7.15.

Table 7.15: *The $p_t^{rel}(\mu)$ in the sample with $p_t(\mu) > 6\,GeV/c$ for several K_S^0 cuts. The numbers in parenthesis give the number of events in the sample.*

selection	real data $< p_t^{rel}(\mu) >$ [GeV/c]	Monte Carlo $< p_t^{rel}(\mu) >$ [GeV/c]
initial sample, non-isolated muons with $p_t(\mu) > 6\,GeV/c$	0.58 ± 0.01 (2188)	0.655 ± 0.008
$\Delta R(K_S^0, j_\mu) < 0.7$	0.59 ± 0.02 (218)	0.66 ± 0.02
$\Delta R < 0.7$; $p_t^{rel}(K_S^0) > 0.6\,GeV$	0.77 ± 0.04 (59)	0.81 ± 0.05
$\Delta R < 0.7$; leading K_S^0 in j_μ	0.57 ± 0.03 (132)	0.58 ± 0.03
$\Delta R < 0.7$; leading K_S^0 in j_μ; $p_t^{rel}(K_S^0) > 0.6\,GeV/c$	0.84 ± 0.05 (40)	0.83 ± 0.06

As expected, the average $p_t^{rel}(\mu)$ is large in the sample with a kaon within the cone of $\Delta R < 0.7$ and $p_t^{rel}(K_S^0) > 0.6\,GeV/c$. The fraction of the $b\bar{b}$ events in the event sample with a leading kaon in the muon jet is 0.5 ± 0.4, as can be calculated using table 7.11 (and solving for the $b\bar{b}$ fraction x in 0.68x+0.44(1-x)=0.57). Hereby we assumed, that the muon background has about the same distribution, as the $c\bar{c}$ events.

The analysis of the $p_t^{rel}(K_S^0)$ of a leading kaon in a muon jet gives in this sample (with $p_t(\mu) > 6\,GeV/c$) $< p_t^{rel}(K_S^0) >= 0.52 \pm 0.03\,GeV/c$. The equality of this value with the average $< p_t^{rel}(K_S^0) >$ obtained in an event sample with less background (see section 7.4.4, eq. 7.8) is compatible with a conclusion, that the selection of a leading kaon in muon jet selects mainly $b\bar{b}$ and $c\bar{c}$ events.

The distribution of the $p_t^{rel}(K_S^0)$ of a leading kaon is shown in fig 7.10, where we have normalized the ISAJET predictions to the number of events in real data with $p_t(\mu) > 6\,GeV/c$. The more accurate measurements of the $b\bar{b}$ fraction are discussed in appendix B.

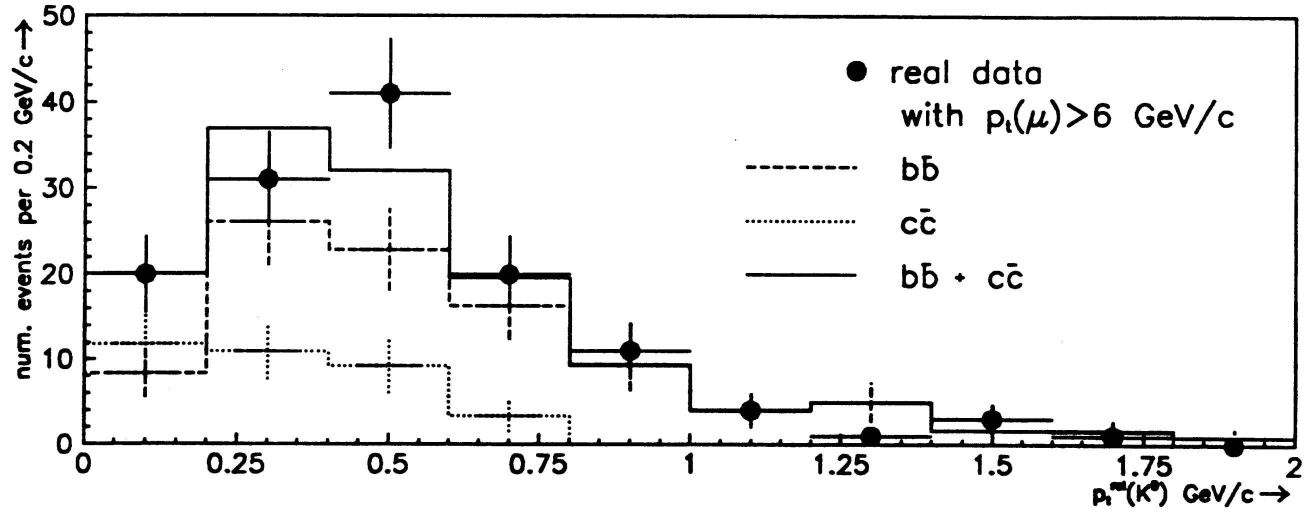

Figure 7.10: *The $p_t^{rel}(K_S^0)$ in real data (with $p_t(\mu) > 6\,GeV/c$) compared to ISAJET predictions for the $b\bar{b}$ and the $c\bar{c}$ contributions. The Monte Carlo predictions have been normalized to the number of events in real data.*

In conclusion, the behavior of data is as expected from the heavy flavour production.

Chapter 8

Summary and conclusions.

The present work was done within the UA1 collaboration at the CERN $p\bar{p}$ Collider at the CM energy of $\sqrt{s} = 630\,GeV$. Its objective was to study the use of neutral kaons for the identification of jets produced by the heavy b and c quarks.

Jets are highly collimated streams of particles produced in the fragmentation of quarks and gluons. For the study of the properties of the heavy quarks it is necessary to identify their jets.

As muons can be detected in jets, they have been used so far to tag the production of the heavy quarks in their semileptonic decay mode. Neutral kaons can also be detected in jets measured in the UA1 Central Detector. As discussed in chapter 2, the 'Standard Model' describes the production of the b and c quarks in $p\bar{p}$ collisions. Within this model neutral kaons can be produced in the decay chain of the heavy quarks (for example $b \rightarrow c \rightarrow s$ is the favorite decay mode of the b quark). Therefore an attempt was made to use these neutral kaons instead of, or in conjunction with the muons.

For the study of neutral kaons in jets a data sample has been used with events containing at least one muon with transverse momentum above 6 GeV/c and with one or more calorimeter jets, the so called 'single muon events'. As compared to the jets detected in the calorimeter, the Central Detector provides a better spatial measurement of the jet axis. The relative transverse momentum of the muon with respect to the axis of this jet in the Central Detector measures the probability for the quark flavour producing the jet. Previous studies of this data sample using the $p_t^{rel}(\mu)$ distribution have shown, that about 51% of the muons with the transverse momentum $p_t(\mu)$ of 10 GeV/c come from a semileptonic decay of a b quark and about 16% from a c quark [10]. However, the full data sample with $p_t(\mu) > 6\,GeV/c$ is dominated by up to 70% background from $\pi^{\pm}$ and $K^{\pm}$ decays into muons (see chapter 3). An additional information from the neutral kaon helps to reduce this background.

The K_S^0 was reconstructed in the UA1 Central Detector from its decay into a $\pi^+\pi^-$ pair with a signal to background ratio of $\geq 4.4 \pm 0.2$ (depending on the set of cuts used), see chapter 4. The reconstruction efficiency is about 15%, see chapter 5. The total inclusive K_S^0 production cross section in the 'single muon events' with a kaon rapidity within $|y| < 2.5$ and transverse momentum above 0.2 GeV/c is $164 \pm 17 \pm 25\,nb$; the first error is statistical and the second is systematical (chapter 6).

There are about 1.3 K_S^0's per event after the efficiency correction in the single muon sample. This multiplicity is comparable to the K_S^0 multiplicity of about 0.6 in the 'minimum bias events'. The 'minimum bias events' result from the simultaneous break up of both the proton and the antiproton in their collision. But, in general, they contain neither heavy quarks nor jet activity. A precise comparison of the K_S^0 multiplicities in both types of events was not possible due to the (technical) differences in their normalization. However, the K_S^0 inclusive cross section falls less steeply with increasing transverse momentum of the kaon in the 'single muon events', than in the 'minimum bias events'. Thus, in general, neutral kaons with a high transverse momentum (over 0.5 or 1 GeV/c) are produced in jets.

There is indeed a clustering of kaons in the direction of the jets observed in the real data (see chapter 7). However, this did not help much for the identification of the quarks producing the jets, because a high momentum K^0_S can be produced in any kind of a gluon or a quark jet.

The number of K^0_S's per jet have been studied with Monte Carlo data for different types of jets. It has been concluded, that the differences in the K^0_S multiplicity in various jets are small and cannot be used for the jet identification. The relative transverse momenta of the kaons with respect to the jet axis are similar in various types of jets and cannot be used for the jet identification either. One important exception are the Central Detector jets containing a muon. In these muon jets the difference in the average $< p_t^{rel}(K^0_S) >$ obtained in the Monte Carlo data between the jets from a b quark and the jets from a c quark is about 0.13 GeV/c.

The differences in the $p_t^{rel}(K^0_S)$ between the b quark and the c quark jets originate mainly from a leading kaon. (A leading kaon in a muon jet has transverse momentum larger than all other particles in the jet in the Central Detector, except the muon.) A leading kaon could be found in almost 50% of the 'single muon events' with a K^0 in the muon jet. In general, a kaon is produced at the end of the decay chain of a heavy quark, therefore the effect of the heavy quark mass on the $p_t^{rel}(K^0_S)$ is diluted. If, however, a K^0 from a heavy quark is leading, then either the K^0 has been produced directly, or the contribution from the intermediary decaying particles to the jet p_t is small. In the muon jets the difference in the average relative transverse momentum of a leading kaon between the jets from a b quark and the jets from a c quark is about 0.26 GeV/c. Furthermore, the $p_t^{rel}(K^0_S)$ of a leading kaon with respect to the muon jet axis contains essentially the same information on the heavy flavour production, as the $p_t^{rel}(\mu)$ of the muon itself. Therefore, as the Monte Carlo data show, the $p_t^{rel}(K^0_S)$ of a leading kaon in the muon jet can be used for a separation of the $b\bar{b}$ events from the $c\bar{c}$ events and from the background.

The multiplicities of K^0_S and the relative transverse momenta $p_t^{rel}(K^0_S)$ in jets measured in the real data are comparable to the values expected from the $b\bar{b}/c\bar{c}$ Monte Carlo. The Monte Carlo $b\bar{b}$ and $c\bar{c}$ $p_t^{rel}(\mu)$ distributions have been fitted to the experimental $p_t^{rel}(\mu)$ distribution in muon jets containing a neutral kaon. A fraction of $b\bar{b}$ events of 0.65 ± 0.12 has been obtained in the sample with $p_t(\mu) > 7\,GeV/c$ and 0.55 ± 0.09 in the sample with $p_t(\mu) > 6\,GeV/c$, see appendix B. The $p_t^{rel}(K^0_S)$ of the leading K^0_S has been used for the calculation of the $b\bar{b}$ fraction in the single muon events with compatible results. Thus, a data sample with less muon background is selected by requiring a kaon in the muon jet.

The method of the analysis of heavy flavour production in single muon events with a K^0_S in the muon jet has the severe disadvantage of a low K^0_S reconstruction efficiency, of the order of 15% in the UA1 Central Detector. Therefore the heavy flavour separation with muons only is far more efficient. The use of neutral kaons would be justified in jets without the muon tag for the heavy flavour. However, in jets not tagged by a muon no meaningful kaon signal could be deduced from the investigated data samples.

Chapter 9

Samenvatting

Het beschreven onderzoek maakt deel uit van de UA1 experiment by de CERN $p\bar{p}$ Collider by een zwaartepuntsenergie $\sqrt{s} = 630\,GeV$. Het doel van het onderzoek was jets die geproduceerd zijn door de zware b en c quarks, te identificeren met behulp van neutrale kaonen.

Jets zijn sterk gecollimeerde stromen deeltjes die ontstaan bij de fragmentatie van quarks en gluonen. Om de eigenschappen van de zware quarks te kunnen bestuderen moet men hun jets identificeren.

De muonen zijn tot nu toe gebruikt als kenmerk voor de productie van de zware quarks voor zover deze semileptonisch vervallen, omdat muonen in jets waargenomen kunnen worden. Ook neutrale kaonen kunnen worden waargenomen in jets die in de Centrale Detector van UA1 gemeten worden. Zoals besproken wordt in hst. 2, beschrijft het 'Standaard Model' de productie van de zware b and c quarks in $p\bar{p}$ botsingen. Binnen dit model kunnen neutrale kaonen worden geproduceerd in de vervalsketen van de zware quarks (bijvoorbeeld $b \to c \to s$ is de meest waarschijnlijke vervalswijse van het b quark). Daarom is gepoogd deze neutrale kaonen als kenmerk te gebruiken in plaats van of tezamen met de muonen.

Om neutrale kaonen in jets te bestuderen is een verzameling data gebruikt met een of meer muon gebeurtenissen met een transversale impuls groter dan 6 GeV/c en met een of meer jets in de calorimeter, de zogenaame 'één-muon' gebeurtenissen. Vergeleken met de jets die in de calorimeter worden gemeten, biedt de Centrale Detector een betere bepaling van de richting van de as van de jet. De relative transversale impuls van het muon ten opzichte van de as van zijn jet in de Centrale Detector is een maat voor de waarschijnlijkheid dat een bepaalde quark 'smaak' de jet produceert. Eerder onderzoek aan deze verzameling data met behulp van de $p_t^{rel}(\mu)$ verdeling heeft aangetoond dat ongeveer 51% van de muonen met een transversale impuls $p_t(\mu)$ boven 10 GeV/c ontstaan bij semileptonisch verval van een b quark en ongeveer 16% by een c quark. Echter de volledige verzameling data ($p_t(\mu) > 6\,GeV/c$) wordt overheerst door, een tot 70% oplopende, achtergrond afkomstig van $\pi^{\pm}$ en $K^{\pm}$ verval naar muonen (zie hst. 3). Extra informatie van de neutrale kaonen helpt deze achtergrond te reduceren.

Het K_S^0 werd gereconstrueerd in de Centrale Detector van UA1 van zijn verval in een $\pi^+\pi^-$ paar met een signal/achtergrond verhouding van $\geq 4.4 \pm 0.2$ (afhankelijk van de gebruikte afsnijdingen), zie hst. 4. De reconstructie efficiëntie is ongeveer 15%, zie hst. 5. De totale inclusieve werkzame doorsnede voor de productie van K_S^0 in de 'één–muon' gebeurtenissen met kaon rapiditeit $|y| < 2.5$ en transversale impuls groter dan 0.2 GeV/c, is $164 \pm 17 \pm 25\,nb$; de eerste fout is statistisch en de tweede systematisch (zie hst. 6).

Na correctie voor de reconstructie efficiëntie zijn er ongeveer 1.3 K_S^0 deeltjes per gebeurtenis in de 'één–muon' data. Deze multipliciteit is vergelijkbaar met de K_S^0 multipliciteit in de 'minimum bias' gebeurtenissen van ongeveer 0.6. Deze 'minimum bias' gebeurtenissen ontstaan waneer bij de botsing zowel het proton als het antiproton dissociëren. In het algemeen bevatten deze gebeurtenissen echter noch zware quarks, noch jet activiteit. Een precieze vergelijking van de K_S^0 multipliciteiten in beide soorten gebeurtenissen is niet mogelijk vanwege de (technische) verschillen in hun normalisatie. Echter, de inclusive werkzame doorsnede voor de productie van K_S^0 neemt minder snel af met toenemende transversale impuls van het kaon bij 'één–muon' gebeurtenissen dan bij de 'minimum bias' gebeurtenissen. Dus worden neutrale kaonen met een grote transversale impuls (groter dan 0.5 of 1 GeV/c) in het algemeen in jets geproduceerd.

Er treedt inderdaad opeenhoping op van kaonen in de richting van jets die in de reële data worden waargenomen (zie hst. 7). Dit draagt echter niet veel bij tot de identificatie van de quarks die deze jets produceren, omdat een K_S^0 met grote impuls in elke soort quark- of gluonjet geproduceerd kan worden.

Het aantal K_S^0 deeltjes per jet is bestudeerd met Monte Carlo data voor verschillende soorten jets. De verschillen in K_S^0 multipliciteit in de verschillende jets zijn klein en kunnen niet worden gebruikt om deze jets te identificeren. De relatieve transversale impuls van de kaonen ten opzichte van de as van de jet is ongeveer gelijk in verschillende soorten jets en kan evenmin worden gebruikt om de jets te identificeren. Een belangrijke uitzondering vormen de jets in de Centrale Detector die een muon bevatten. In deze muon jets is het verschil in de gemiddelde $< p_t^{rel}(K_S^0) >$ (zoals verkregen uit de Monte Carlo data) tussen jets afkomstig van een b quark en jets afkomstig van een c quark ongeveer 0.13 GeV/c.

De verschillen in $p_t^{rel}(K_S^0)$ tussen b quark jets en c quark jets zijn hoofdzakelijk afkomstig van een 'leidend' kaon. (Een leidend kaon in een muon jet heeft een grotere transversale impuls dan elk ander deeltje in de jet in de Centrale Detector, uitgezonderd het muon). In bijna 50% van de 'één–muon' gebeurtenissen met een K^0 in de muon jet kwam een leidend kaon voor. Omdat in het algemeen een kaon wordt geproduceerd aan het eind van de vervalsketen van een zware quark, is het effect van de massa van de zware quark op $p_t^{rel}(K_S^0)$ verzwakt. Als echter een K_S^0 afkomstig van een zware quark leidend is, dan is ofwel het K_S^0 rechtsteeks geproduceerd, ofwel de bijdrage van de vervallende tussenproducten aan de transversale impuls van de jet is klein. In de muon jets is het verschil in de gemiddelde relatieve transversale impuls van een leidend kaon tussen de jets afkomstig van een b quark en van een c quark ongeveer 0.26 GeV/c. Verder bevat de $p_t^{rel}(K_S^0)$ van een leidend kaon ten opzichte van de as van de muon jet in wezen dezelfde informatie over de productie van zwaare quarks als de $p_t^{rel}(\mu)$ van het muon zelf. Daarom kan, zoals de Monte Carlo data laten zien, de $p_t^{rel}(K_S^0)$ van een leidend kaon in de muon jet gebruikt worden om $b\bar{b}$ gebeurtenissen te scheiden van $c\bar{c}$ gebeurtenissen en van de achtergrond.

De K_S^0 multipliciteiten en de relatieve transversale impulsen $p_t^{rel}(K_S^0)$ in jets in de reële data zijn vergelijkbaar met de waarden die men verwacht uit de $b\bar{b}/c\bar{c}$ Monte Carlo. De Monte Carlo $b\bar{b}$ en $c\bar{c}$ $p_t^{rel}(\mu)$ verdelingen zijn aangepast aan de experimentele $p_t^{rel}(\mu)$ in de muon jet, die een neutrale kaon bevatten. Een fractie $b\bar{b}$ gebeurtenissen van 0.65 ± 0.12 werd gevonden in de dataverzameling met $p_t(\mu) > 7\,GeV/c$ en 0.55 ± 0.09 in de verzameling met $p_t(\mu) > 6\,GeV/c$, zie appendix B. De $p_t^{rel}(K_S^0)$ van het leidende kaon is gebruikt om de $b\bar{b}$ fractie in de 'één–muon' gebeurtenissen te berekenen, met de zelfde uitkomsten. Door op deze wijze kaonen in de muon jet in de 'één–muon' data met $p_t(\mu) > 6\,GeV/c$ te selecteren, kan de data verkregen worden met minder muon achtergrond.

De beschreven analyse methode voor de productie van zware quarks in 'één–muon' gebeurtenissen met een kaon in de muon jet heeft het ernstige nadeel dat de K_S^0 reconstructie efficiëntie in de Centrale Detector van UA1 slechts ongeveer 15% bedraagt. Daarom is de identificatie van zware quarks met alleen muonen veruit voordeliger. Het gebruik van neutrale kaonen zou gerechtwaardigd zijn in jets zonder het muon kenmerk voor de zware quarks. Uit de onderzochte data kon echter geen zinvol kaon signal in deze jets worden afgeleid.

КРАТКИЙ ОБЗОР

Настоящая работа представляет собой часть эксперимента UA1, выполненного на $p\bar{p}$ коллайдере в ЦЕРНе при энергии центра масс сталкивающихся частиц равной $\sqrt{s}$ = 630 ГэВ. Работа посвящена исследованию нейтральных каонов для опознавания кварковых струй, в частности для опознавания струй тяжелых b и c кварков.

Струи возникают в результате фрагментации кварков и представляют собой узкоколлимированные потоки частиц. Опознавание струй, другими словами, определение "аромата" кварка, создающего эту струю, необходимо для изучения свойств кварков.

В UA1 эксперименте для опознавания струй тяжелых кварков до сих пор всегда использовались мюоны, так как мюоны могут быть выявлены в струях, возникающих при семилептонном распаде этих кварков. Нейтральные каоны также могут быть выявлены в струях, детектируемых в дрейфовой камере UA1. Как обсуждалось в главе 2, рождение b и c кварков во взаимодействии протонов с антипротонами на коллайдере описывается "Стандартной моделью". В этой модели нейтральные каоны возникают, как правило, в конце распада тяжелых кварков (например, в ступенчатом распаде $b \to c \to s$ тяжелого b кварка). Поэтому была исследована возможность использования нейтральных каонов для опознавания струй тяжелых кварков вместо мюонов или совместно с мюонами.

Для изучения нейтральных каонов в струях были использованы экспериментальные события, содержащие по крайней мере один мюон с поперечным импульсом выше 6 ГэВ/с и при одном или большем числе струй, зарегистрированных в калориметре. Это, так называемые, "одномюонные" события. По сравнению со струями в калориметре, дрейфовая камера установки UA1 позволяет измерять направление оси струи с большей точностью. Поперечный импульс мюона относительно оси струи $-p_T^{rel}(\mu)-$ в дрейфовой камере измеряет вероятность определенного аромата кварка, создающего эту струю. Предыдущие исследования этих экспериментальных данных, использующие распределение по $p_T^{rel}(\mu)$ показали, что около 51% и 16% мюонов с поперечными импульсами выше 10 ГэВ/с рождаются в семилептонных распадах b и c кварков, соответственно [10]. Однако полный набор событий, содержащий мюоны с $p_T(\mu)>6$ ГэВ/с содержит до 70% фона от $\pi^{\pm}$ и $K^{\pm}$ распадов в мюоны (см. главу 3). Дополнительная информация, которую дает нейтральный каон помогает уменьшить этот фон.

Короткоживущие нейтральные каоны K_S^0 были восстановлены из продуктов распада в $\pi^+\pi^-$ в дрейфовой камере установки UA1 с соотношением сигнал/шум $> 4,4 \pm 0,2$ это значение зависит от имеющих место отборов, (см. главу 4). Эффективность восстановления составляет около 75% (см. главу 5). Полное инклюзивное сечение продукции K_S^0 в "одномюонных" событиях с быстротами каона $|y| < 2,5$ и поперечными импульсами, превышающими 0,2 ГэВ/с, составляет $164 \pm 17 \pm 25$ нб (первая погрешность статистическая, вторая систематическая по характеру, см. главу 6).

Количество K_S^0 на событие составляет около 1,3 (после поправки на эффективность реконструкции). Эта множественность сравнима с множественностью короткоживущих нейтральных каонов в событиях "минимального смещения", где она составляет около 0,6. События "минимального смещения" получаются в результате одновременной диссоциации протона и антипротона при их столкновении. Обычно они не содержат ни струй, ни тяжелых кварков. Точное сравнение множественности K_S^0 в обоих типах событий технически не было возможно из-за различной нормализации этих событий. Однако зависимость инклюзивного сечения нейтральных каонов падает намного медленнее с увеличением поперечного импульса каонов в "одномюонных событиях", чем в событиях "минимального смещения". Следовательно, в общем случае, нейтральные каоны с большими поперечными импульсами (больше 0,5 или 1,0 ГэВ/с) рождаются в кварковых или глюонных струях.

Кластеризация нейтральных каонов по оси струи была действительно обнаружена в одномюонных событиях, см. главу 7. Этот факт не помогает, однако, при определении аромата кварка, создающего струю, потому что нейтральные каоны могут быть рождены от глюонов или кварков любых ароматов.

Количество K_S^0 на струю для различных кварков, создающих струю, было изучено с помощью программы розыгрыша событий по системе Монте Карло. Был сделан вывод, что различия в множественности нейтральных каонов для различных струй незначительны. Таким образом, множественность нейтральных каонов в струях не может быть использована для опознавания струй. Поперечный импульс нейтральных каонов относительно оси струи для различных кварков обладает приблизительно одинаковым значением. Важным исключением являются струи с мюоном, измеренные в дрейфовой камере. В таких мюонных струях разница в средних значениях $<p_T^{rel}(K_S^0)>$ между струями от b и c кварков, полученная по результатам Монте Карло составляет приблизительно 0,13 ГэВ/с.

Обычно каон рождается в конце ступенчатого распада тяжелого кварка, поэтому влияние кварковой массы на величину относительного поперечного импульса распределяется между многими частицами. Однако, если нейтральный каон является ведущим, то можно сделать вывод, что либо он был рожден в самом начале распада, либо вклад промежуточных частиц в поперечный импульс струи незначителен. Таким образом, в мюонных струях разница в средних значениях лидирующего каона между струями b и c кварков составляет около 0,26 ГэВ/с. Более того, поперечный импульс лидирующего нейтрального каона относительно оси мюонной струи несет ту же информацию о продукции тяжелых кварков, что и $p_T^{rel}(\mu)$ самого мюона. Поэтому, согласно результатам, полученным по событиям Монте Карло, $p_T^{rel}(K_S^0)$ лидирующего каона в мюонных струях может быть использован для отделения событий со струями b кварков от событий со струями c кварков и от фоновых событий.

Множественность K_S^0 и поперечный импульс относительно оси струи, измеренные в реальных одномюонных событиях, приблизительно равны значениям ожидаемым по Монте Карло. Распределения $p_T^{rel}(\mu)$ мюона в струях b и c кварков, полученные по данным Монте Карло, были использованы для определения доли реальных событий, содержащих струи b или c кварков. Было найдено, что в одномюонных событиях при $p_T(\mu)>7$ ГэВ/с доля кварковых событий $b\bar{b}$ составляет 0,65±0,12, а при $p_T(\mu)>6$ ГэВ/с она составляет $0{,}55 \pm 0{,}09$ (см. приложение Б). Измерение $p_T^{rel}(K_S^0)$ лидирующего каона в одномюонных событиях привело к тем же результатам. Таким образом, путем отбора событий с каоном в мюонной струе был получен набор событий, содержащий меньшее число фоновых событий.

Описанный метод отбора событий с нейтральным каоном в мионной струе имеет существенный недостаток, выражающийся в низкой эффективности восстановления нейтральных каонов (около 15%) в дрейфовой камере установки UA1. Поэтому отбор событий, содержащих тяжелые кварки с использованием только мюонов, намного эффективнее. Использование нейтральных каонов было бы оправдано для опознавания струй, не содержащих мюоны. Но в таких струях получить соответствующий сигнал с нейтральным каоном не удалось.

Appendix A

Tables for K_S^0 reconstruction efficiency.

The efficiency of K_S^0 reconstruction is calculated from the 'Single K_S^0' efficiency with corrections for the Monte Carlo overestimation. The 'Single K_S^0' efficiency is calculated by generating a K_S^0 decay in an otherwise empty Central Detector. The new kaon selection cuts discussed in the chapter 4.2 have been used. The 'Single K_S^0' tables have been calculated for a flat $p_t(K_S^0)$ range of [0.2,0.5], [0.5,1.0], [1.0,3.0], [3.0,5.0] GeV/c. The (uniform) rapidity (y) and azimuthal angle (ϕ) ranges in each p_t interval are [0,0.5], [0.5,1.0], [1.0,1.5], [1.5,2.0], [2.0,2.5] for the rapidity and [0,22.5], [22.5,45], [45,67.5], [67.5,90] degree for the ϕ angle. The efficiencies are presented in tables A.1- A.4.

The variation of the efficiency with p_t of the kaon is a stronger effect than the coarse p_t ranges above suggest. Therefore we have calculated the efficiency for a central rapidity and ϕ intervals of $1.0 < y < 1.5$ and $45 < \phi < 67.5°$ in small p_t steps of 0.2 GeV/c in the whole transverse momentum range of 0.2 to 5 GeV/c. The results are presented in table A.5. The 'Single K_S^0' efficiency $A(p_t, y, \phi)$ is obtained from the tables A.1- A.5 by:

$$A(p_t, y, \phi) = \frac{E_1^s(p_t, y, \phi)}{E_1^s(p_t, y_0, \phi_0)} \cdot E_2^s(p_t, y_0, \phi_0) \tag{A.1}$$

where E_1^s are the tables A.1- A.4 and E_2^s is the table A.5, y_0 and ϕ_0 are the central values of rapidity and azimuthal angle, for which E_2^s is calculated. In the equation A.1 we assumed, that the form of the rapidity and ϕ efficiency distribution is about the same inside a single p_t interval of tables E_1^s.

This assumption has been checked by computing the difference between $A(p_t, y, \phi)$ calculated with equation A.1 and by calculating the 'Single K_S^0' efficiency directly for a number of points at the boundary of the p_t, y, ϕ intervals. It has been found, that the values agree with each other within $\Delta A \approx 0.02$.

The value $\Delta A = 0.02$ has been taken as a floor error on the efficiency calculation. The statistical errors given also in tables A.1- A.5 are added quadratically:

$$\frac{\Delta A(p_t, y, \phi)}{A(p_t, y, \phi)} = \sqrt{\left(\frac{\Delta E_1^s(p_t, y, \phi)}{E_1^s(p_t, y, \phi)}\right)^2 + \left(\frac{\Delta E_1^s(p_t, y_0, \phi_0)}{E_1^s(p_t, y_0, \phi_0)}\right)^2 + \left(\frac{\Delta E_2^s(p_t, y_0, \phi_0)}{E_1^s(p_t, y_0, \phi_0)}\right)^2 + (0.02)^2} \tag{A.2}$$

To obtain a realistic efficiency the 'Single K_S^0' efficiency $A(p_t, y, \phi)$ has to be multiplied by the Monte Carlo correction factor C_{mc} defined in eq. 5.1. Also the background from track combinations accidentally passing the V^0 reconstruction cuts has to be subtracted. The procedure to calculate the cross section is described in chapter 6.

Table A.1: *Single kaon efficiency in % for* $0.2 < p_t < 0.5\,GeV/c$.

ϕ[deg]/y	0.0-0.5	0.5-1.0	1.0-1.5	1.5-2.0	2.0-2.5
0-22.5	2.5 ± 0.3	11.9 ± 0.6	20.9 ± 0.8	13.9 ± 0.6	5.0 ± 0.3
22.5-45	12.6 ± 0.6	8.4 ± 0.5	26.2 ± 1.0	20.6 ± 0.8	7.5 ± 0.5
45-67.5	24.6 ± 0.9	15.8 ± 0.7	26.8 ± 1.0	21.5 ± 0.8	7.9 ± 0.5
67.5-90	28.1 ± 1.0	25.4 ± 1.0	30.5 ± 1.0	23.5 ± 0.9	9.4 ± 0.5

Table A.2: *Single kaon efficiency in % for* $0.5 < p_t < 1.0\,GeV/c$.

ϕ[deg]/y	0.0-0.5	0.5-1.0	1.0-1.5	1.5-2.0	2.0-2.5
0-22.5	6.2 ± 0.4	22.8 ± 0.9	28.7 ± 1.0	22.2 ± 0.9	12.3 ± 0.6
22.5-45	22.1 ± 0.9	20.8 ± 0.8	37.7 ± 1.2	33.8 ± 1.1	22.5 ± 0.9
45-67.5	38.5 ± 1.2	31.3 ± 1.0	39.6 ± 1.2	36.8 ± 1.2	22.0 ± 0.9
67.5-90	45.1 ± 1.3	42.3 ± 1.3	43.5 ± 1.3	38.3 ± 1.2	22.7 ± 0.9

Table A.3: *Single kaon efficiency in % for* $1.0 < p_t < 3.0\,GeV/c$.

ϕ[deg]/y	0.0-0.5	0.5-1.0	1.0-1.5	1.5-2.0	2.0-2.5
0-22.5	8.6 ± 0.5	29.5 ± 1.0	34.9 ± 1.1	30.9 ± 1.1	21.1 ± 0.8
22.5-45	24.4 ± 0.9	27.0 ± 1.0	35.6 ± 1.1	31.5 ± 1.1	24.9 ± 0.9
45-67.5	33.7 ± 1.1	34.4 ± 1.1	36.6 ± 1.2	33.7 ± 1.1	25.1 ± 0.9
67.5-90	41.8 ± 1.3	39.2 ± 1.2	38.3 ± 1.2	34.6 ± 1.1	23.2 ± 0.9

Table A.4: *Single kaon efficiency in % for* $3.0 < p_t < 5.0\,GeV/c$.

ϕ[deg]/y	0.0-0.5	0.5-1.0	1.0-1.5	1.5-2.0	2.0-2.5
0-22.5	6.2 ± 0.4	24.5 ± 0.9	26.3 ± 0.9	21.8 ± 0.9	17.5 ± 0.7
22.5-45	11.1 ± 0.6	23.3 ± 0.9	22.7 ± 1.0	24.6 ± 0.9	20.1 ± 0.8
45-67.5	17.6 ± 0.7	22.2 ± 0.9	27.5 ± 1.0	25.8 ± 0.9	17.3 ± 0.7
67.5-90	19.4 ± 0.8	23.2 ± 0.9	26.6 ± 1.0	24.2 ± 0.9	16.8 ± 0.7

Table A.5: *Single kaon efficiency in % for* $0.2 < p_t < 5.0\,GeV/c$ *and a central rapidity and* ϕ *interval:* $1.0 < y < 1.5$ *and* $45 < \phi < 67.5°$.

$p_t\,GeV/c$	E_2^s[%]	$p_t\,GeV/c$	E_2^s[%]	$p_t\,GeV/c$	E_2^s[%]	$p_t\,GeV/c$	E_2^s[%]
0.2-0.4	25.6 ± 0.9	1.4-1.6	43.0 ± 1.3	2.6-2.8	34.4 ± 1.1	3.8-4.0	25.2 ± 0.9
0.4-0.6	31.7 ± 1.1	1.6-1.8	43.7 ± 1.3	2.8-3.0	35.6 ± 1.1	4.0-4.2	24.2 ± 0.9
0.6-0.8	36.0 ± 1.1	1.8-2.0	41.2 ± 1.2	3.0-3.2	32.1 ± 1.1	4.2-4.4	22.1 ± 0.9
0.8-1.0	40.0 ± 1.2	2.0-2.2	40.6 ± 1.2	3.2-3.4	29.6 ± 1.0	4.4-4.6	21.2 ± 0.8
1.0-1.2	43.6 ± 1.3	2.2-2.4	38.6 ± 1.2	3.4-3.6	27.2 ± 1.0	4.6-4.8	19.8 ± 0.8
1.2-1.4	42.1 ± 1.3	2.4-2.6	36.0 ± 1.1	3.6-3.8	27.1 ± 1.0	4.8-5.0	19.7 ± 0.8

Appendix B

Measurement of the b$\bar{\text{b}}$ fraction.

In chapter 7 we have calculated the fraction of the $b\bar{b}$ events in the muon data samples with a leading neutral kaon using $p_t^{rel}(K_S^0)$ with respect to the muon jet axis. The fraction of $b\bar{b}$ is 0.7 ± 0.3 in both data samples with $p_t(\mu) > 7\,GeV/c$ and with $p_t(\mu) > 6\,GeV/c$. In this appendix we describe a method to measure the $b\bar{b}$ fraction more accurate.

Large errors in the above $b\bar{b}$ fractions are coming from three sources. First of all, the accuracy is limited by the statistics of the real data: there are only 75 events in the muon data sample with $p_t(\mu) > 7\,GeV/c$; it is slightly better in the sample with $p_t(\mu) > 6\,GeV/c$, containing 132 events. Second, the Monte Carlo data sample of the $b\bar{b}$ and the $c\bar{c}$ events containing a leading K_S^0 after the detector reconstruction is rather small. There are 99 $b\bar{b}$ events and 33 $c\bar{c}$ events. Third, the use of the $< p_t^{rel} >$ averages of the corresponding distributions to calculate the $b\bar{b}$ fraction enhances the error in the $b\bar{b}$ fraction.

To measure accurately the $b\bar{b}$ fraction using $p_t^{rel}(K_S^0)$ of a leading kaon in the muon jet we have fit the Monte Carlo distributions to the real data. For this fit the statistics of the Monte Carlo data, especially the number of the $c\bar{c}$ events had to be increased. A large increase in the number of the available Monte Carlo events can be achieved by using the data without the detector simulation. This way is prohibited, however, because the jet definition must be changed drastically and therefore the selection parameters have to be changed as well. An example is given by the cut on the transverse mass of a jet (m_t). Events, that were passing this cut after the reconstruction in the detector, obtained contributions to m_t from unreconstructed tracks and therefore did not satisfy the $m_t < 2\,GeV/c^2$ cut any more. To overcome these difficulties, we selected the muon events after the detector simulation and used kaons without their reconstruction in the detector. As discussed in chapter 5, the kinematical parameters of the kaons after the detector simulation do not deviate strongly from their initial parameters. However, it is necessary to weight the events with these 'bare' kaons by the corresponding efficiency (see appendix A), otherwise the observed kaon spectrum is too hard. After weighting we obtained the following results for the $< p_t^{rel}(K_S^0) >$ of the leading kaon in the Monte Carlo data:

$$< p_t^{rel}(K_S^0) >_{Lead} = \begin{cases} 0.65 \pm 0.02\,GeV/c\ (438) & b\bar{b} \\ 0.37 \pm 0.02\,GeV/c\ (175) & c\bar{c} \end{cases} \tag{B.1}$$

The number of events is given in the parenthesis.

Using these distributions of $p_t^{rel}(K_S^0)$ of the $b\bar{b}$ and the $c\bar{c}$ events we have fit the real data with $p_t(\mu) > 7\,GeV/c$ (fig. B.1) and with $p_t(\mu) > 6\,GeV/c$ (fig. B.2). As in chapter 7, we assume the background distribution has the same shape as the $c\bar{c}$ distribution.

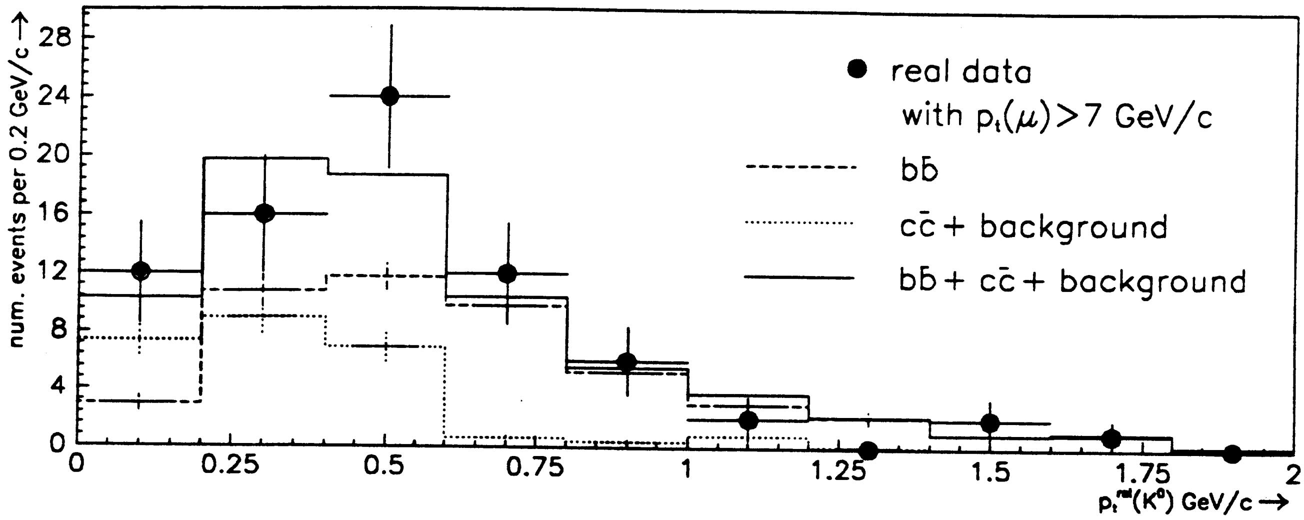

Figure B.1: *The $p_t^{rel}(K_S^0)$ in real data (with $p_t(\mu) > 7\,GeV/c$) fit with the improved ISAJET predictions for the $b\bar{b}$ and the $c\bar{c}$ contributions. The Monte Carlo predictions have been normalized to the number of events in real data.*

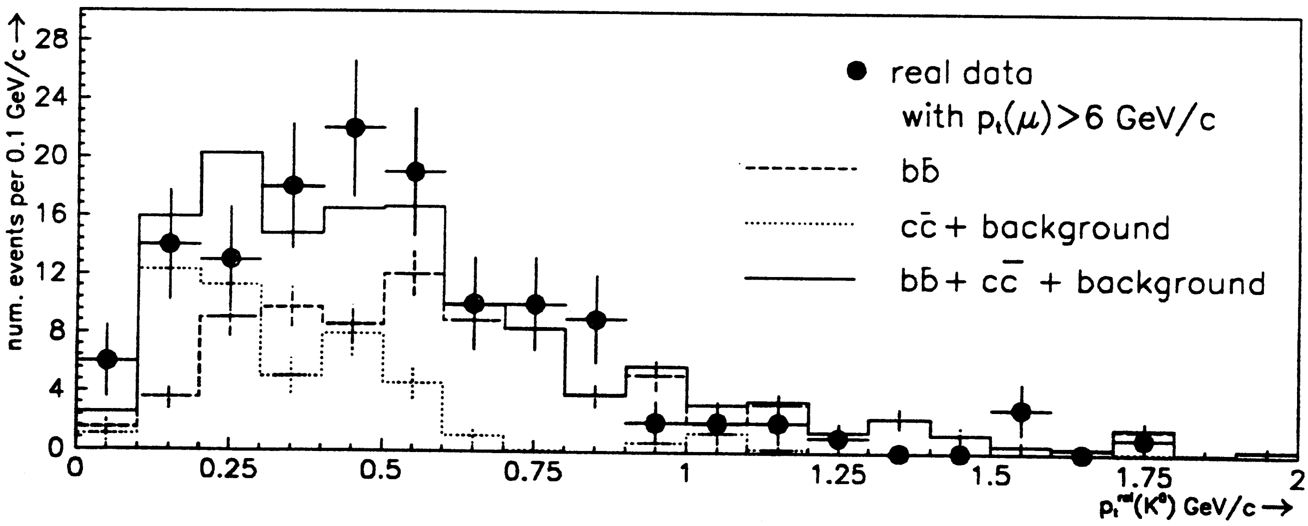

Figure B.2: *The $p_t^{rel}(K_S^0)$ in real data (with $p_t(\mu) > 6\,GeV/c$) fit with the improved ISAJET predictions for the $b\bar{b}$ and the $c\bar{c}$ contributions. The Monte Carlo predictions have been normalized to the number of events in real data.*

The numerical results are:

$$fraction\ b\bar{b} = \begin{cases} 0.65 \pm 0.15 & \text{for } p_t(\mu) > 7\,GeV/c \\ 0.63 \pm 0.14 & \text{for } p_t(\mu) > 6\,GeV/c \end{cases} \tag{B.2}$$

The χ^2/df values of the fit are 4.7/8 and 36.2/15 for the $p_t(\mu) > 7\,GeV/c$ and the $p_t(\mu) > 6\,GeV/c$ data samples respectively. We observe, that the statistics of the real data is still the main limiting factor of the accuracy of the measurement. The χ^2 of the fit to the data sample with $p_t(\mu) > 6\,GeV/c$ is rather high; probably the assumption of background varying similar to the $c\bar{c}$ distribution is less justified in this case. In summary, the improved results emphasize the conclusion of the present thesis, that the data selection with a leading kaon in the muon jet has the ability to reduce the background in the single muon data sample.

The $b\bar{b}$ fraction of 0.65 ± 0.15 in the sample with leading kaons is almost 2 times larger than the $b\bar{b}$ fraction of 0.35 ± 0.04 in the muon sample with $p_t(\mu) > 7\,GeV/c$ [39], quoted in chapter 7.

The reason for this background reduction is understood within the Independent Fragmentation Model (chapter 2) by counting the different possibilities. Recall first, that the background in single muon events is caused by decays of charged kaons and pions produced in the fragmentation of light u, d or s quarks. The ratio of K/π has been measured to about 0.4 for $p_t(\mu) > 6\,GeV/c$ [39]. The specific combination of a charged particle at the first step and a neutral kaon at the second step in the fragmentation of a light quark is not very common. The largest contribution comes from an u quark, that can make a charged kaon or a charged pion:

- To make a charged pion ($\pi^+ = (u\bar{d})$) it picks a $(d\bar{d})$ pair from the sea. The remaining d quark lifts an $(s\bar{s})$ pair from the sea to make a $K^0 = (d\bar{s})$. The probability to pick an $s\bar{s}$ pair is about 0.2.

- To make a charged kaon ($K^+ = (u\bar{s})$) the u quark picks an $(s\bar{s})$ pair from the sea. The remaining s quark lifts a $(d\bar{d})$ pair from the sea to make a $\bar{K}^0 = (\bar{d}s)$. The probability to pick an $d\bar{d}$ pair is about 0.4.

Since the K/π ratio is 0.4 (i.e. 71% $\pi^\pm$ and 29% $K^\pm$) the probability for a charged pion or kaon and then a K^0 from an u quark is 0.25. In d or s jets the probability for this combination is smaller by a factor of 8, since the neutral kaon at the second fragmentation step has to be produced via an intermediary K^*. The probability of about 0.03 has been obtained for the d or s quark jets.

Thus, after the selection of a leading kaon in the muon jet the background from u quark jets goes down by a factor of 4, while the heavy quark signal is less by a factor of 2 (see chapter 7). The fraction of heavy quarks in the single muon data sample with $p_t(\mu) > 6\,GeV/c$ grows from 0.3 to about 0.5, if the background events contain only the u quark jets. The percentage of the heavy quarks goes up to 70% if the u quarks contribute only for 1/3 to the muon background. Thus, the selection of a leading neutral kaon in the muon jet reduces the muon background more than a factor of 4, in proportion dependent on the quark content of this background.

The explanation for the background reduction discussed above is not restricted to neutral kaons produced in the second step of the fragmentation. The calculated probabilities for the production of a neutral kaon apply everywhere in the fragmentation chain. Therefore, for the background reduction, the only presence of a K^0 in the muon jet should be sufficient. To prove this statment the Monte Carlo $b\bar{b}$ and $c\bar{c}$ $p_t^{rel}(\mu)$ distributions have been fitted to the experimental data. The fits are shown in fig. B.3 for the sample with $p_t(\mu) > 7\,GeV/c$ and fig. B.4 for the sample with $p_t(\mu) > 6\,GeV/c$. Note, that the muon relative transverse momentum distribution with respect to its jet in the Central detector has been used in this calculation, because the difference in the average $< p_t^{rel}(K_S^0) >$ between the $b\bar{b}$ and the $c\bar{c}$ jets is only $0.13\,GeV/c$ (see chapter 7), if the kaon is not leading.

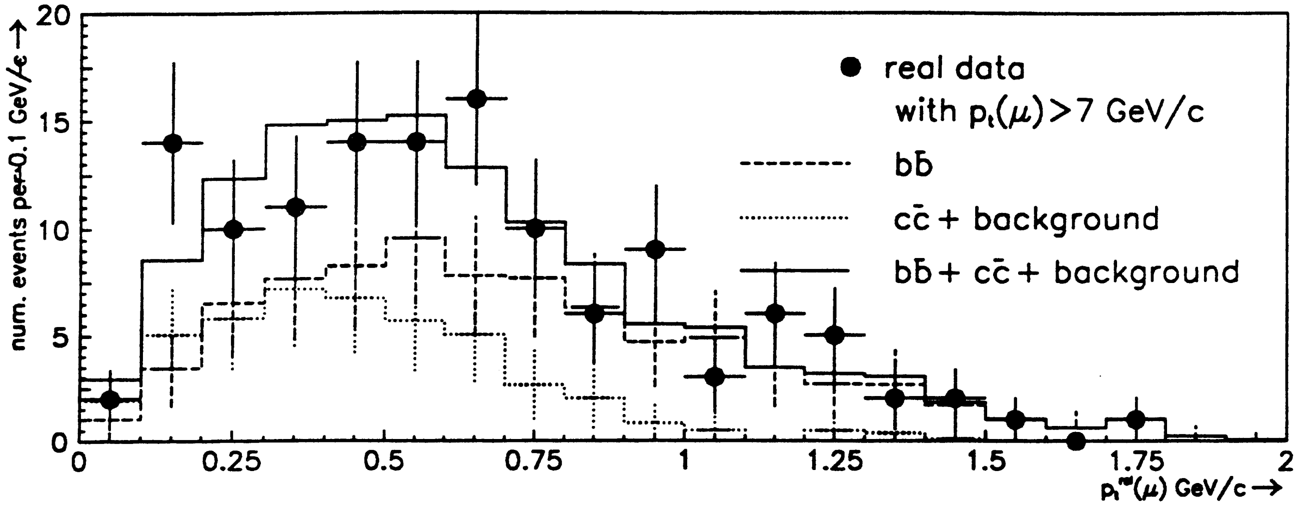

Figure B.3: *The $p_t^{rel}(\mu)$ in real data (with $p_t(\mu) > 7\,GeV/c$) fit with the improved ISAJET predictions for the $b\bar{b}$ and the $c\bar{c}$ contributions. The Monte Carlo predictions have been normalized to the number of events in real data.*

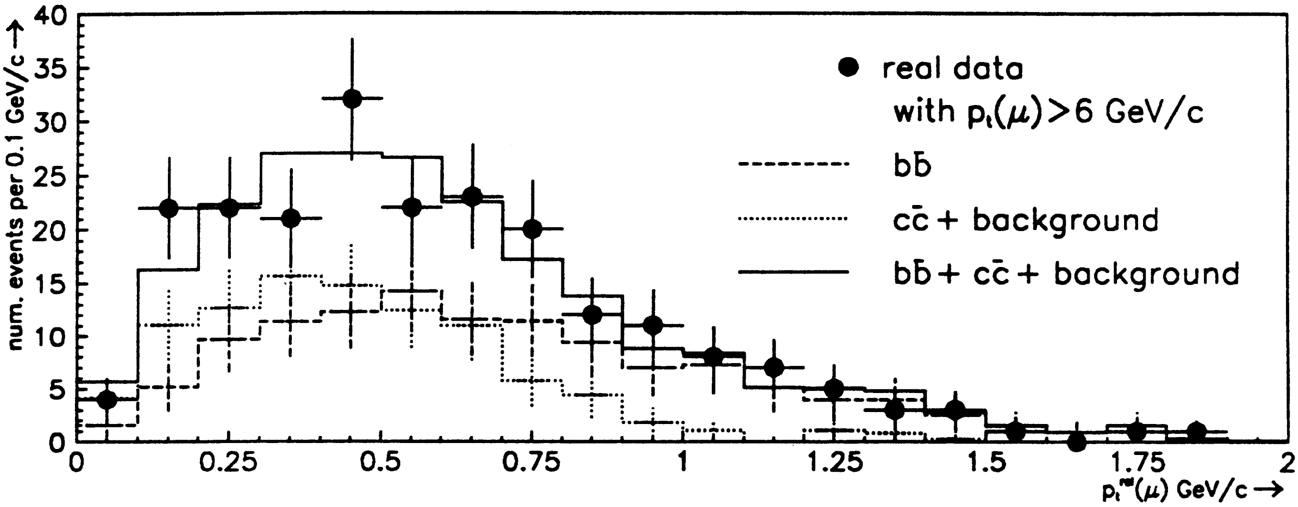

Figure B.4: *The $p_t^{rel}(\mu)$ in real data (with $p_t(\mu) > 6\,GeV/c$) fit with the improved ISAJET predictions for the $b\bar{b}$ and the $c\bar{c}$ contributions. The Monte Carlo predictions have been normalized to the number of events in real data.*

The numerical results are:

$$fraction\ b\bar{b} = \begin{cases} 0.65 \pm 0.12 & \text{for } p_t(\mu) > 7\,GeV/c \\ 0.55 \pm 0.09 & \text{for } p_t(\mu) > 6\,GeV/c \end{cases} \tag{B.3}$$

The χ^2/df values of the fit are 11.8/17 and 9.43/18 for the $p_t(\mu) > 7\,GeV/c$ and the $p_t(\mu) > 6\,GeV/c$ data samples respectively. Therefore the selection of neutral kaons in the muon jet allow to reduce the background in the single muon events.

In conclusion, the described method of data selection allows to obtain a sample with a high heavy quark percentage in the single muon events with $p_t(\mu) > 6\,GeV/c$.

Bibliography

[1] C. Rubbia, P. McIntyre, D. Cline, Proc. Int. Neutrino Conf., Aachen, 1976.

[2] S. L. Glashow, Nucl. Phys., 22, 579 (1961)
S. Weinberg, Phys. Rev. Lett., 19, 1264 (1967)
A. Salam, in Elementary particle theory, ed. N.Svartholm, Almquist and Wiksell, Stockholm 1968, p. 367.

[3] P. Braham et al., Nucl. Instrum. and Methods, 125 (1975) 201.

[4] A. Astbury et al., A 4π solid angle detector for the SPS used as a proton–antiproton collider at a center of mass energy of 540 GeV, Proposal, CERN/SPSC/78-06, January 1978.

[5] G. Arnison et al., Phys. Lett. 122B (1983), 1.
G. Arnison et al., Phys. Lett. 126B (1983), 398.

[6] See review article: W.J.Marciano and Pagels, Phys. Rep. 36C, 137 (1978)

[7] C. Albajar et al. Search for new heavy quarks at the CERN proton-antiproton Collider, Z.Phys. C73, (1988).

[8] C. Albajar et al., Phys. Lett. 186B (1987) 237 and 247

[9] C. Albajar et al., High transverse momentum J/ψ production at the CERN proton–antiproton Collider, Phys. Lett. 200B (1988), 380.

[10] C. Albajar et al., Study of heavy flavour production in events with a muon accompanied by jet(s) at the CERN proton-antiproton collider, Z.Phys. C37,489-503(1988).

[11] V. Karimäki, Formulae for the UA1 V^0 finding algorithm, UA1-TN 84/31
V. Karimäki, R. Raja, V^0 pattern recognition and kinematic fitting, UA1-TN 85/88.

[12] I. Zacharov, UA1 Technical Note (in preparation).

[13] P. Erhard, Ph. D. Thesis, (1988)

[14] L.S.Kim, The search for truth within the Standard Model, Ph.D. Thesis, Univ. of Wisconsin, Madison, MAD/PH/416 (1988)

[15] M. Kobayashi, K. Maskawa, Prog. Theor. Phys. 49 (1973), 652.

[16] B.L.Ioffe, V.A.Khoze, L.N.Lipatov, Hard Processes, Vol. 1, North Holland, 1984

[17] V.S.Mursin, L.I.Sarytcheva, Fizika adronnych processov (Physics of Hadronic processes), Moskaw, 1986.

[18] G.Altarelli, G.Parisi, Nucl. Phys. B126, 298 (1977).

[19] Eichten et al., Rev. Mod. Phys, 56, 579 (1984).

[20] Eichten, Theoretical expectations at collider energies, FERMILAB-Conf-85/178-T (May, 1986)

[21] F.E.Paige, S.D.Protopopescu, ISAJET 5.30: A Monte Carlo event generator for pp and $p\bar{p}$ interactions, Brookhaven National Laboratory, BNL 38774 (1986)..

[22] B. van Eijk, Ph.D. Thesis, Univ. of Amsterdam, 1987.

[23] R.P.Feynman, R.D.Field, G.C.Fox, Phys. Rev. D18, 3320 (1978)
R.P.Feynman, R.D.Field, Nucl. Phys. B136, 1 (1978)

[24] C. Peterson et al., Phys. Rev. D27, 105 (1983)

[25] Rev. of Particle Properties, Particle Data Group, Phys. Lett. 170B (1986).

[26] C.Albajar et al., Measurement of the Bottom Quark production cross section in proton–antiproton collisions at $\sqrt{s} = 0.63\,TeV$, CERN-EP/88-100, August 1988.

[27] See e.g. L. R. Evans, Performance limitations of the SPS Collider, in Physics of particle accelerators, Vol. 2, M.Month (ed.), M.Dienes (ed.), SLAC Summer school july 15-26 1985 and Fermilab Summer school, august 13-24, 1984.

[28] A. Astbury et al., The UA1 Calorimeter trigger, Nucl. Instruments and Methods, A238, 288 (1985).

[29] J. Dorenbosch et al., Selection of Muon Events in the 168E, UA1-TN 85/31 (1985)
I. ten Have, Efficiency of the Second Level Trigger using Mutime, UA1-TN 85/70 (1985)
M. Preischl, University Graduation Thesis, University of Kiel (1985).

[30] T. R. Edgecock, J/Ψ production in proton-antiproton collisions at $\sqrt{s} = 630\,GeV$, Ph.D. Thesis, 1986.

[31] M. Pimiä, Track finding in the UA1 Central Detector at the CERN $p\bar{p}$ Collider, Ph.D. Thesis, 1985.

[32] V.Karimäki, Fast trajectory fitting in uniform field. UA1-TN 31/84 (1984). (unpublished).

[33] V.Karimäki, J. Kroll, Vertex Finding in the Central Detector, UA1-TN 87/100, December 1987

[34] R.Wigmans, Energy loss of particles in dense matter calorimetry, NIKHEF-H/87-12, August 1987.

[35] V.Karimäki, Kink Finding in the Central Detector, UA1-TN 86/03, January 1986.

[36] N.Ellis, V.Karimäki, Automatic Identification of Cosmic Rays in Muon Trigger Data, UA1-TN 83/91, November 1983.

[37] F.Ceradini, G.Ciapetti, A. Di Ciaccio, F.Lacava, Finding efficiency and energy correction for low E_t jets in UA1, UA1-TN 86/108, November, 1986.

[38] K.Wacker, Inclusive muon selection from 1984 data, UA1-TN 86/26;
N.Ellis et al., Selection of muon events from the 1985 run, UA1-TN 86/45;
J.Richman, Update to selection of muon events from the 1985 run, UA1-TN 86/74.

[39] M. P. Jimack, A study of heavy flavour production in muon events at the CERN $p\bar{p}$ collider, Ph.D. Thesis, RAL-T-053 (1987).

[40] D.J.Holthuizen, I.E.Zacharov, K^0 and $\Lambda/\bar{\Lambda}$ selection in single muon events, UA1-TN 88/19.

[41] D.Charlton et al., Monte-Carlo production using ISAJET 5.23, UA1-TN 86/97, October 1986.

[42] D.J.Holthuizen, I.E.Zacharov, Efficiency of K^0_S reconstruction in the UA1 Central Detector, UA1-TN 88/11.

[43] R.C.Fernow, Introduction to experimental particle physics, Cambridge Univ. Press, 1986.

[44] G.Ciapetti, V.Karimäki, J.Kroll, L.Nisati, K^0_S production in Minimum Bias Trigger Events at $\sqrt{s} = 630\ GeV$, UA1-TN 87/73

[45] J.Kroll, Private Communication.

[46] G.J.Alner et al, Kaon production in $p\bar{p}$ reactions at a center of mass energy of 540 GeV, Nuclear Physics B, 1985.

[47] E. Byckling, K. Kajantie, Particle Kinematics, John Wiley and Sons, Ltd., 1973.

[48] M. Bozzo et al., Phys. Lett. 147B (1984), 385
D. Bernard et al., Phys. Lett. 186B (1987), 227.

[49] R. E. Ansorge et al., Kaon production at 200 and 900 GeV CM energy, Phys. Lett. 199B (1987), 311.

Contents

1 Introduction. **1**

2 Theory of the $p\bar{p}$ collisions. **3**

2.1 Introduction. 3
2.2 Theory of Quantum Chromodynamics. 3
2.2.1 Introduction. 3
2.2.2 The Quark-Parton Model. 4
2.2.3 Parton confinement. 4
2.2.4 Fragmentation of quarks and gluons in jets. 5
2.2.5 Weak decays of the heavy quarks. 6
2.3 Summary of hadron production. 6
2.3.1 ISAJET Monte Carlo program. 7

3 Description of the UA1 experiment. **10**

3.1 $Sp\bar{p}S$. 10
3.2 The Detector. 10
3.3 Event reconstruction in the Central Detector. 12
3.4 Jet reconstruction. 14
3.5 Muon identification and reconstruction. 16
3.6 Single muon events selection. 17

4 V^0 reconstruction in the CD. **19**

4.1 Introduction 19
4.2 The V^0 finding cuts. 19
4.3 The analysis procedure. 21
4.4 Properties of the Signal and the Background bands. 22
4.4.1 The experimental mass distribution. 22
4.4.2 Random background in the V^0 search. 22
4.4.3 Secondary interactions and γ-conversions in the CD walls. 24
4.4.4 Decay Probability of a K^0 for the Signal Band. 26
4.4.5 Decay angle of a K^0 for the Signal Band. 27
4.4.6 Decay plane orientation of a K^0 for the Signal Band. 27
4.4.7 Uncertainties of the mass determination. 31
4.4.8 Summary of the study of the mass spectrum. 31
4.5 Identification of a V^0 decay. 33
4.6 Summary of V^0 reconstruction procedure. 34

5 The efficiency of K_S^0 reconstruction. **35**
5.1 Introduction. 35
5.2 The merging of Monte Carlo K^0 into real events. 36
5.2.1 The analysis procedure. 36
5.2.2 The merging program. 36
5.2.3 Deviation of the vertex and the track parameters after mixing. 38
5.3 The V^0 reconstruction analysis for the old cuts. 40
5.3.1 The V^0 reconstruction for the single K^0 Monte Carlo events 40
5.3.2 The V^0 reconstruction in mixed events. 41
5.3.3 Comparison of the V^0 reconstruction efficiency with previous results. . . . 44
5.4 Efficiency of K_S^0 reconstruction with the new cuts. 45

6 The inclusive K_S^0 cross section. **47**

7 K_S^0 production in jets. **51**
7.1 Introduction 51
7.2 Selection of the data sample. 52
7.2.1 The μ and the calorimeter jet selection cuts. 52
7.2.2 Selection of the non-isolated muons. 52
7.2.3 Selection of the muon balancing jet. 53
7.2.4 The K_S^0 selection cuts. 54
7.2.5 Data selection summary and expectations for a $b\bar{b}/c\bar{c}$ signal. 54
7.3 Monte Carlo study of K_S^0 properties in jets. 56
7.3.1 Monte Carlo event generation. 56
7.3.2 General properties of the Monte Carlo data. 57
7.3.3 K_S^0 multiplicity in the Monte Carlo data. 58
7.3.4 $p_t^{rel}(K_S^0)$ in the Monte Carlo data. 60
7.3.5 $p_t^{rel}(K_S^0)$ for a leading K_S^0 in the Monte Carlo data. 60
7.3.6 Summary of the Monte Carlo study. 63
7.4 The K_S^0 properties in real data. 63
7.4.1 K_S^0 multiplicity in real data. 63
7.4.2 The $p_t^{rel}(\mu)$ after the K_S^0 selection in the real data. 64
7.4.3 The $p_t^{rel}(\mu)$ in jets with leading K_S^0. 67
7.4.4 The $p_t^{rel}(K_S^0)$ for a leading kaon in real data. 67
7.4.5 The K_S^0 selection in the data sample with $p_t(\mu) > 6\,GeV/c$. 70

8 Summary and conclusions. **72**

9 Samenvatting **74**

10 Kratky obzor. **76**

A Tables for K_S^0 reconstruction efficiency. **79**

B Measurement of the $b\bar{b}$ fraction. **82**

List of Figures

2.1 Inclusive differential b-quark production cross section at the Collider. 9
2.2 Topology of the heavy quark production. 9

3.1 The UA1 detector with two halves separated. 11
3.2 The UA1 Central Detector. 12
3.3 Distribution of the estimated error in the vertex position in x-coordinate. 14
3.4 Muon detector arrangement. 16
3.5 The inclusive muon spectrum. 18

4.1 An experimental mass distribution after the cuts $\chi_i^2 > 4.0$ and $b(K^0) < 3\,mm$. . . 23
4.2 V^0 background form from the $b\bar{b}$, $c\bar{c}$ M.C. events. 23
4.3 An experimental transverse momentum distribution of V^0's. 23
4.4 An experimental distribution of V^0 decay vertices in the XY-plane. 25
4.5 Scatter Plot of V^0 momentum and the opening angle. 25
4.6 An experimental decay probability distribution. 27
4.7 An experimental $cos\theta^*$ distribution of V^0's. 28
4.8 An experimental distribution of the decay plane angle ϕ of a K^0. 29
4.9 An experimental mass distribution for several decay plane dip angles. 30
4.10 An experimental mass distribution for several values of a mass uncertainty. . . . 32
4.11 An experimental mass distribution for $\Lambda/\bar{\Lambda}$ decay hypotheses. 33

5.1 Skeleton of the main program for the V^0 reconstruction analysis using the mixing technique. 37
5.2 Momentum shift of the Monte Carlo tracks after mixing with dimuon events. . . 40
5.3 Track splitting in CD. 42
5.4 Track crossing uncertainty in the CD. 43
5.5 The K^0 reconstruction efficiency as function of $p_t(K^0)$. 45

6.1 Inclusive differential K_S^0 production cross section. 49
6.2 Comparison of the K_S^0 production in minimum bias and single muon events. . . . 50

7.1 The inclusive p_t and rapidity spectra of kaons. 55
7.2 Distribution of neutral kaons relative to a muon jet for $p_t^{rel}(\mu) > 0.6$. 65
7.3 Distribution of neutral kaons relative to a muon balancing jet for $p_t^{rel}(\mu) > 0.6$. . 65
7.4 Distribution of neutral kaons relative to a muon jet for $p_t^{rel}(\mu) < 0.6$. 66
7.5 Distribution of neutral kaons relative to a muon balancing jet for $p_t^{rel}(\mu <> 0.6$. . 66
7.6 Spatial separation between a kaon and a muon within a jet. 68
7.7 The muon p_t relative to its jet containing a kaon. 68
7.8 The difference in azimuthal angle between K_S^0 and a muon relative to jet axis. . . 69
7.9 The $p_t^{rel}(K_S^0)$ in real data with $p_t(\mu) > 7\,GeV/c$ compared to ISAJET predictions. 70

7.10 The $p_t^{rel}(K_S^0)$ compared to ISAJET predictions for real data with $p_t(\mu) > 6\,GeV/c$. 71

B.1 The $p_t^{rel}(K_S^0)$ fit with the improved ISAJET predictions for real data with $p_t(\mu) > 7\,GeV/c$. 83

B.2 The $p_t^{rel}(K_S^0)$ fit with the improved ISAJET predictions for real data with $p_t(\mu) > 6\,GeV/c$. 83

B.3 The $p_t^{rel}(\mu)$ fit with the improved ISAJET predictions for real data with $p_t(\mu) > 7\,GeV/c$. 85

B.4 The $p_t^{rel}(\mu)$ fit with the improved ISAJET predictions for real data with $p_t(\mu) > 6\,GeV/c$. 85

List of Tables

2.1 Some quark properties. 3

3.1 Main parameters of the calorimeters. 15

4.1 S/B ratio for a kaon signal in single muon events for several χ_i^2 and $b(K^0)$ values. 22
4.2 S/B ratio for a kaon signal in single muon events for several $p_t(V^0)$ values. 24
4.3 S/B ratio for a kaon signal after P_d cut. 27
4.4 S/B ratio and the number of kaons for several $cos\theta^*$ values. 28
4.5 S/B ratio and the number of kaons after the cut $\lambda_d < 0.3$ for several $p_t(V^0)$ values. 30
4.6 S/B ratio and the number of kaons after the cut $\sigma < 40\,MeV/c^2$ for several $p_t(V^0)$ values. 31
4.7 S/B ratio for a kaon signal in single muon events for simultaneous cuts. 31
4.8 S/B ratio and the number of $\Lambda/\bar{\Lambda}$'s. 33

5.1 Deviation of the Monte Carlo track parameters after mixing. 39
5.2 Track acceptance in the UA1 CD as function of K^0 transverse momentum. . . . 40
5.3 The r.m.s. width of the Monte Carlo $K^0 \rightarrow \pi^+\pi^-$ mass spectrum as function of $p_t(K^0)$. 41
5.4 The Monte Carlo efficiency correction factor as a function of kaon transverse momentum. 44
5.5 Efficiency of the $K_S^0 \rightarrow \pi^+\pi^-$ reconstruction. 46

6.1 Inclusive differential K_S^0 cross section in single muon events. 48

7.1 Selection of events. 55
7.2 Estimation of the number of the heavy flavour events. 55
7.3 Jet-parton association in the ISAJET Monte Carlo. 57
7.4 Heavy Flavour separation. 57
7.5 K_S^0 sources for several cuts. 58
7.6 The probability of K_S^0 production for jets originating from different quarks. . . . 58
7.7 K_S^0 multiplicity in the ISAJET Monte Carlo data for jets of different origin. . . . 59
7.8 The $p_t^{rel}(K_S^0)$ in the ISAJET Monte Carlo data for jets of different origin. 60
7.9 Percentage of the M.C. kaons that are leading and 'next to leading' in different types of jets. 61
7.10 The $p_t^{rel}(K_S^0)$ for leading and 'next to leading' kaons in the Monte Carlo data. . . 61
7.11 The $p_t^{rel}(\mu)$ for leading kaons in the Monte Carlo data. 62
7.12 K_S^0 multiplicity for the muon jets and their recoil jets. 64
7.13 The $p_t^{rel}(\mu)$ for leading kaons in the real data. 67
7.14 Percentage of leading K_S^0 for the muon jets and their recoil jets. 69
7.15 The $p_t^{rel}(\mu)$ in the sample with $p_t(\mu) > 6\,GeV/c$ for several K_S^0 cuts. 71

A.1 Single kaon efficiency for $0.2 < p_t < 0.5\,GeV/c$. 80
A.2 Single kaon efficiency for $0.5 < p_t < 1.0\,GeV/c$. 80
A.3 Single kaon efficiency for $1.0 < p_t < 3.0\,GeV/c$. 80
A.4 Single kaon efficiency for $3.0 < p_t < 5.0\,GeV/c$. 81
A.5 Single kaon efficiency for $0.2 < p_t < 5.0\,GeV/c$ and a central y, ϕ interval. 81

Acknowledgements

Any major result of the data analysis in the High Energy Physics is a combined effort of many people. I with to express my gratitude to all members of the UA1 Collaboration, who worked day and night to keep the experiment going, to collect the data and to put all the knowledge together, which I was lucky to use in the present thesis.

However, I would like to name specially all these people, who have contribute directly to my thesis. In the first place my co-promotor Dr. D. J. Holthuizen, who came with enlightening ideas when the analysis seemed to run into a blind alley and my promotor Prof. Dr. A. N. Diddens, who took the patience to read my reports and to teach me better English along with physics.

This thesis would not be possible without my co-promotor Dr. A. Norton, who introduced me to the analysis of the production of neutral particles and suggested the subject for this thesis. Many thanks to Prof. Dr. V. Karimäki, who developed the basic software for the neutral particles reconstruction and showed a continued interest in my work, helping me to understand the subject.

I have had many useful discussions with Dr. M. Della Negra, Dr. D. Denegri, Dr. J. Dorenbosch, Dr. N. Ellis, Dr. J. Kroll, Dr. L. Nisati; these discussions helped to determine the direction of the analysis. I apologize to all those, whose names I forgot to mention here.

I acknowledge the discussion with Prof. Dr. K. Gaemers and Dr. J. Vermaseren at the theory division at NIKHEF-H, who helped me to understand better the complicated modern theories of Elementary Particles.

Finally, I'm thinking back to the first year within the UA1 Collaboration, when I was working on the UA1 graphics system and Dr. J.-P. Vialle introduced me to the intrinsics of the UA1 software. I have learned a lot of the computer graphics at the CERN Data Division from Dr. D. Myers and J. Bettels.

Many warm gratitudes to my mother Larisa for her support and for helping me with print work and to my friends Anatoly Ivangorodsky and Hans van Zwol for their help with the translation of the summary section.

Curriculum Vitae

Igor Evgenievitch Zacharov was born 15 August 1959 in Odessa. He completed the high school education at the 'Rudolf Koch Schule' gymnasium in Offenbach (W. Germany) in 1978 with the 'Zeugnis der Allgemeinen Hochschulreife' Diploma.

He started to study physics at the University of Amsterdam in 1978 and obtained the 'kandidaats' Diploma (comparable to a bachelor of science degree) with majors in physics and computer science in 1981. He completed with honors the university study in 1984 with the graduation thesis in experimental nuclear physics entitled 'Electron Scattering from $^{48,50}Ti$'. The work resulting in the university graduation was performed in 1981-1984 at NIKHEF-K (Amsterdam) in the electron scattering group headed by Prof. Dr. C. de Vries.

He started to work on his Ph. D. in 1985 at the High Energy Physics department at NIKHEF in the group collaborating in the UA1 Experiment at CERN headed by Prof. Dr. C. Rubbia. During this time he worked on the graphics software for an interactive three dimensional analysis of the Collider data on Apollo workstations. The Ph. D. in experimental physics has been completed by the present thesis in 1988 (supervisor Prof. Dr. A. N. Diddens). This thesis describes the reconstruction of neutral kaons in the UA1 detector and the analysis of heavy quark production using neutral kaons.

Stellingen behorende bij het proefschrift

K^0 production in μ–tagged jets at the CERN $p\bar{p}$ Collider.

van Igor Evgenievitch Zacharov

In 1988 the UA1 detector is a dedicated muon detection facility [1]. An experiment to improve the limits of the top mass will be more successful by studying $B^0 - \bar{B}^0$ mixing via the muon signal than by a direct top search.

[1] The UA1 Program for the 1988 Collider run, CERN SPSC 88-29, SPSC/M 437.

The perturbation series for the strong coupling constant $\alpha_s(\mu)$ is not expected to converge, because of the non–perturbative effects of the QCD. Therefore the hope that $\alpha_s(\mu)$ will not depend on the renormalization scale μ, when calculated to all orders in the perturbation theory[2], is not justified.

[2] see e.g. J.Stirling, *Proceedings of the CERN Summer School 1988*, in preparation.

At the future LHC/SSC accelerators the proposed warm liquid calorimeter with Uranium–TMP or TMS [3] is either too slow, or too dangerous in operation.

[3] C.Rubbia in Festi-Val — Festschrift for Val Telegdi, ed. K.Winter, Elsevier Science Publishers, 1988, p.213.

In the life time calculation for a e^- beam in a storage ring with an internal target, Spencer [3] does not justify the neglect of the restoring effect of the synchrotron radiation. If these damping effects are included, the calculated life time of the beam can be more than a factor 2 longer.

[3] J.E.Spencer, in *Workshop on Electronuclear Physics with internal targets*, ed. R.G.Arnold, R.C.Minehart, SLAC-REPORT-316, 1987, p.37.

The Principal Component Analysis searches 'automatically' for a minimal set of independent parameters [5]. In practice, however, the human experimentator has to decide upon the most important parameters, based on physics arguments and intuition.

[5] see e.g. H.Wind in Formulae and Methods in experimental data evaluation, ed. R.K.Bock et al., Vol. 3, CERN 1983.

The existence of solutions of the 'General Theory of Relativity' (GTR), that are interpreted as 'Black Holes', is philosophically unsatisfactory. It is more natural to assume that at high matter densities the classical equations of GTR loose their meaning in favour of a quantum interpretation of the gravitational phenomena.

The scientific value of a Ph.D. thesis is, in general, not proportional to the costs of its printing and distribution. Therefore the formal requirements for a thesis in the Netherlands have to be reduced.

A chess game guided by a coordinated effort of all the pieces for the most important strategic aim cannot be lost.

Scientific theories are based on the typical, common elements of the perceived reality. Myths are also based on these elements, giving them a reality, independent of the perception.

A false theory can be confirmed only by a criminal practice.